NASA CONTRACTOR REPORT 177368

# Test and Evaluate Passive Orbital Disconnect Struts (PODS-III)

R. T. Parmley

S. A. Katz

I. Spradley

Lockheed Missiles & Space Company
Research & Development Division
Palo Alto, California 94304

W. C. Henninger
ACRI
Santa Cruz, California 95061

Prepared for
Ames Research Center
Under Contract NAS2-11946

AUGUST 1985

National Aeronautics and
Space Administration

Ames Research Center
Moffett Field, California 94035

## FOREWORD

This work was conducted for the National Aeronautics and Space Administration (NASA) through the Ames Research Center, Moffett Field, California, Dr. Peter Kittel, Program Manager.

The Lockheed Palo Alto Research Laboratory (LPARL) conducted the program within the Cryogenic Technology Group of the Thermal Sciences Laboratory, with Applied Computer Resources, Inc. (ACRI) support. Key individuals who contributed to this program are:

- D. Bushnell - developed DEWAR optimization program
- W. C. Henninger (ACRI) - predicted modal resonance
- S. A. Katz - performed modal resonance testing and reduced data
- I. Spradley - performed benefit study

R. T. Parmley
Principal Investigator

CONTENTS

## ILLUSTRATIONS

## ILLUSTRATIONS (Cont.)



## TABLES

# Section 1
# INTRODUCTION AND SUMMARY

## 1.1 INTRODUCTION

The Passive Orbital Disconnect Strut (PODS) support system was developed under contract NAS2-10848 (Refs. 1, 2, 3). Struts were analyzed, designed, fabricated, and tested structurally and thermally. Tests on a single strut included thermal conductance to helium temperature, thermal expansion data, loads to thermally short out the strut, ultimate loads, evacuation rates, and fatigue tests at liquid-nitrogen temperature. Load tests on a set of six struts included axial and side-load tests and the effect on strut shorting of simulated asymmetric temperatures of the vacuum shell.

The Task 1 modal resonance tests described in this report complete the test series on the PODS-III version of the strut. The Task 2 benefit study in this report addresses use of PODS-III supports on Orbit Transfer Vehicle (OTV) and Space Station (SS) liquid-oxygen and liquid-hydrogen tanks and compares PODS-III supports to other disconnect strut supports.

The PODS-III support is ready for use on flight dewars or other support applications. A new version of the strut (PODS-IV) with improved resistance to side loads is being developed on contract NAS2-11946, amendment 1. The PODS-IV support is the current selection for supporting the 1580-l superfluid helium tank on the Gravity Probe-B program. Other missions where the PODS supports may be used include SIRTF, LDR, OTVs, Space Station, and other NASA and DoD missions.

## 1.2 SUMMARY

The objectives of this program are: (1) to perform modal resonance testing of the PODS-III supports and compare the results to predicted values so that all engineering data required for use on flight systems are available; and (2) to determine possible performance improvements as compared to nondisconnect struts in large liquid-oxygen/liquid-hydrogen ($LO_2/LH_2$) tank space applications.

Task 1 - Modal Vibration Tests

Using the PODS-III supports and the dewar simulator developed under contract NAS2-10848, a modal resonance survey is performed on the set of six struts assembled in the dewar simulator. Survey conditions simulate launch and simulate orbital loadings of the struts. The orbital load range spans a full to an empty tank. The frequencies surveyed cover the range consistent with Space Transport System (STS) qualification requirements and the principal resonant modes of the strut system. The results of these tests are compared to predicted results based on strut dimensions and measured modulus values.

Task 2 - Benefit Study

The benefit of using PODS-III supports on OTV and Space Station $LO_2$ and $LH_2$ reference tanks is compared to using present state-of-the-art (SOTA) nondisconnect struts. These studies are performed on four different $LO_2$ and $LH_2$ tanks (1) holding the launch resonance at 35 Hz and varying the orbit resonance from 1 to 20 Hz, (2) analyzing both full and empty tanks at launch, (3) varying orbit boundary temperatures from 150 to 250 K, (4) varying the number of struts from 6 to 12, (5) varying orbit times up to 5 years, and (6) using or not using vapor cooling.

## Section 2
## PODS-III DESIGN CONCEPT

Figure 2-1 presents the PODS-III support concept. A minimum of six struts (three pairs) is required to support a cryogen tank. (Six struts provide a statically determinate support system in all axes.) As the tank diameter changes due to cooldown or pressurization, the angled pinned-end struts are free to move in and out as the tank moves up or down slightly a value of H. A similar adjustment occurs automatically as the vacuum shell changes diameter in orbit due to temperature changes.

For purposes of installation, the warm end of the strut provides a length adjustment feature. The threads on the rod-end fitting and length adjustment are a different pitch; consequenty, by rotating the adjustment hex, precise length adjustments can be made during strut installation without rotating the strut. This feature allows length adjustments after the vapor-cooled shields are attached to the struts.

The cold end of the strut provides the passive orbital disconnect feature. The cold rod end fitting/stem is connected to the body by a thin-wall fiberglass or graphite/epoxy orbit tube and adjustment bushing. The conical stem load-bearing surfaces are separated from the nut (tension) and body (compression) by an axial gap of ~0.076 mm (0.003 in.) at operating temperature. At ambient temperature, the gaps are set to take into account the differential shrinkage between the various parts. During one-g thermal test or orbital flight, the conical surfaces do not touch. Consequently, heat is transferred from the body to the thin-wall orbit tube/stem/rod end fitting subassembly by radiation and by conduction along the orbit tube.

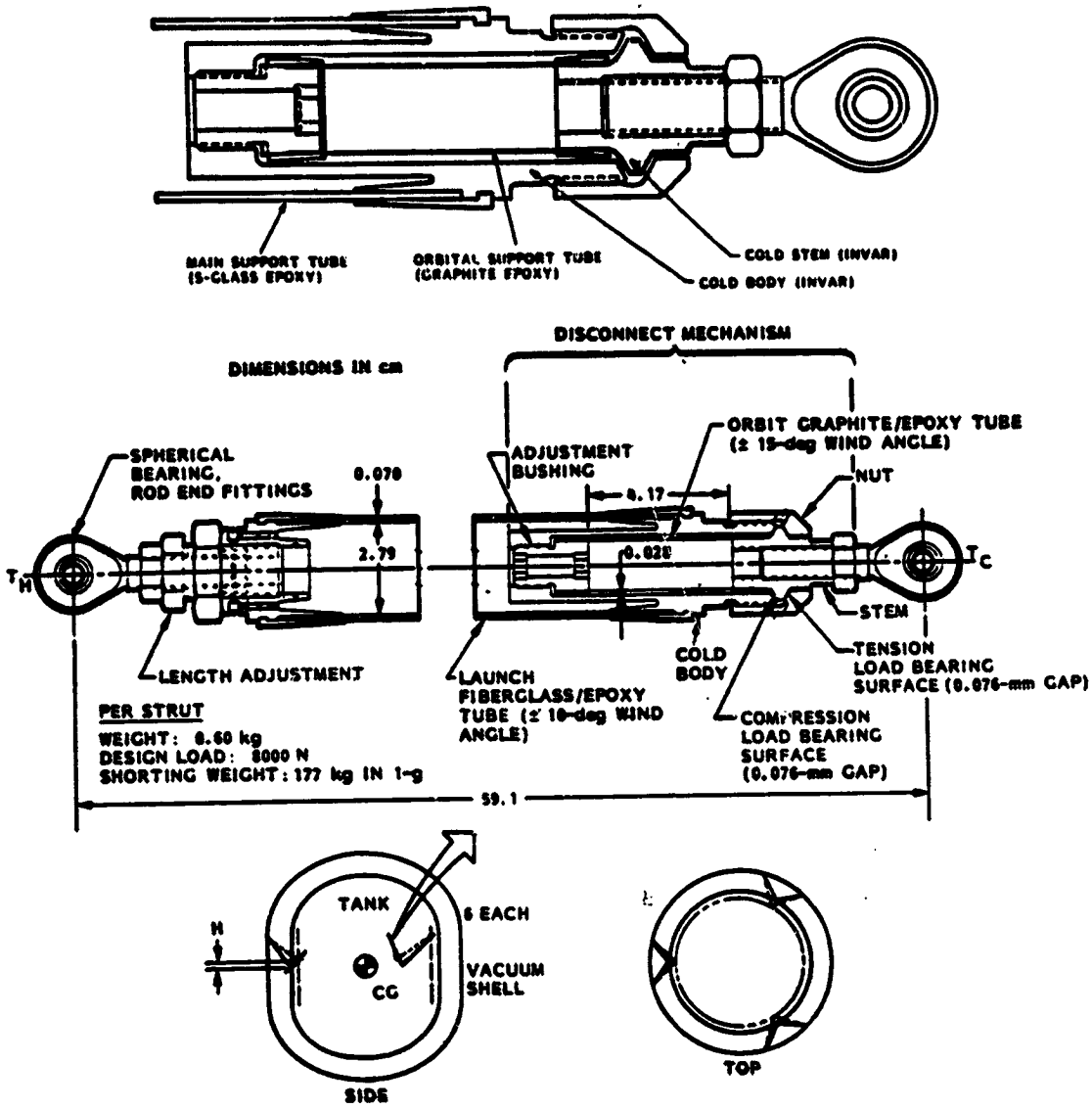


Fig. 2-1 PODS-III Support Concept

During launch, the g load elastically deforms the orbit tube along its axis; the conical shoulder of the stem rests hard on the body (compression) or nut (tension). The load path bypasses the orbit tube. The major thermal resistance and load path during launch is now the launch tube. Upon achieving orbit, the conical shoulder of the stem passively disconnects from the body or nut, and the major thermal resistance is again the thin-wall orbit tube.

This design combines the desirable features of a thermal disconnect during ground hold and orbit with the high reliability of a completely passive design. Since the struts do not short out in one-g, the orbital performance of the struts can be demonstrated in one-g thermal qualification tests and the ground hold heat leak is lower. These are both highly desirable features. Details of prior analyses, design, fabrication, and structural and thermal test results are provided in Refs. 1, 2, and 3.

## Section 3
## TASK 1 - MODAL VIBRATION TESTS

### 3.1 TEST ARTICLE AND SETUP

Figure 3-1 shows the PODS-III test article. Strut number six from Ref. 3 was instrumented for these tests. Table 3-1 provides measured characteristics of the strut.

A dewar simulator was designed so that simulated ground hold, launch, or orbit loads could be applied during the modal resonance tests. These include simulated loads from the weight of the tank, helium, vapor-cooled shields, and insulation.

The simulator was fabricated and installed in a three-post load machine as shown in Fig. 3-2. A 56-kg (123.5-lb) triangular aluminum plate and six adjustable clevis fittings simulate the aluminum tank attachments. Three aluminum blocks are attached to the three load posts. Six adjustable clevis fittings attached to the blocks simulate the vacuum shell attachments. The six struts are installed as shown at a 55-deg angle from the horizontal.

Axial compression or tension hydraulic loads were applied at the geometric center of the simulated tank through a load cell and large spherical bearing. For some tests, the weight of the simulated tank was taken off the struts by suspending the weight from a pinned clevis on the top center of the triangular aluminum plate. All struts were electrically wired using six light bulbs and a power supply to indicate when each strut shorted under load.

Triaxial accelerometers were mounted to a steel block which in turn was mounted to a steel hose clamp (Fig. 3-2). The clamp was mounted on the PODS-III fiberglass tube at different locations during the tests. To ensure that the clamp contributed no spurious frequency responses, the triaxial

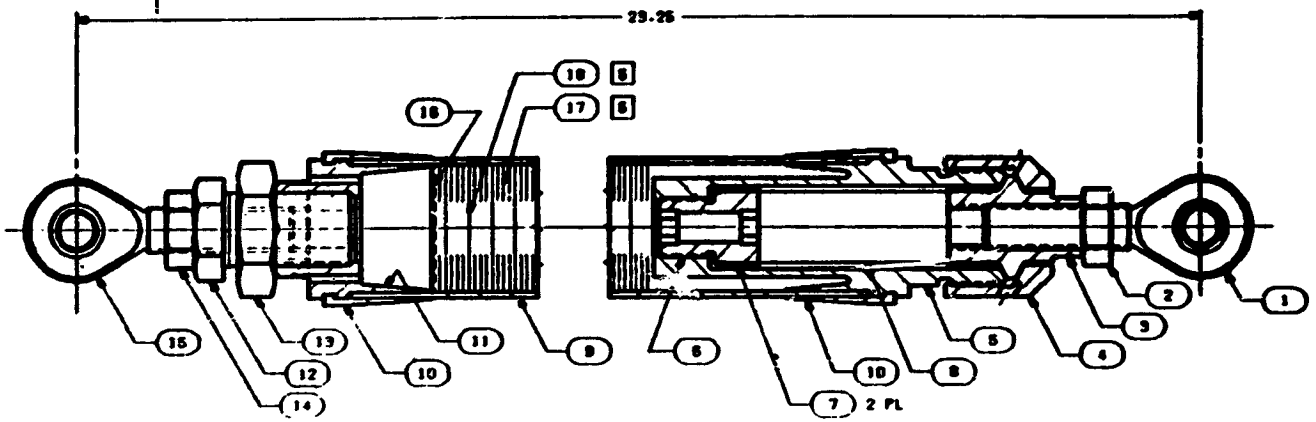


| | | | | | | | |
|---|---|---|---|---|---|---|---|
| 204 | | SFH-208-001 | RADM SHIELD | | | | 19 |
| 1858 | | SFH-208-009 | SPACER | | | | 17 |
| 1 | | SFH-208-005 | SPACER | | | | 18 |
| 1 | 81378 | 2SREA-SA-009 | ROD END.WARM | SOUTHWEST PRODUCTS CO. | HOUSTON,TX 81018 | | 15 |
| 1 | 08887 | LSB819-6 | JAM NUT | | | | 14 |
| 1 | | SFH-179-001 | JAM NUT | | | | 13 |
| 1 | | SFH-170-001 | LENGTH ADJ. | | | | 12 |
| 1 | | SFH-168-001 | BODY.WARM END | | | | 11 |
| 2 | | SFH-171-001 | CLAMSHELL.LGE | | | | 10 |
| 1 | | SFH-183-001 | LARGE TUBE | | | | 9 |
| 1 | | SFH-184-001 | SMALL TUBE | | | | 9 |
| 2 | | SFH-172-001 | CLAMSHELL.SM | | | | 7 |
| - | | SFH-189-001 | ADJ. BUSHING | | | | 5 |
| 1 | | SFH-185-001 | BODY.COLD END | | | | 5 |
| 1 | | SFH-188-001 | NUT | | | | 4 |
| 1 | | SFH-187-001 | STEM | | | | 3 |
| 1 | | -8819L6 | JAM NUT | | | | 2 |
| 1 | 813 | FLH-SA-008 | ROD END.COLD | SOUTHWEST PRODUCTS CO. | HOUSTON,TX 81018 | | 1 |
| QTY REQD | CODE IDENT. | PART OR IDENTIFYING NO. | DESCRIPTION | MATERIAL SPECIFICATION NO. OR SIZE | MANUFACTURER'S NAME AND ADDRESS | ZONE | ITEM NO. |

-501 PARTS LIST

SUPPORT STRUT

SFH-100 -501 NEXT ASSY | USED ON

SFH COOLER USED ON

0 | 17077 | SFH-107

NOTES:

1. CLEAN PER SPEC LAC 0170.
2. PROTECT PER SPEC LAC 1001.
3. IDENTIFY PER SPEC LAC 3575-011998.
4. ASSEMBLE PER SPEC SFH-500.
5. ACTUAL NUMBER OF ITEMS 17 & 18 SHOWN ARE OMITTED FOR CLARITY.

Fig. 3-1 PODS-III Support Strut Assembly

Table 3-1 CHARACTERISTICS OF PODS-III STRUT NO. 6

Length, rod end to rod end centers: 0.5907 m (23.256 in.)

Fiberglass Tube

- Unsupported Length: 0.422 m (16.60 in.)
- ID: 0.02799 m (1.1018 in.)
- OD: 0.02938 m (1.1566 in.)
- Cross Sectional Area: $6.27 \times 10^{-5}$ $m^2$ (0.0972 $in.^2$)
- Modulus: $5.4 \times 10^{10}$ $N/m^2$ ($7.8 \times 10^6$ psi)

Graphite Tube

- Unsupported Length: 0.0417 m (1.64 in.)
- ID: 0.01524 m (0.600 in.)
- OD: 0.01582 m (0.623 in.)
- Cross Sectional Area: $1.45 \times 10^{-5}$ $m^2$ (0.0221 $in.^2$)
- Modulus: $10.8 \times 10^{10}$ $N/m^2$ ($15.7 \times 10^6$ psi)

Weight (Fig. 3-1)

| Item No. | | g | Item No. | | g |
|---|---|---|---|---|---|
| 1 | Rod End, Cold | 42.5 | 10 | Clamshell, Large | 21.0 (ea) |
| 2 | Jam Nut | 3.6 | 11 | Body, Warm End | 64.4 |
| 3 | Stem | 33.0 | 12 | Length Adj. | 39.7 |
| 4 | Nut | 60.0 | 13 | Jam Nut | 21.7 |
| 5 | Body, Cold End | 148.3 | 14 | Jam Nut | 3.6 |
| 6 | Adj. Bushing | 19.2 | 15 | Rod End, Warm | 42.5 |
| 7 | Clamshell, Small | 1.8 (ea) | 16 | Spacer | 0.1 |
| 8 | Small Tube (Graphite) | 1.1 | 17 | Spacer | 16.2 |
| | | | 18 | Radiation Shield | 1.1 |
| 9 | Large Tube (Fiberglass) | 58.0 | | | 600.6 |

accelerometer block was also mounted directly to the PODS-III end fittings with beeswax in a separate test. A comparison of the data showed the clamp had no effect on the frequency response of the strut. Data were acquired and

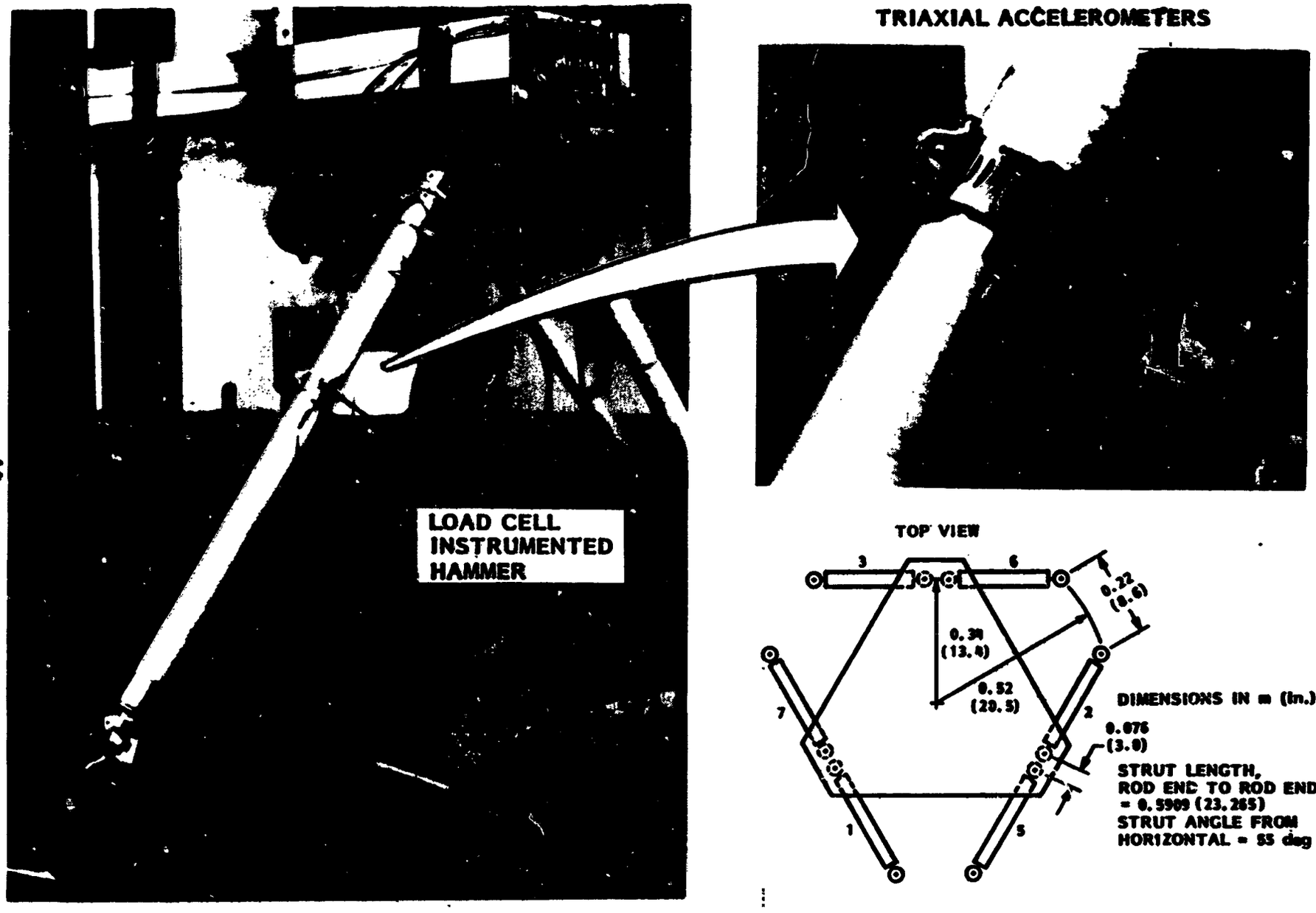


Fig. 3-2 Dewar Simulator With PODS-III Strut No. 6 Instrumented for Modal Resonance Tests

analyzed using a GENRAD 2515 Dynamic Data Analyzer and a load cell instrumented hammer/tap test technique.

## 3.2 TEST PROCEDURE

The triaxial accelerometers were mounted to the hex jam nut (item 13, Fig. 3-1) with beeswax. The strut was tapped on the length adjustment (item 12, Fig. 3-1) with the load cell instrumented hammer while different axial loads were applied to the struts (Fig. 3-3). The traixial accelerometer was then attached to the steel clamp, and the clamp was attached to the fiberglass tubes in one of six locations (Fig. 3-4). Different loads were applied to the struts (Table 3-2), and the strut shorting was monitored with the light bulbs.

Each of the eight modal tests was repeated six times with the triaxial accelerometers moved to the six locations shown in Fig. 3-4. The excitation was performed using the load cell instrumented hammer. The X-axis was the axis of excitation. The point of hammer impact was the hex face of the jam nut (item 13, Fig. 3-1) below accelerometer locations 1 and 2.

Modal data were analyzed on the GENRAD 2515. Since the structure tested was a simple cylindrical shape, the computer model used to describe its modal dynamics was a rectangle formed by the bisecting Y-axis plane of the strut about which the accelerometer locations were placed. Figure 3-4 (as-analyzed diagram) describes the computer model. The accelerometer locations and axial orientation of both the "as-tested" and the "as-analyzed" configurations are identical.

## 3.3 TEST RESULTS

The modal analysis revealed two types of fundamental modes: column bending and strut torsion. In a few cases a complex mode consisting of a combination of both bending and torsion was seen. The dynamic modes and associated fundamental frequencies and damping coefficients are summarized in Table 3-3 and plotted in Fig. 3-5.

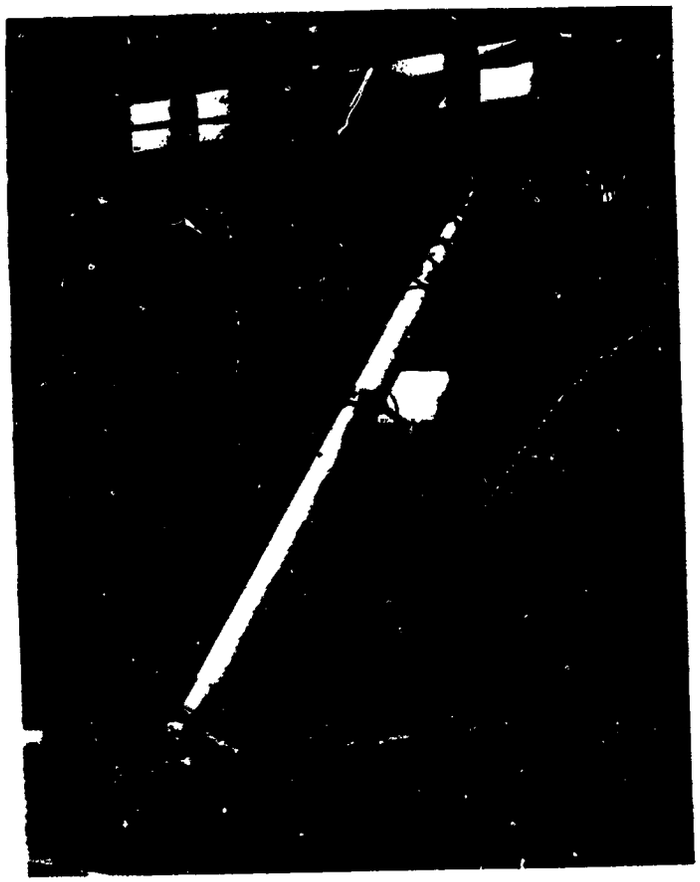

Fig. 3-3 Strut Excitation

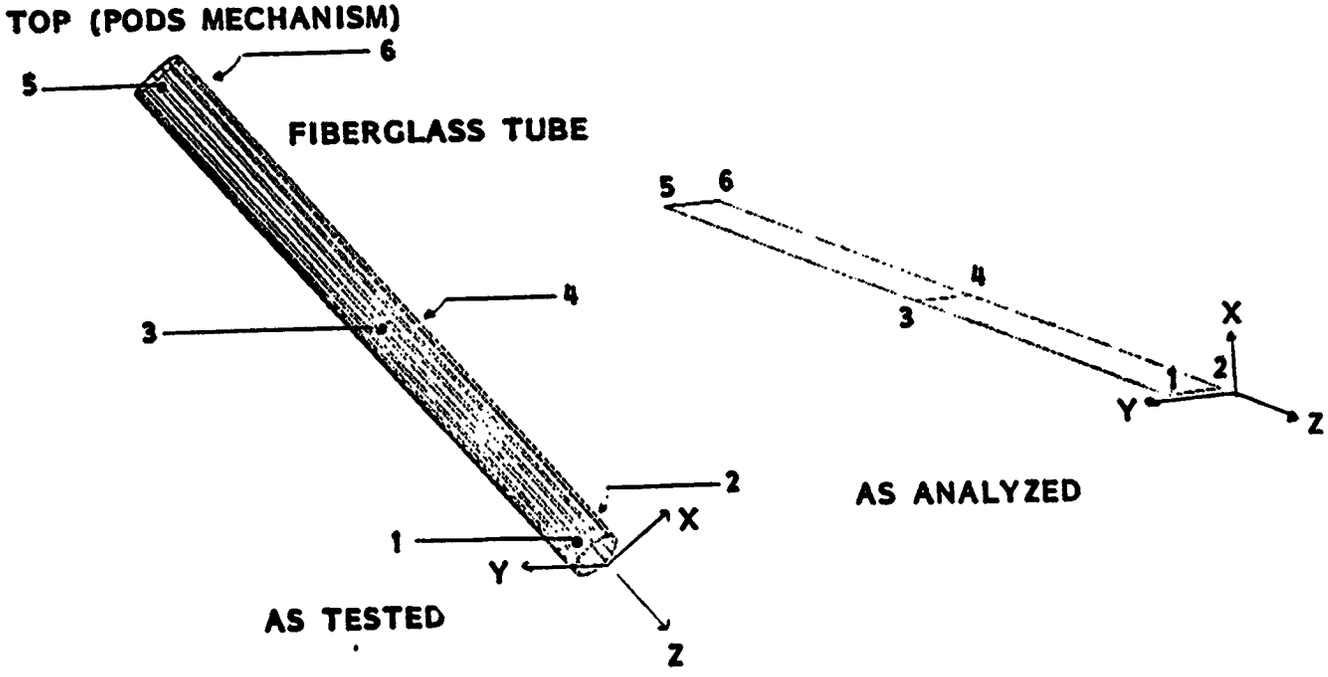


Fig. 3-4 Accelerometer Locations

Table 3-2 LOAD CASES TESTED

| Test No. | Load Direction: C-Compression T-Tension | Load On On All Six Struts N ($lb_f$) | Strut: Shorted-S NonShorted-NS | Simulates: Ground Hold (GH) Orbit (O) Launch (L) |
|---|---|---|---|---|
| 1 | -- | 0 | NS | O |
| 2 | T | 8,896 (2000) | NS | GH |
| 3 | T | 17,792 (4000) | S | L |
| 4 | T | 35,584 (8000) | S | L |
| 5 | C | 549 (123.5) | NS | GH |
| 6 | C | 2,224 (500) | NS | GH |
| 7 | C | 8,896 (2000) | S | L |
| 8 | C | 35,584 (8000) | S | L |

In Fig. 3-5, the lowest fundamental frequency is plotted versus the square root of the applied axial load. There appears to be a slight step change in slope between the shorted and nonshorted cases.

Mode shape estimations were performed in reference to the center accelerometer locations (3 and 4). All other location responses were integrated into the modal models. To develop a high degree of confidence in the computer modal model estimations, admittance function phase data were examined. Accelerometer location sets (i.e., 1&2, 3&4, 5&6) were at the same longitudinal location on the strut but were rotated 180 deg. Consequently, the clamp/accelerometer assembly was merely rotated 180 deg to accommodate the opposite set location. This did not effect Z-axis measurements; however X- and Y-axis measurements of opposite locations were 180 deg out of phase. Figure 3-6 illustrates this. These are admittance function plots of locations 3 and 4 in the X-axis (the upper plot is location 4 in the X- direction, the

Table 3-3 MODAL TEST RESULTS

| Test No. (Table 3-2) | Fundamental Freq. (Hz) | Damping Coeff. | Mode Dynamics |
|---|---|---|---|
| 1 | 99.8 | 0.02183 | Primary Bending |
| | 222.5 | 0.01491 | Primary Bending |
| 2 | 142.4 | 0.02401 | Primary Bending |
| | 254.0 | 0.00756 | Primary Bending |
| | 483.3 | 0.00940 | Primary Torsional |
| 3 | 174.8 | 0.03657 | Primary Bending |
| | 449.6 | 0.01062 | Primary Bending |
| | 474.1 | 0.02748 | Primary Torsional |
| 4 | 194.9 | 0.01226 | Primary Bending |
| | 459.1 | 0.00706 | Primary Bending |
| | 462.2 | 0.00069 | Primary Torsional |
| | 482.2 | 0.00731 | Primary Bending |
| 5 | 125.2 | 0.01450 | Primary Bending |
| | 137.6 | 0.01782 | Primary Bending |
| | 423.5 | 0.02618 | Complex Bending/Torsional |
| | 454.1 | 0.00869 | Complex Bending/Torsional |
| 6 | 111.9 | 0.01352 | Primary Bending |
| | 120.4 | 0.04342 | Primary Bending |
| | 222.1 | 0.09968 | Complex Bending/Torsional |
| 7 | 132.9 | 0.09755 | Primary Bending |
| | 148.9 | 0.00612 | Primary Bending |
| | 428.0 | 0.03669 | Primary Torsional |
| 8 | 124.5 | 0.01602 | Primary Bending |
| | 137.3 | 0.01117 | Primary Bending |
| | 422.9 | 0.03585 | Primary Torsional |

Cautionary Note: During tests 1 and 5, the strut tended to "rattle" on its mountings when dynamically excited, so the associated data contain some uncertainty.

lower plot is location 3 in the X+ direction). Comparing the phase angles (accelerometer direction) at the circled fundamental frequencies reveals that accelerometers are 180 deg out of phase. Since the accelerometers are physically 180 deg out of phase, simultaneous motion of the two accelerometers

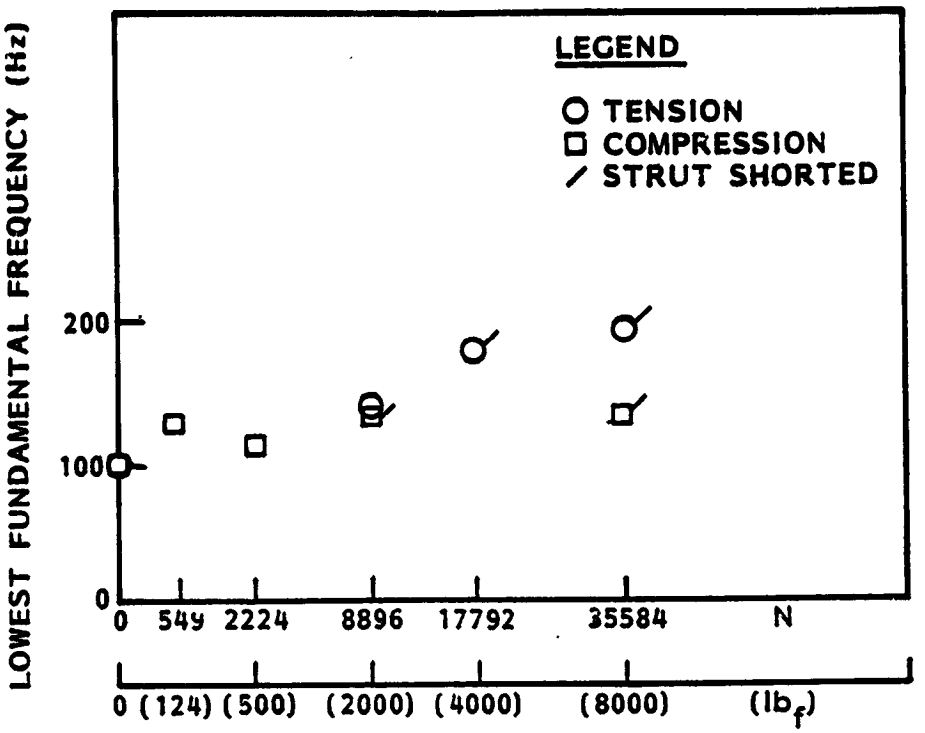


Fig. 3-5 Modal Test Results

in the same direction is indicated, and the associated mode is bending. Conversely, if the phase angles are the same, simultaneous opposite motion occurs, indicating a torsional mode.

Admittance functions in the Y- and Z-axes were also examined to determine any off-axis fundamental modes. No such modes were found. Appendix A presents admittance functions for all of the static loadings at locations 3X+, 4X-, 5X+, 3Y+, and 3Z-.

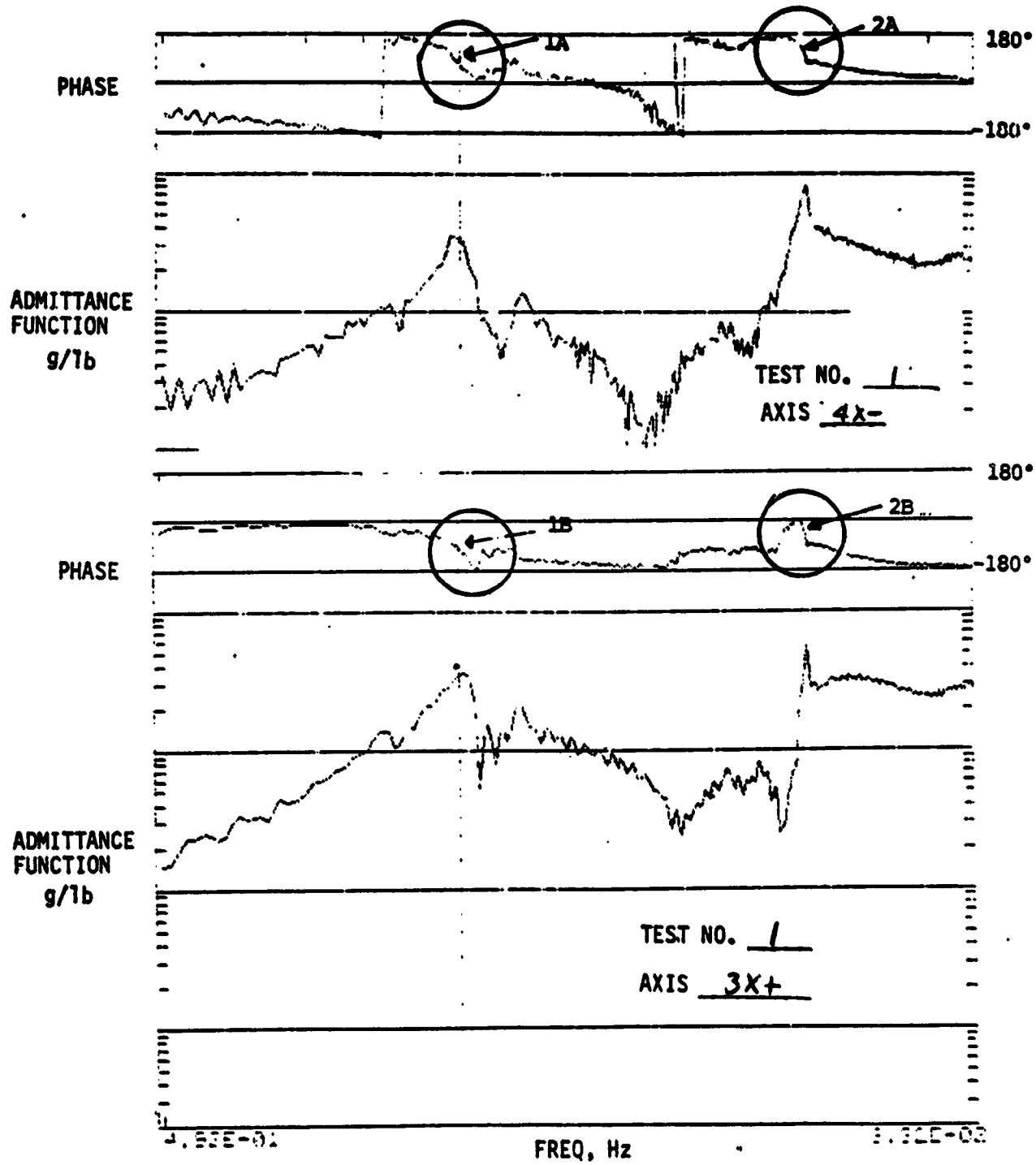


Fig. 3-6 Mode Phasing Comparison

## 3.4 PREDICTED TEST RESULTS

### 3.4.1 Model Used

Finite element analysis (FEA) models of the PODS-III test article were developed using Lockheed's ASTRO computer program (Ref. 9). Initial analyses for all preload cases tested revealed that the strut's fundamental mode did not include any participation of the 56-kg (123.5-lb) triangular plate; hence, for the analyses reported herein, the FEA models represent a single PODS-III strut.

Two versions of the strut model were developed. The first version, depicted in Fig. 3-7, simulates the strut's test configuration by incorporating the lumped weight of the triaxial accelerometer assembly (17.5 g) and the hose clamp (27.4 g). Since the accelerometer/clamp-assembly weight equaled 85 percent of the fiberglass tube's unsupported weight, it was necessary to add this weight to obtain frequency results that compare with the test data. As in the tests, the location of the accelerometer/clamp assembly was varied. The averaged frequency results determine the strut's fundamental frequency for each preload case. The second version, depicted in Fig. 3-8, simulates the strut's as-built configuration.

The strut FEA models consisted of eight beam elements as shown in Figs. 3-7 and 3-8. The center four elements represent the strut's unsupported fiberglass tube length with properties as summarized in Table 3-1. The end beam element was employed to simulate the orbit and ground-hold (open gap) and launch (closed gap) configurations. Rigid elements used to offset the accelerometer and clamp weights are shown in Fig. 3-7. The weight of the fiberglass tube was evenly distributed over the five intermediate nodes and other strut-end item weights (Table 3-1) were lumped at the tube's end nodes, with half the weight lumped to ground.

As noted, the model's end beam element was used to simulate orbit and launch models. The orbit model, due to its increased flexibility, was tuned by

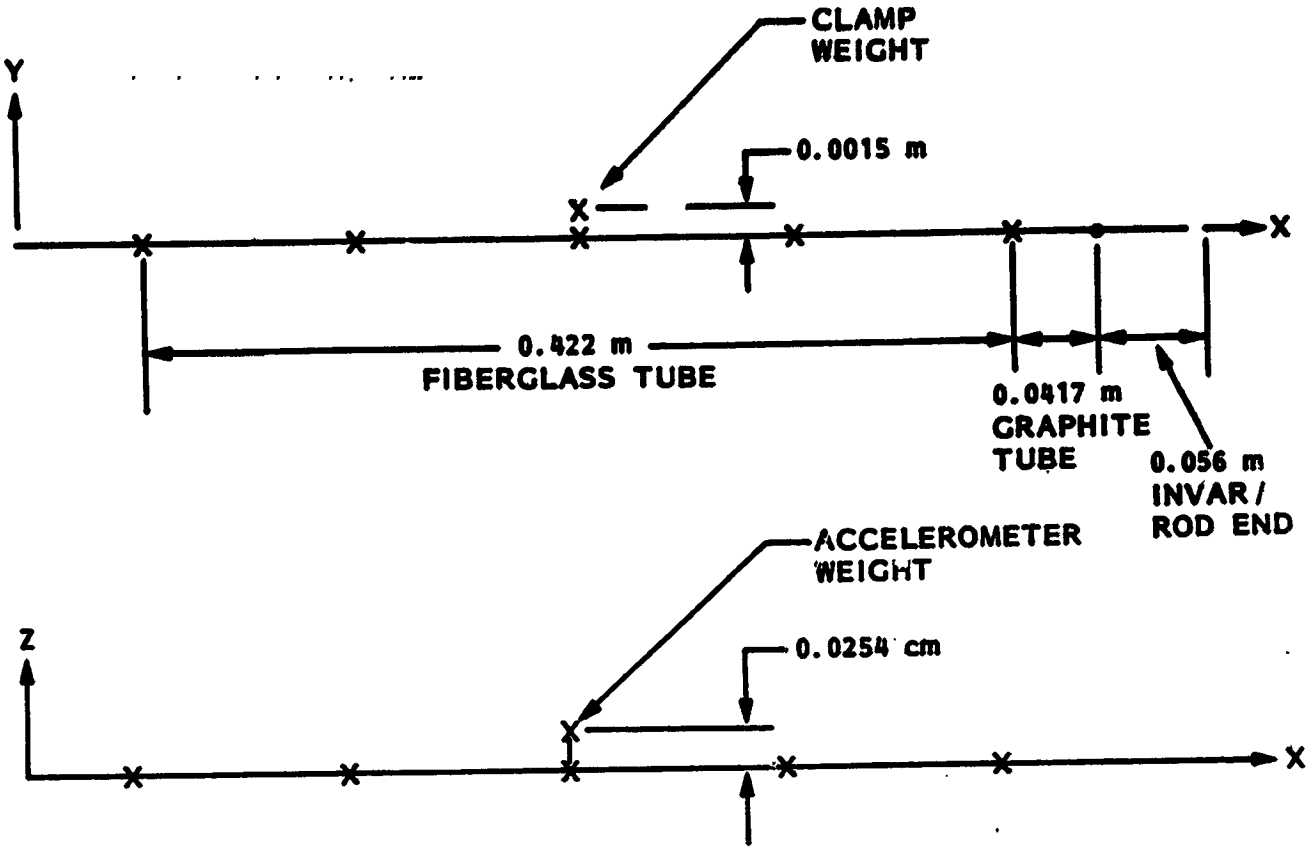


Fig. 3-7 Strut Model With Accelerometers and Clamp

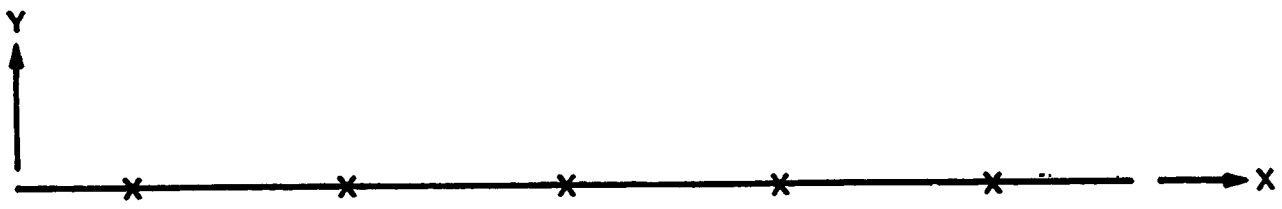


Fig. 3-8 Strut Model Without Accelerometer

adjusting the end beam's stiffness to agree with results of Test 2 and then analyzed for the other relevant preload conditions. The launch model end members were simulated by rigid beam elements to reflect the additional stiffness of the strut while in this configuration.

### 3.4.2 Predicted Versus Test Results

The goal of the analyses summarized herein was to define and analyze an analytical model and to compare the model's fundamental frequency with that obtained experimentally. Table 3-4 summarizes the analyses performed for the test and as-built FEA models. In general, the launch model test configuration frequencies compare very well with test results for all cases except Test 8. Orbit and ground-hold model test simulation results demonstrate frequencies substantially higher than determined by test, except for Test 2 for which the analytical model was tuned. As-built simulation-model frequencies are consistently higher due to removal of the accelerometer/clamp lumped weight.

Table 3-4 MODEL ANALYSIS VERSUS TEST RESULTS

| Test No. | Test Results | Test Simulation (With Accelerometers) | As-Built Simulation (Without Accelerometers) | Model Configuration |
|---|---|---|---|---|
| 1 | 99.8 | 130.1 | 142.5 | Orbit |
| 2 | 142.4 | 141.1 | 154.4 | Ground Hold |
| 3 | 174.8 | 172.6 | 192.3 | Launch |
| 4 | 194.9 | 193.5 | 215.4 | Launch |
| 5 | 125.2 | 129.4 | 141.7 | Ground Hold |
| 6 | 111.9 | 126.3 | 138.3 | Ground Hold |
| 7 | 132.9 | 134.8 | 150.2 | Launch |
| 8 | 124.5 | 79.4 | 88.5 | Launch |

# Section 4
# TASK 2 - BENEFIT STUDY

To determine the benefit of using PODS-III supports, reference $LO_2$ and $LH_2$ tanks were established (Ref. 7) for both an OTV mission of 1 month or less and space station storage (SSS) tanks with storage times of up to 5 years. The PODS-III supports were compared with state-of-the-art (SOTA) fiberglass struts. An alternate SOTA support, tension bands, is heavier for supporting such large tanks due to the large structures required to react the tension loads. For smaller tanks, the vacuum shell reacts the support loads. For these large tanks, vacuum shells are too heavy. PODS and SOTA struts were optimized using the DEWAR optimization program for full tanks at STS launch, empty tanks at STS launch, 35-Hz launch resonance, and 1- to 20-Hz orbit resonances.

Four thermal models were set up for both PODS and SOTA supports with and without vapor cooling. These models included the supports, multilayer insulation (MLI), vapor-cooled shields where applicable, and fill and vent lines. The optimized dimensions of the supports for the different cases were input into the thermal models and run for hot boundary temperatures of 150, 200, and 250 K, vapor cooling or no vapor cooling for the SSS tanks and no vapor cooling for the OTV tanks, and storage times up to 1 month for the OTV tanks and 5 years for the SSS tanks. These total heat loads to the tanks were then used as the basis for the support evaluation and recommendations. Table 4-1 summarizes the parameters that were used in the study.

## 4.1 REFERENCE TANKS

The reference 2219 aluminum $LO_2$ and $LH_2$ tanks used in the study are shown in Fig. 4-1. The support-structure dimensions and tank dimensions were held constant and the strut angles were allowed to optimize. The MLI is double aluminized mylar/silk net with a degradation factor of 1.5. The tanks have

Table 4-1 PARAMETERS USED TO EVALUATE THF SUPPORTS

| Conditions Evaluated | OTV Tanks | SSS Tanks |
|---|---|---|
| Minimum launch Resonance | 35 Hz | 35 Hz |
| Minimum Orbit Resonance | 5 to 20 Hz | 1 to 20 Hz |
| Initial Launch Condition | Full/Empty | Full/Empty |
| Hot Boundary Temperature Range | 150 to 250 K | 150 to 250 K |
| Struts | 6-12 | 6-12 |
| Orbit Times | Up to 1 month | Up to 5 years |
| Vapor-Cooled Shields | Without | With/Without |

titanium fill and vent lines with approximately one-half the conductivity of stainless steel, aluminum vapor-cooled shields (SSS tanks only where applicable), and purge bag plus plumbing components if launched with cryogen. A summary of the launch weights for both full and empty tanks is provided in Table 4-2. The weights were calculated using the factors shown in Table 4-3. The SSS $LO_2$ tank is only partially loaded in the "full" column due to STS launch constraints of ~28,000 kg (62,000 lb). These weights are used in the DEWAR optimization program to size the supports.

## 4.2 SUPPORT OPTIMIZATION

### 4.2.1 Support Optimization Program (DEWAR)

The objective of this support thermal/structural optimization program is to minimize the flow of heat from the outer structure to which the struts are attached. In addition, enough structural rigidity must be maintained to keep the lowest frequencies at launch and during orbital conditions above certain specified values, and stresses due to assembly and launch loads must be kept below those that would cause buckling or material failure.

In the analysis, the outer structure and the tank to which it is attached are assumed to be rigid, and the supports are assumed to be massless. For more detailed calculations, the rigidity of the structure and tank and support mass

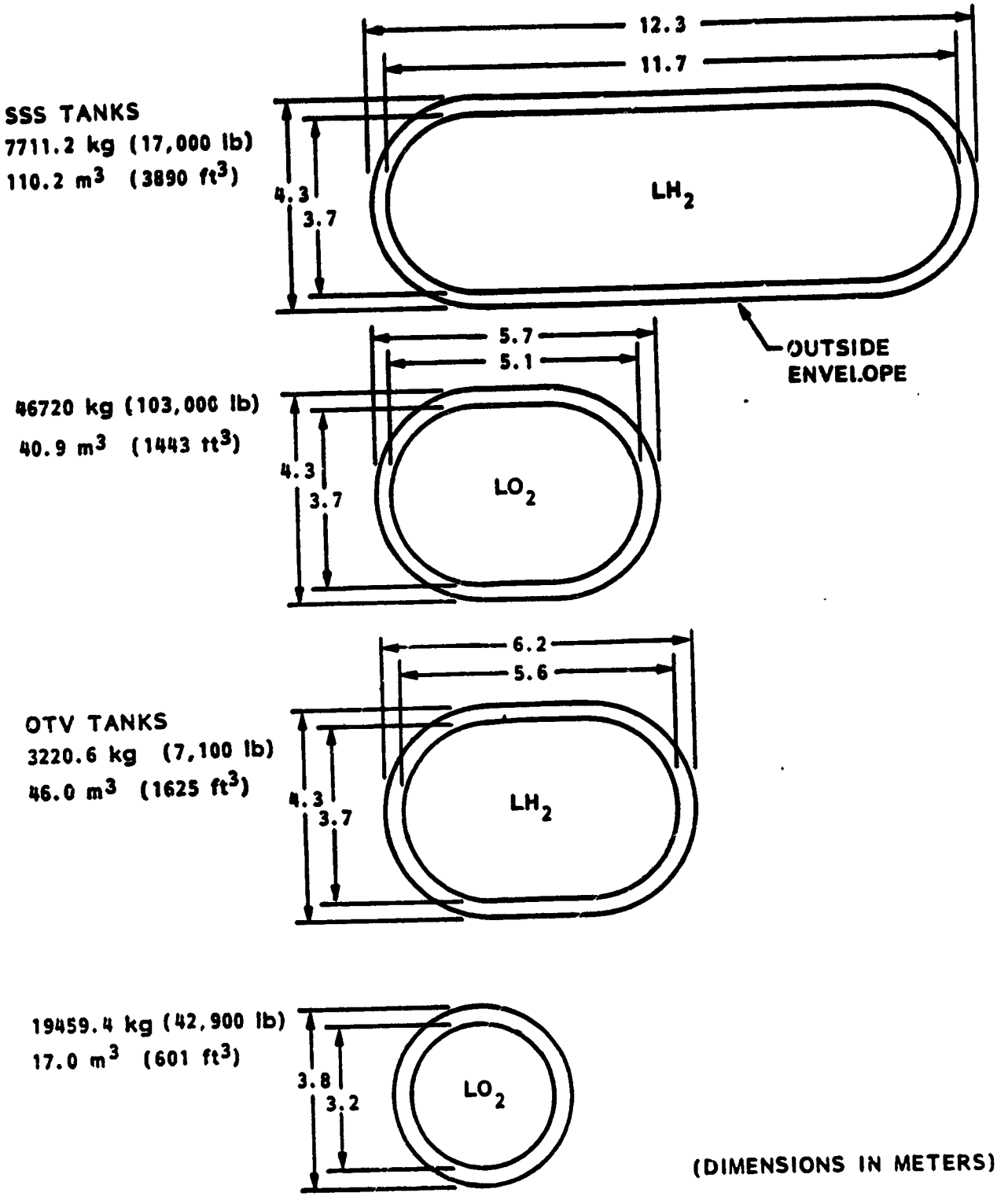


Fig. 4-1 Cryogen Tank Characteristics

## Table 4-2 TANK LAUNCH WEIGHTS

| Tank Components | | OTV $LO_2$ Tank | | OTV $LH_2$ Tank | | SSS $LO_2$ Tank | | SSS $LH_2$ Tank | | SSS $LO_2$ Tank with Vapor-Cooled Shields | | SSS $LH_2$ Tank with Vapor-Cooled Shieds | |
|---|---|---|---|---|---|---|---|---|---|---|---|---|---|
| | | 1.8-cm MLI Thickness | | 5.1-cm MLI Thickness | | 3.8-cm MLI Thickness | | 12.7-cm MLI Thickness | | 3.8-cm MLI Thickness | | 12.7-cm MLI Thickness | |
| | | Full 12 Struts | Empty 6 Struts | Full 12 Struts | Empty 6 Struts | Full 12 Struts | Empty 6 Struts | Full 12 Struts | Empty 12 Struts | Full 12 Struts | Empty 6 Struts | Full 12 Struts | Empty 12 Struts |
| Cryogen | kg | 19459.4 | 0 | 3220.6 | 0 | 27216.0* | 0 | 7711.2 | 0 | 27216.0 | 0 | 7711.2 | 0 |
| | (lb) | (42,900) | (0) | (7,100) | (0) | (60,000) | (0) | (17,000) | (0) | (60,000) | (0) | (17,000) | (0) |
| Tank | kg | 233.6 | 233.6 | 676.3 | 676.3 | 560.6 | 560.6 | 1619.4 | 1619.4 | 560.6 | 560.6 | 1619.4 | 1619.4 |
| | (lb) | (515) | (515) | (1491) | (1491) | (1236) | (1236) | (3570) | (3570) | (1236) | (1236) | (3570) | (3570) |
| MLI (DAM/ Silk Net) | kg | 17.7 | 17.7 | 103.0 | 103.0 | 70.3 | 70.3 | 549.8 | 549.8 | 70.3 | 70.3 | 549.8 | 549.8 |
| | (lb) | (39) | (39) | (227) | (227) | (155) | (155) | (1212) | (1212) | (155) | (155) | (1212) | (1212) |
| Vapor-Cooled Shields | kg | 0 | 0 | 0 | 0 | 0 | 0 | 0 | 0 | 174.6 | 174.6 | 406.0 | 406.0 |
| | (lb) | (0) | (0) | (0) | (0) | (0) | (0) | (0) | (0) | (385) | (385) | (895) | (895) |
| Fill/Vent Plumbing | kg | 68.0 | 68.0 | 90.7 | 90.7 | 68.0 | 68.0 | 90.7 | 90.7 | 68.0 | 68.0 | 90.7 | 90.7 |
| | (lb) | (150) | (150) | (200) | (200) | (150) | (150) | (200) | (200) | (150) | (150) | (200) | (200) |
| Purge Bag | kg | 15.9 | 0 | 33.1 | 0 | 29.9 | 0 | 71.7 | 0 | 29.9 | 0 | 71.7 | 0 |
| | (lb) | (35) | (0) | (73) | (0) | (66) | (0) | (158) | (0) | (66) | (0) | (158) | (0) |
| Purge Plumbing (Tank + $GN_2$) | kg | 13.6 | 0 | 0 | 0 | 36.3 | 0 | 0 | 0 | 36.3 | 0 | 0 | 0 |
| | (lb) | (30) | (0) | (0) | (0) | (80) | (0) | (0) | (0) | (80) | (0) | (0) | (0) |
| Purge Plumbing (Tank + GHe) | kg | 0 | 0 | 39.5 | 0 | 0 | 0 | 205.9 | 0 | 0 | 0 | 205.9 | 0 |
| | (lb) | (0) | (0) | (87) | (0) | (0) | (0) | (454) | (0) | (0) | (0) | (454) | (0) |
| Total | kg | 19808.3 | 319.3 | 4163.1 | 870.0 | 27981.2 | 699.0 | 10248.6 | 2259.8 | 28155.9* | 873.6 | 10654.6 | 2665.8 |
| | (lb) | (43,669) | (704) | (9178) | (1918) | (61687) | (1541) | (22594) | (4982) | (62072) | (1926) | (23489) | (5877) |

*Maximum load due to Orbiter limitations.

Table 4-3 FACTORS USED TO CALCULATE WEIGHTS

| Item | $LO_2$ | $LH_2$ |
|---|---|---|
| Tanks | $\frac{0.012\text{-kg tank}}{1\text{ kg }LO_2}$ | $\frac{0.21\text{-kg tank}}{1\text{ kg }LH_2}$ |
| MLI<br>$\rho$ = 30.8 kg/m$^3$<br>(1.92 lb/ft$^3$) | 1.8 cm (OTV) (Ref. 8)<br>3.8 cm (SSS) (Ref. 7)<br>(Thicknesses set based on study results of other programs.) | 5.1 cm (OTV) (Ref. 8)<br>12.7 cm (SSS) (Ref. 7) |
| Vapor-Cooled Shields | 0.98 kg/m$^2$ (0.20 lb/ft$^2$) | 0.98 kg/m$^2$ (0.20 lb/ft$^2$) |
| Plumbing | 68 kg (150 lb) | 91 kg (200 lb) |
| Purge Bag | 0.5 kg/m$^2$ (0.1 lb/ft$^2$) | 0.5 kg/m$^2$ (0.1 lb/ft$^2$) |
| Purge Plumbing | High-pressure $GN_2$ bottle sized for 5 volume changes plus plumbing | High-pressure GHe bottle sized for 5 volume changes plus plumbing |

should be accounted for. It is also assumed that the vapor-cooled shields and insulation are rigid, supported by elastic struts which carry loads only along their axes (pinned ends).

In the PODS concept, the effective axial stiffness $(EA/L)_{eff}$ and heat flow conductance $(KA/L)_{eff}$ change abruptly from the launch condition to the orbital conditions due to a "disconnect" feature within each strut, so the design of each of these support systems involves solving of two optimization problems, one corresponding to the launch phase and the other corresponding to the orbital phase. The SOTA support strut involves solving one optimization problem corresponding to the launch condition only, since the nature of this support system does not change for the orbital phase and the launch phase represents the more severe environment.

The program inputs include: (1) weights and dimensions of the insulated tanks, (2) quasistatic and dynamic acceleration g-factors, (3) launch and

orbital frequency constraints, (4) Young's modulus and the maximum allowable stress of the fiberglass or graphite tubes, and (5) thermal conductivity of the tubes. Program outputs include: (1) center of gravity locations and polar and tilting moments of inertia of the supported tanks; (2) design margins at launch of maximum stress, tube column (Euler) buckling, and tube shell (local) buckling; (3) strut length and diameter, strut spacing and angles, and cross-sectional area and wall thickness of the launch tube; (4) launch and orbital frequency margins in lateral, tilt, axial, and torsional modes; and (5) the axial length and cross-sectional area of the orbit tube for the PODS support.

Optimization is carried out by a nonlinear programming algorithm called CONMIN (Refs. 4,5). This program, written by Vanderplaats in the early 1970s, is based on a nonlinear constrained search algorithm due to Zoutendijk (Ref. 6). The basic analytic technique used in CONMIN is to minimize an objective function (e.g., heat flow) until one or more constraints, in this case vibration frequencies, buckling loads, maximum stress or strain, and upper and lower bounds on design variables, become active. The minimization process then continues by following the constraint boundaries in design variable space in a direction such that the value of the objective function continues to decrease. When a point is reached such that no further decrease in the objective function is obtained, the process is terminated.

### 4.2.2. DEWAR Inputs and Constraints

Figure 4-2 provides criteria for selecting the appropriate composite for the PODS-III "orbit" tube on the $LH_2$ tank. Both thermal conductivity (k) and modulus (E) values affect the choice. The lower the k and the higher the E (lowest k/E ratio), the more desirable the choice. The modulus affects the spring rate (K) and consequently the resonance value ($\Omega$) of the supports ($\Omega \alpha \sqrt{K}$) plus the column buckling and local crippling strength. If constraints such as minimum wall gage are encountered during the optimization procedure, the modulus value cannot be used to full advantage.

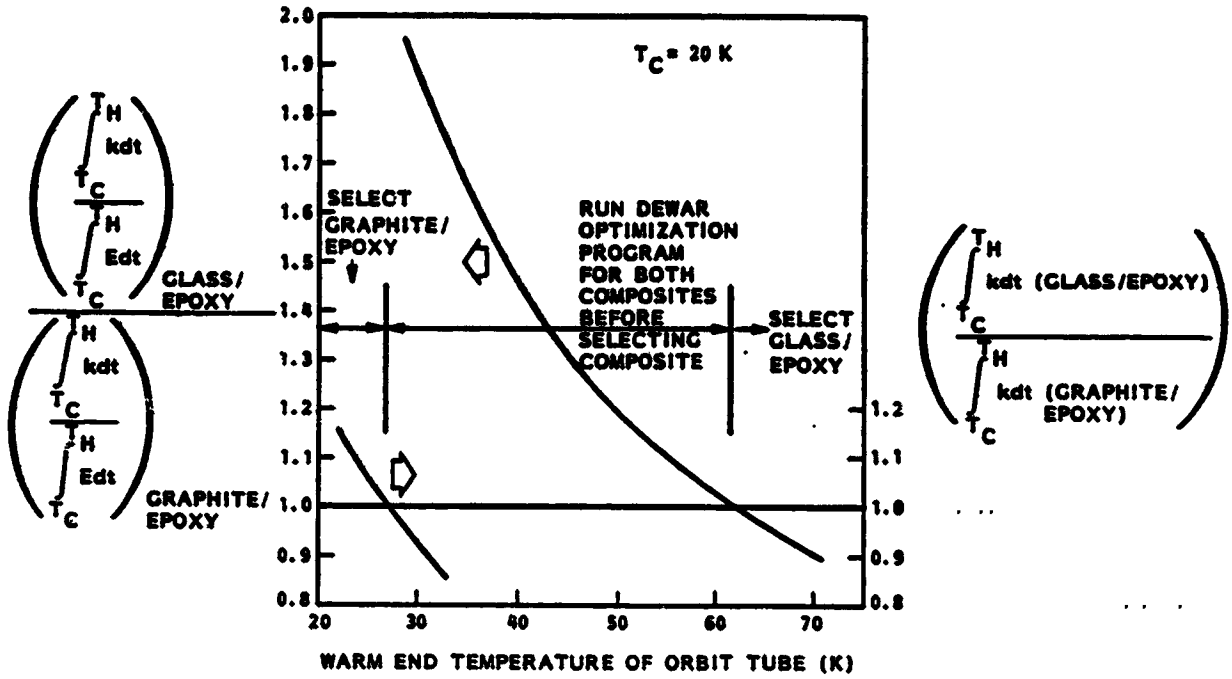


Fig. 4-2 Selection Criteria for Orbit Tube Composite

When the orbit tube warm-end temperature is below 27 K, the integrated thermal conductivity and k/E values of graphite/epoxy are below that of glass/epoxy (Fig. 4-2). Between 27 K and 61.5 K, the integrated k/E ratio of graphite/epoxy is below that of glass/epoxy but not the k value. Consequently, in this range the DEWAR optimization program must be run with both composites before a choice can be made.

Above 61.5 K, glass/epoxy is the optimum choice in all cases for the orbit tube on the $LH_2$ tank due to the lower k and k/E ratio. The optimum choice for the PODS-III launch tube on the $LH_2$ tank and the launch or orbit tubes for the $LO_2$ tank is fiberglass/epoxy due to the higher temperature ranges (90 K and higher) and higher graphite/epoxy conductivity.

For all analyses in this section, fiberglass/epoxy tubes were assumed for both cryogens and the launch or orbit tubes. (The minimum wall gage constraint was

exercised 12 out of 18 times for the $LH_2$ orbit tube as shown in Table 4-5.) If additional analyses were run on both composites in the 27- to 61.5-K range for the $LH_2$ tank, a graphite/epoxy orbit tube for the $LH_2$ tank may be optimum for some of the cases shown, providing additional performance improvement of the PODS-III support over the SOTA strut.

Table 4-4 presents inputs and constraints to the DEWAR program. The tank "density" values were calculated from the tank dimensions (Fig. 4-1) and tank weights (Table 4-2). The modulus value used was measured in Ref. 3. The maximum allowable stress is 22 percent of ultimate to allow for $10^5$ fatigue load cycles (Ref. 3, Fig. 2-6). The axial and lateral g loads were assumed to be equal for these calculations and are the sum of the STS quasistatic (3.17 g) and dynamic ($g = 204.5 \times W_s^{-0.5372}$) accelerations where $W_s$ is the supported weight in kilograms (Ref. 3, Fig. 6-4).

The minimum launch resonance was taken from Ref. 1. The orbit resonances were varied over a broad range to determine their impact on PODS-III performance. Minimum wall thicknesses were set based on manufacturing limitations. The outer diameter of the orbit tube is always smaller than the inner diameter of the launch tube due to the design of the PODS-III support.

### 4.2.3 DEWAR Results

Table 4-5 summarizes the DEWAR optimization results for the PODS-III supports. The SOTA strut dimensions were assumed to be the same as those of the PODS-III support (excluding the orbit tube).

## 4.3 THERMAL ANALYSES

Finite-element thermal models were developed using THERM and the reference tank data from Section 4.1 and the optimized support data from Section 4.2. The resulting heat rate data allowed a comparison between PODS-III supports and SOTA struts for a variety of different cases.

## Table 4-4 DEWAR INPUTS AND CONSTRAINTS

| Properties and Constraints | | OTV $LO_2$ Tanks | OTV $LH_2$ Tanks | SSS $LO_2$ Tanks | SSS $LH_2$ Tanks | SSS $LO_2$ Tanks with Vapor-Cooled Shields | SSS $LH_2$ Tanks with Vapor-Cooled Shields |
|---|---|---|---|---|---|---|---|
| Tank Density per 6 Struts, $kg/m^3$ ($lb/in.^3$) | Full | 1721.6 (0.0622) | 3731.1 (0.1348) | 2546.5 (0.0920) | 3670.2 (0.1326) | 2546.5 (0.0920) | 3670.2 (0.1326) |
| | Empty | 2460.7 (0.0889) | 3731.1 (0.1348) | 3349.2 (0.121) | 3670.2 (0.1326) | 3349.2 (0.121) | 3670.2 (0.1326) |
| Tank Content Density per 6 Struts, $kg/m^3$ ($lb/in.^3$) | Full | 1151.5 (0.0416) | 75.8 (0.00274) | 669.8 (0.0242) | 78.3 (0.00283) | 675.4 (0.0244) | 81.9 (0.00296) |
| | Empty | 5.0 (0.000182) | 4.2 (0.000122) | 3.4 (0.000122) | 5.8 (0.00021) | 7.7 (0.000277) | 9.5 (0.000343) |
| Young's Modulus of Fiberglass/ Epoxy Launch or Orbit Tube, kPa (psi) | | $5.4 \times 10^7$ ($7.8 \times 10^6$) | $5.4 \times 10^7$ ($7.8 \times 10^6$) | $5.4 \times 10^7$ ($7.8 \times 10^6$) | $5.4 \times 10^7$ ($7.8 \times 10^6$) | $5.4 \times 10^7$ ($7.8 \times 10^6$) | $5.4 \times 10^7$ ($7.8 \times 10^6$) |
| Maximum Allowable Stress in Fiberglass/Epoxy Launch or Orbit Tube, kPa (psi) | | $3.4 \times 10^5$ (50,000) | $3.4 \times 10^5$ (50,000) | $3.4 \times 10^5$ (50,0009) | $3.4 \times 10^5$ (50,000) | $3.4 \times 10^5$ (50,000) | $3.4 \times 10^5$ (50,000) |
| Axial or Lateral Loading,* g's | Full | 4.17 | 5.49 | 4.0 | 4.60 | 4.0 | 4.57 |
| | Empty | 12.39 | 8.55 | 9.23 | 6.39 | 8.54 | 6.12 |
| Minimum Launch Resonance, Hz | | 35 | 35 | 35 | 35 | 35 | 35 |
| Launch Tube Length, cm (in.) | | 30.5 → 91.4 (12 → 36) | 30.5 → 91.4 (12 → 36) | 30.5 → 91.4 (12 → 36) | 30.5 → 91.4 (12 → 36) | 30.5 → 91.4 (12 → 36) | 30.5 → 91.4 (12 → 36) |
| Inner Diameter of Launch Tube, cm (in.) | | 2.5 → 15.2 (1 → 6) | 2.5 → 15.2 (1 → 6) | 2.5 → 15.2 (1 → 6) | 2.5 → 15.2 (1 → 6) | 2.5 → 15.2 (1 → 6) | 2.5 → 15.2 (1 → 6) |
| Launch Tube Thickness, cm (in.) | | 0.071 → 2.54 (0.028 → 1.0) | 0.071 → 2.54 (0.028 → 1.0) | 0.071 → 2.54 (0.028 → 1.0) | 0.071 → 2.54 (0.028 → 1.0) | 0.071 → 2.54 (0.028 → 1.0) | 0.071 → 2.54 (0.028 → 1.0) |
| Outer Diameter of Orbit Tube, cm (in.) | | 1.58 → * (0.624 → **) | 1.58 → * (0.624 → **) | 1.58 → * (0.624 → **) | 1.58 → * (0.624 → **) | 1.58 → * (0.624 → **) | 1.58 → * (0.624 → **) |
| Orbit Tube Thickness, cm (in.) | | 0.028 → 0.254 (0.011 → 0.1) | 0.028 → 0.254 (0.011 → 0.1) | 0.028 → 0.254 (0.011 → 0.1) | 0.028 → 0.254 (0.011 → 0.1) | 0.028 → 0.254 (0.011 → 0.1) | 0.028 → 0.254 (0.011 → 0.1) |
| Orbit Tube Length, cm (in.) | | 2.54 → 25.4 (1 → 10) | 2.54 → 25.4 (1 → 10) | 2.54 → 25.4 (1 → 10) | 2.54 → 25.4 (1 → 10) | 2.54 → 25.4 (1 → 10) | 2.54 → 25.4 (1 → 10) |

*Sum of quasistatic plus dynamic accelerations for STS launch
**Upper limit dependent upon inner diameter of outer tube

## Table 4-5 PODS-III OPTIMIZED DIMENSIONS

| Case | Initial Tank Launch Condition | Minimum Orbit Resonance (Hz) | Length of Launch Tube cm (in.) | Inner Diameter of Launch Tube cm (in.) | Thickness of Launch Tube cm (in.) | Outer Diameter of Orbit Tube cm (in.) | Thickness of Orbit Tube cm (in.) | Length of Orbit Tube cm (in.) | Azimuthal Angle, θ* deg |
|---|---|---|---|---|---|---|---|---|---|
| OTV $LO_2$ Tank | Full 12 Struts | 5 | 49.02 (19.30) | 15.24 (6.00) | 0.292 (0.115) | 1.58 (0.624) | 0.028 (0.011) | 14.71 (5.79) | 45 |
| | | 12.5 | 49.02 (19.30) | 15.24 (6.00) | 0.292 (0.115) | 2.32 (0.914) | 0.045 (0.0176) | 5.08 (2.00) | 45 |
| | | 20 | 49.02 (19.30) | 15.24 (6.00) | 0.292 (0.115) | 2.98 (1.175) | 0.060 (0.0235) | 2.54 (1.00) | 45 |
| | Empty 6 Struts | 5 | 62.53 (24.62) | 3.42 (1.346) | 0.071 (0.028) | 1.58 (0.624) | 0.028 (0.011) | 25.4 (10.00) | 58 |
| | | 12.5 | 62.53 (24.62) | 3.42 (1.346) | 0.071 (0.028) | 1.58 (0.624) | 0.028 (0.011) | 25.4 (10.00) | 58 |
| | | 20 | 62.53 (24.62) | 3.42 (1.346) | 0.071 (0.028) | 1.58 (0.624) | 0.028 (0.011) | 18.52 (7.29) | 58 |
| OTV $LH_2$ Tank | Full 6 Struts | 5 | 50.17 (19.75) | 13.77 (5.42) | 0.183 (0.0719) | 1.58 (0.624) | 0.028 (0.011) | 25.4 (10.00) | 41 |
| | | 12.5 | 50.17 (19.75) | 13.77 (5.42) | 0.183 (0.0719) | 1.58 (0.624) | 0.034 (0.0132) | 5.08 (2.00) | 41 |
| | | 20 | 50.17 (19.75) | 13.77 (5.42) | 0.183 (0.0719) | 1.74 (0.686) | 0.055 (0.0215) | 2.54 (1.00) | 41 |
| | Empty 6 Struts | 5 | 52.68 (20.74) | 3.24 (1.274) | 0.190 (0.0747) | 1.58 (0.624) | 0.028 (0.011) | 25.4 (10.00) | 39 |
| | | 12.5 | 52.68 (20.74) | 3.24 (1.274) | 0.190 (0.0747) | 1.58 (0.624) | 0.028 (0.011) | 16.15 (6.36) | 39 |
| | | 20 | 52.68 (20.74) | 3.24 (1.274) | 0.190 (0.0747) | 1.58 (0.624) | 0.028 (0.011) | 4.93 (1.94) | 39 |
| SSS $LO_2$ Tank | Full 12 Struts | 1 | 47.98 (18.89) | 15.24 (6.00) | 0.407 (0.1603) | 1.58 (0.624) | 0.028 (0.011) | 25.4 (10.00) | 44 |
| | | 10 | 47.98 (18.89) | 15.24 (6.00) | 0.407 (0.1603) | 1.58 (0.624) | 0.0292 (0.0115) | 2.54 (1.00) | 44 |
| | | 20 | 47.98 (18.89) | 15.24 (6.00) | 0.407 (0.1603) | 4.97 (1.958) | 0.0958 (0.0377) | 5.08 (2.00) | 44 |
| | Empty 6 Struts | 1 | 64.52 (25.40) | 5.54 (2.183) | 0.109 (0.0431) | 1.58 (0.624) | 0.028 (0.011) | 25.4 (10.00) | 54 |
| | | 10 | 64.52 (25.40) | 5.54 (2.183) | 0.109 (0.0431) | 1.58 (0.624) | 0.028 (0.011) | 25.4 (10.00) | 54 |
| | | 20 | 64.52 (25.40) | 5.54 (2.183) | 0.109 (0.0431) | 1.58 (0.624) | 0.028 (0.011) | 6.81 (2.68) | 54 |
| SSS $LH_2$ Tank | Full 12 Struts | 1 | 52.93 (20.84) | 9.76 (3.844) | 0.376 (0.1482) | 1.58 (0.624) | 0.028 (0.011) | 25.4 (10.00) | 41 |
| | | 10 | 52.93 (20.84) | 9.76 (3.844) | 0.376 (0.1482) | 1.58 (0.624) | 0.028 (0.011) | 4.65 (1.83) | 41 |
| | | 20 | 52.93 (20.84) | 9.76 (3.844) | 0.376 (0.1482) | 1.58 (0.624) | 0.088 (0.0345) | 2.54 (1.00) | 41 |
| | Empty 12 Struts | 1 | 55.75 (21.95) | 9.95 (3.919) | 0.101 (0.0398) | 1.58 (0.624) | 0.028 (0.011) | 25.4 (10.00) | 40 |
| | | 10 | 55.75 (21.95) | 9.95 (3.919) | 0.101 (0.0398) | 1.58 (0.624) | 0.028 (0.011) | 18.51 (7.288) | 40 |
| | | 20 | 55.75 (21.95) | 9.95 (3.919) | 0.101 (0.0398) | 1.58 (0.624) | 0.033 (0.013) | 5.08 (2.00) | 40 |

*Circumferential angle, $\phi$, is 30 deg for all cases

## Table 4-5 (Cont.)

| Case | Initial Tank Launch Condition | Minimum Orbit Resonance (Hz) | Length of Launch Tube cm (in.) | Inner Diameter of Launch Tube cm (in.) | Thickness of Launch Tube cm (in.) | Outer Diameter of Orbit Tube cm (in.) | Thickness of Orbit Tube cm (in.) | Length of Orbit Tube cm (in.) | Azimuthal Angle, θ* deg |
|---|---|---|---|---|---|---|---|---|---|
| SSS $LO_2$ Tank With Vapor-Cooled Shields | Full 12 Struts | 1 | 49.40 (19.45) | 15.23 (5.995) | 0.417 (0.164) | 1.58 (0.624) | 0.028 (0.011) | 25.4 (10.00) | 45 |
| | | 10 | 49.40 (19.45) | 15.23 (5.995) | 0.417 (0.164) | 1.58 (0.624) | 0.031 (0.0123) | 2.72 (1.07) | 45 |
| | | 20 | 49.40 (19.45) | 15.23 (5.995) | 0.417 (0.164) | 3.57 (1.404) | 0.070 (0.0276) | 2.54 (1.00) | 45 |
| | Empty 6 Struts | 1 | 50.32 (19.81) | 6.35 (2.50) | 0.0866 (0.0341) | 1.58 (0.624) | 0.028 (0.011) | 25.4 (10.00) | 39 |
| | | 10 | 50.32 (19.81) | 6.35 (2.50) | 0.0866 (0.0341) | 1.58 (0.624) | 0.028 (0.011) | 25.4 (10.00) | 39 |
| | | 20 | 50.32 (19.81) | 6.35 (2.50) | 0.0866 (0.0341) | 1.58 (0.624) | 0.028 (0.011) | 5.38 (2.118) | 39 |
| SSS $LH_2$ Tank With Vapor-Cooled Shields | Full 12 Struts | 1 | 53.21 (20.95) | 15.24 (6.00) | 0.254 (0.0999) | 1.58 (0.624) | 0.028 (0.011) | 25.4 (10.00) | 41 |
| | | 10 | 53.21 (20.95) | 15.24 (6.00) | 0.254 (0.0999) | 1.58 (0.624) | 0.028 (0.011) | 4.47 (1.76) | 41 |
| | | 20 | 53.21 (20.95) | 15.24 (6.00) | 0.254 (0.0999) | 1.58 (0.624) | 0.088 (0.0348) | 2.54 (1.00) | 41 |
| | Empty 12 Struts | 1 | 55.12 (21.70) | 11.89 (4.681) | 0.0965 (0.038) | 1.58 (0.624) | 0.028 (0.011) | 25.4 (10.00) | 40 |
| | | 10 | 55.12 (21.70) | 11.89 (4.681) | 0.0965 (0.038) | 1.58 (0.624) | 0.028 (0.011) | 16.03 (6.31) | 40 |
| | | 20 | 55.12 (21.70) | 11.89 (4.681) | 0.0965 (0.038) | 1.92 (0.755) | 0.037 (0.0145) | 5.08 (2.00) | 40 |

### 4.3.1 THERM

Detail design analyses are done with THERM, the Lockheed thermal analyzer computer program, on the UNIVAC 1110 computer. The configuration is arbitrarily divided into nodes by the designer, and THERM uses a finite-difference solution for the three-dimensional heat transfer equation at each node. Programs with well over 1000 nodes have been run with no difficulty. Steady state occurs when the largest temperature difference of any node between consecutive iterations is less than a value specified in the program. Subroutines for THERM can be performed at many places in the calculation. Two examples are: (1) at each iteration, the temperature-dependent properties can be recalculated and (2) heat maps can be obtained for different nodes.

### 4.3.2 Thermal Models

Four finite-element thermal models were developed for the following cases.

| Support | Cryogen | Vapor Cooled | Fig. No. |
|---|---|---|---|
| PODS-III | $LO_2$ or $LH_2$ | No | 4-3 |
| SOTA Strut | $LO_2$ or $LH_2$ | No | 4-4 |
| PODS-III | $LO_2$ or $LH_2$ | Yes | 4-5 |
| SOTA Strut | $LO_2$ or $LH_2$ | Yes | 4-6 |

Table 4-6 provides the modeled system resistors. Areas for the MLI were calculated from data in Fig. 4-1, and MLI thicknesses were taken from Table 4-2. An MLI degradation factor of 1.5 was used in the conductivity algorithms (Ref. 1). The optimized PODS-III and SOTA support dimensions were taken from Table 4-5. Table 4-6 presents the fill and vent line characteristics.

The vapor-cooled modeling used the cathode follower method. The method determines the amount of heat [$Q = \dot{m}C_p(T_H - T_C)$] a fluid can pick up as it flows from node to node. Sink nodes are used to remove the heat from the model. The struts and vent line were thermally grounded to all three vapor-cooled shields. The fill line was grounded to only the inner shield.

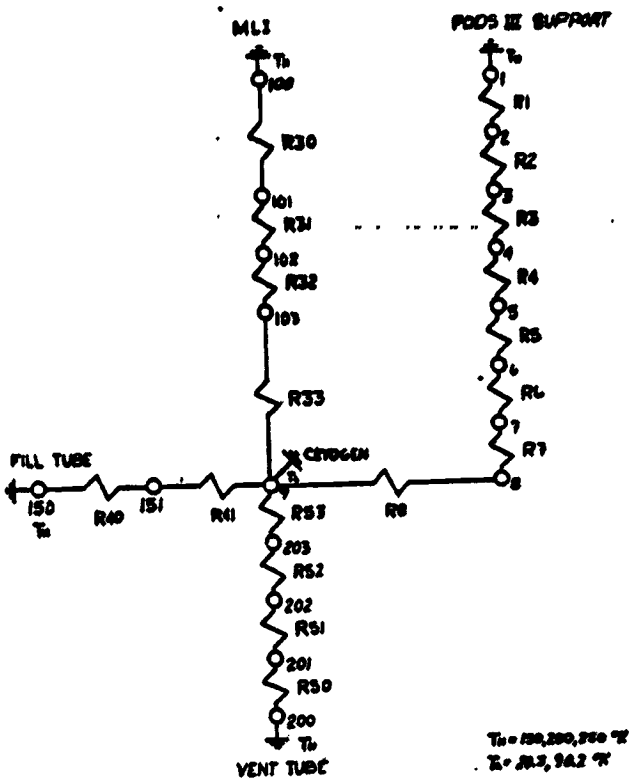


Fig. 4-3 PODS-III/Tank Thermal Model Without Vapor-Cooled Shields

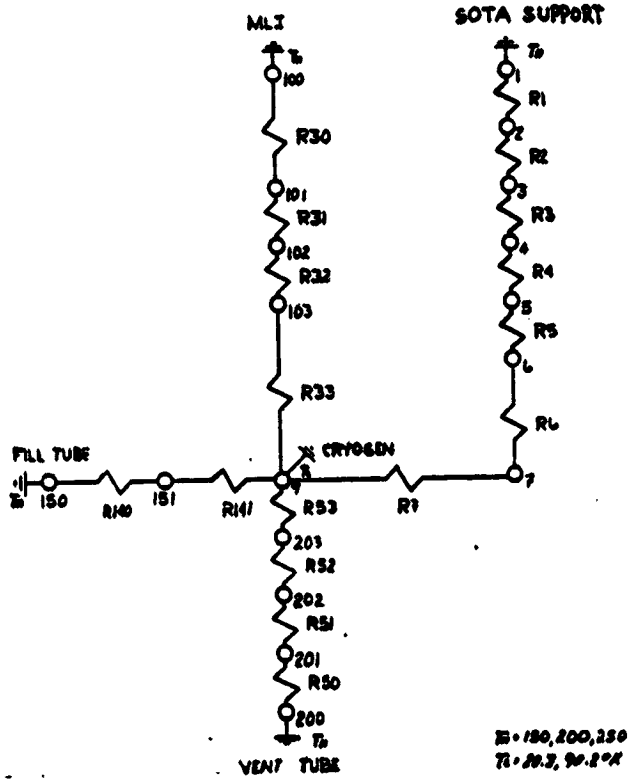


Fig. 4-4 SOTA Strut/Tank Thermal Model Without Vapor-Cooled Shields

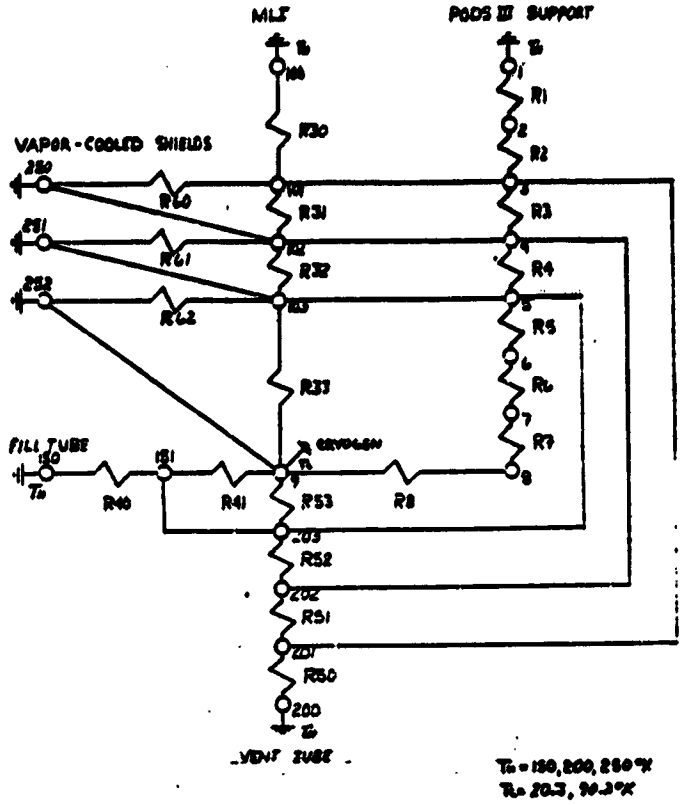


Fig. 4-5 PODS-III/Tank Thermal Model With Vapor-Cooled Shields

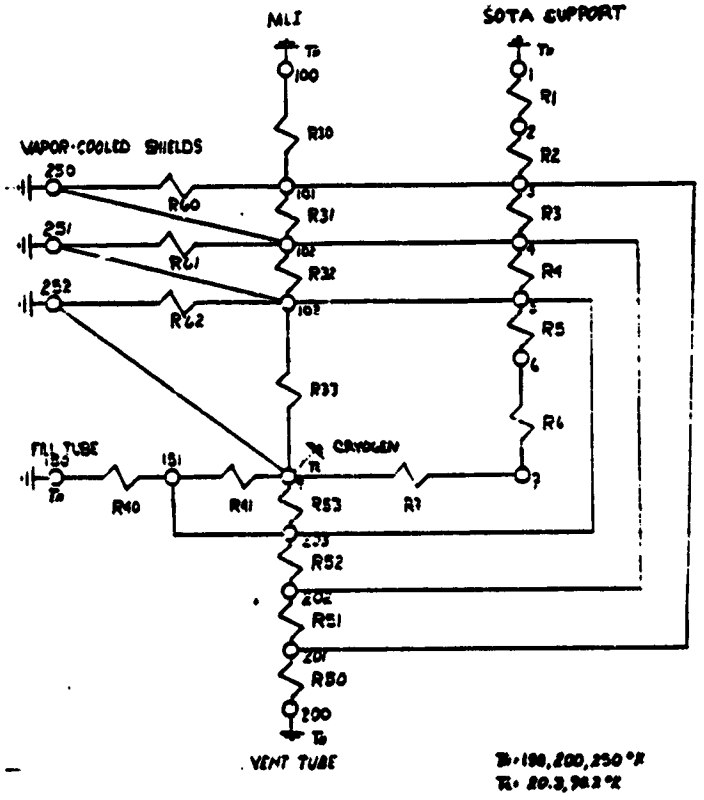


Fig. 4-6 SOTA Strut/Tank Thermal Model With Vapor-Cooled Shields

Table 4-6 MODELED SYSTEM RESISTORS

| System Components | Resistors | Material |
|---|---|---|
| PODS-III | | |
| Rod End, Warm | 1 | Inconel 718 |
| Length Adjustment | 1 | Invar |
| Body, Warm | 1 | Invar |
| Bond Line | 1 | Epoxy |
| Large Outer Tube | 2-5 | S-Glass/Epoxy |
| Bond Line | 6 | Epoxy |
| Body, Cold | 6 | Invar |
| Adjustment Bushing | 6 | Invar |
| Bond Line | 6 | Epoxy |
| Small Inner Tube | 7 | S-Glass/Epoxy |
| Bond Line | 8 | Epoxy |
| Stem | 8 | Invar |
| Rod End, Cold | 8 | Inconel 718 |
| SOTA - Same as above except for the following: | | |
| Bond Line | 6 | Epoxy |
| Body, Cold | 6 | Invar |
| Stem | 7 | Invar |
| Rod End, Cold | 7 | Inconel 718 |
| MLI | 30-33 | DAM/Silk Net |
| Fill Tube 2.54 cm diam. x 0.051 cm x 61 cm (1.0 in. diam. x 0.020 in. x 24 in.) | 40-41 | Titanium 6 Al 4V |
| Vent Tube 1.27 cm diam. x 0.0254 cm x 101.6 cm (0.5 in. diam. x 0.010 in. x 40 in.) | 50-53 | Titanium 6 Al 4V |
| Vapor-Cooled Shields | 60-62 | 6061 Aluminum |

### 4.3.3 Results

The following tables provide a breakdown of the calculated heat rates as a function of warm boundary temperature, orbit resonance, and full or empty tanks at launch.

| Table No. | Tank | Vapor Cooled |
|---|---|---|
| 4-7 | OTV - $LO_2$ | No |
| 4-8 | OTV - $LH_2$ | No |
| 4-9 | SSS - $LO_2$ | No |
| 4-10 | SSS - $LH_2$ | No |
| 4-11 | SSS - $LO_2$ | Yes |
| 4-12 | SSS - $LH_2$ | Yes |

From these tables, the ratio of the total heat rate for PODS supported SSS tanks to SOTA strut supported tanks is plotted versus the warm boundary temperature, full or empty tanks at launch, and orbit resonance (Figs. 4-7 through 4-10). The inverse of this ratio is also plotted for the struts-only heat leak in Fig. 4-11.

The following trends appear in the data: (1) the MLI heat rate is dominant; (2) lower orbit resonance values (smaller A/L ratios) and lower warm boundary temperatures (where MLI heat rate decreases faster than support heat rates) improve the PODS-III supported tank thermal performance versus SOTA struts; (4) non-vapor-cooled PODS-III support tanks show greater relative performance gain over SOTA struts than when the struts are vapor cooled; and (5) launching tanks empty provides the smallest relative gain in PODS-III tank performance improvement over SOTA struts.

The empty tanks are filled in orbit from a supply tank; consequently, additional cryogen is required for cooling down the warm tank. A second launch may be required to bring up the extra cryogen, and a supply dewar is required.

## Table 4-7 OTV HEAT RATES, $LO_2$ TANK (mW)

| Hot Boundary Temperature (K) | Tank Components | PODS-III Initial Tank Condition | | | | | | SOTA Initial Tank Condition | |
|---|---|---|---|---|---|---|---|---|---|
| | | Full: 19808.3 kg (43,669 lb) Struts = 12 | | | Empty: 319.3 kg (704 lb) Struts = 6 | | | Full 19808.3 kg (43,669 lb) | Empty 319.3 kg (704 lb) |
| | | Orbital Resonance | | | Orbital Resonance | | | Struts | Struts |
| | | 5 Hz | 12.5 Hz | 20 Hz | 5 Hz | 12.5 Hz | 20 Hz | 12 | 6 |
| 150 | Supports | 35.3 | 191.0 | 418.6 | 7.4 | 7.4 | 9.1 | 848.7 | 24.9 |
| | MLI | 1555.7 | 1555.7 | 1555.7 | 1555.7 | 1555.7 | 1555.7 | 1555.7 | 1555.7 |
| | Fill Line | 17.7 | 17.7 | 17.7 | 17.7 | 17.7 | 17.7 | 17.7 | 17.7 |
| | Vent Line | 2.7 | 2.7 | 2.7 | 2.7 | 2.7 | 2.7 | 2.7 | 2.7 |
| | Total | 1611.4 | 1767.1 | 1994.6 | 1583.5 | 1583.5 | 1595.2 | 2424.7 | 1601.0 |
| 200 | Supports | 74.0 | 395.6 | 858.5 | 15.3 | 15.3 | 18.8 | 1726.3 | 50.8 |
| | MLI | 4217.6 | 4217.6 | 4217.6 | 4217.6 | 4217.6 | 4217.6 | 4217.6 | 4217.6 |
| | Fill Line | 36.2 | 36.2 | 36.2 | 36.2 | 36.2 | 36.2 | 36.2 | 36.2 |
| | Vent Line | 5.4 | 5.4 | 5.4 | 5.4 | 5.4 | 5.4 | 5.4 | 5.4 |
| | Total | 4333.1 | 4654.7 | 5117.7 | 4274.4 | 4274.4 | 4278.0 | 5985.4 | 4310.0 |
| 250 | Supports | 117.9 | 630.9 | 1364.8 | 24.5 | 24.5 | 30.1 | 2715.7 | 80.8 |
| | MLI | 9144.8 | 9144.8 | 9144.8 | 9144.8 | 9144.8 | 9144.8 | 9144.8 | 9144.8 |
| | Fill Line | 57.2 | 57.2 | 57.2 | 57.2 | 57.2 | 57.2 | 57.2 | 57.2 |
| | Vent Line | 8.6 | 8.6 | 8.6 | 8.6 | 8.6 | 8.6 | 8.6 | 8.6 |
| | Total | 3328.4 | 9841.4 | 10575.0 | 9235.0 | 9235.0 | 9240.6 | 11926.0 | 9291.3 |

## Table 4-8 OTV HEAT RATES, $LH_2$ TANK (mW)

| Hot Boundary Temperature (K) | Tank Components | PODS-III Initial Tank Condition | | | | | | SOTA Initial Tank Condition | |
|---|---|---|---|---|---|---|---|---|---|
| | | Full: 4163.1 kg (9178 lb) Struts = 6 | | | Empty: 870 kg (1918 lb) Struts = 6 | | | Full 4163.1 kg (9178 lb) | Empty 870 kg (1918 lb) |
| | | Orbital Resonance | | | Orbital Resonance | | | Struts | Struts |
| | | 5 Hz | 12.5 Hz | 20 Hz | 5 Hz | 12.5 Hz | 20 Hz | 6 | 6 |
| 150 | Supports | 18.0 | 97.2 | 212.0 | 16.3 | 23.9 | 55.1 | 459.3 | 128.4 |
| | MLI | 1572.3 | 1572.3 | 1572.3 | 1572.3 | 1572.3 | 1572.3 | 1572.3 | 1572.3 |
| | Fill Line | 30.5 | 30.5 | 30.5 | 30.5 | 30.5 | 30.5 | 30.5 | 30.5 |
| | Vent Line | 4.6 | 4.6 | 4.6 | 4.6 | 4.6 | 4.6 | 4.6 | 4.6 |
| | Total | 1625.4 | 1704.5 | 1819.3 | 1623.7 | 1631.3 | 1662.5 | 2066.7 | 1735.7 |
| 200 | Supports | 29.0 | 154.6 | 337.0 | 26.0 | 38.0 | 87.8 | 732.5 | 205.3 |
| | MLI | 3460.0 | 3460.0 | 3460.0 | 3460.0 | 3460.0 | 3460.0 | 3460.0 | 3460.0 |
| | Fill Line | 48.7 | 48.7 | 48.7 | 48.7 | 48.7 | 48.7 | 48.7 | 48.7 |
| | Vent Line | 7.3 | 7.3 | 7.3 | 7.3 | 7.3 | 7.3 | 7.3 | 7.3 |
| | Total | 3544.9 | 3670.5 | 3852.9 | 3541.9 | 3554.0 | 3603.8 | 4248.4 | 3721.2 |
| 250 | Supports | 42.6 | 224.4 | 480.1 | 38.0 | 55.2 | 125.0 | 1042.1 | 291.9 |
| | MLI | 6954.1 | 6954.1 | 6954.1 | 6954.1 | 6954.1 | 6954.1 | 6954.1 | 6954.1 |
| | Fill Line | 70.8 | 70.8 | 70.8 | 70.8 | 70.8 | 70.8 | 70.8 | 70.8 |
| | Vent Line | 10.5 | 10.5 | 10.5 | 10.5 | 10.5 | 10.5 | 10.5 | 10.5 |
| | Total | 7078.0 | 7259.8 | 7515.5 | 7073.4 | 7090.7 | 7160.5 | 8077.6 | 7327.3 |

## Table 4-9 SSS HEAT RATES, $LO_2$ TANK (mW)

| Hot Boundary Temperature (K) | Tank Components | PODS-III Initial Tank Condition | | | | | | SOTA Initial Tank Condition | |
|---|---|---|---|---|---|---|---|---|---|
| | | Full: 27981.2 kg (61,687 lb) Struts = 12 | | | Empty: 699 kg (1541 lb) Struts = 6 | | | Full 27,981.2 kg (61,687 lb) | Empty 699 kg (1541 lb) |
| | | Orbital Resonance | | | Orbital Resonance | | | Struts | Struts |
| | | 1 Hz | 10 Hz | 20 Hz | 1 Hz | 10 Hz | 20 Hz | 12 | 6 |
| 150 | Supports | 20.9 | 183.6 | 543.4 | 9.0 | 9.0 | 23.5 | 1088.1 | 58.5 |
| | MLI | 1336.4 | 1336.4 | 1336.4 | 1336.4 | 1336.4 | 1336.4 | 1336.4 | 1336.4 |
| | Fill Line | 17.7 | 17.7 | 17.7 | 17.7 | 17.7 | 17.7 | 17.7 | 17.7 |
| | Vent Line | 2.7 | 2.7 | 2.7 | 2.7 | 2.7 | 2.7 | 2.7 | 2.7 |
| | Total | 1377.7 | 1540.3 | 1900.1 | 1365.7 | 1365.7 | 1380.2 | 2444.9 | 1415.2 |
| 200 | Supports | 43.9 | 381.3 | 1112.4 | 18.7 | 18.7 | 48.5 | 2204.1 | 119.9 |
| | MLI | 3623.0 | 3623.0 | 3623.0 | 3623.0 | 3623.0 | 3623.0 | 3623.0 | 3623.0 |
| | Fill Line | 36.2 | 36.2 | 36.2 | 36.2 | 36.2 | 36.2 | 36.2 | 36.2 |
| | Vent Line | 5.4 | 5.4 | 5.4 | 5.4 | 5.4 | 5.4 | 5.4 | 5.4 |
| | Total | 3708.5 | 4045.9 | 4777.0 | 3683.3 | 3683.3 | 3713.1 | 5868.7 | 3784.5 |
| 250 | Supports | 70.0 | 607.4 | 1766.5 | 29.9 | 29.9 | 77.4 | 3452.9 | 189.8 |
| | MLI | 7855.6 | 7855.6 | 7855.6 | 7855.6 | 7855.6 | 7855.6 | 7855.6 | 7855.6 |
| | Fill Line | 57.2 | 57.2 | 57.2 | 57.2 | 57.2 | 57.2 | 57.2 | 57.2 |
| | Vent Line | 8.6 | 8.6 | 8.6 | 8.6 | 8.6 | 8.6 | 8.6 | 8.6 |
| | Total | 7991.3 | 8528.7 | 9687.9 | 7951.3 | 7951.3 | 7998.7 | 11,374.0 | 8111.2 |

## Table 4-10 SSS HEAT RATES, $LH_2$ TANK (mW)

| Hot Boundary Temperature (K) | Tank Components | PODS-III Initial Tank Condition | | | | | | SOTA Initial Tank Condition | |
|---|---|---|---|---|---|---|---|---|---|
| | | Full: 10248.6 kg (22,594 lb) Struts = 12 | | | Empty: 2259.8 kg (4982 lb) Struts = 12 | | | Full 10,248.6 kg (22,594 lb) | Empty 2259.8 kg (4982 lb) |
| | | Orbital Resonance | | | Orbital Resonance | | | Struts | Struts |
| | | 1 Hz | 10 Hz | 20 Hz | 1 Hz | 10 Hz | 20 Hz | 12 | 12 |
| 150 | Supports | 36.3 | 174.5 | 578.9 | 34.1 | 45.2 | 148.7 | 1211.8 | 373.7 |
| | MLI | 1341.4 | 1341.4 | 1341.4 | 1341.4 | 1341.4 | 1341.4 | 1341.4 | 1341.4 |
| | Fill Line | 30.5 | 30.5 | 30.5 | 30.5 | 30.5 | 30.5 | 30.5 | 30.5 |
| | Vent Line | 4.6 | 4.6 | 4.6 | 4.6 | 4.6 | 4.6 | 4.6 | 4.6 |
| | Total | 1412.8 | 1550.9 | 1955.4 | 1410.6 | 1421.7 | 1525.2 | 2588.3 | 1750.2 |
| 200 | Supports | 58.5 | 278.7 | 913.3 | 54.6 | 72.3 | 236.8 | 1933.4 | 486.6 |
| | MLI | 2951.8 | 2951.8 | 2951.8 | 2951.8 | 2951.8 | 2951.8 | 2951.8 | 2951.8 |
| | Fill Line | 48.7 | 48.7 | 48.7 | 48.7 | 48.7 | 48.7 | 48.7 | 48.7 |
| | Vent Line | 7.3 | 7.3 | 7.3 | 7.3 | 7.3 | 7.3 | 7.3 | 7.3 |
| | Total | 3066.3 | 3286.5 | 3927.1 | 3062.4 | 3080.1 | 3244.5 | 4941.2 | 3604.0 |
| 250 | Supports | 86.0 | 406.2 | 1311.4 | 79.9 | 105.5 | 338.0 | 2755.2 | 846.7 |
| | MLI | 5932.8 | 5932.8 | 5932.8 | 5932.8 | 5932.8 | 5932.8 | 5932.8 | 5932.8 |
| | Fill Line | 70.8 | 70.8 | 70.8 | 70.8 | 70.8 | 70.8 | 70.8 | 70.8 |
| | Vent Line | 10.5 | 10.5 | 10.5 | 10.5 | 10.5 | 10.5 | 10.5 | 10.5 |
| | Total | 6100.2 | 6420.4 | 7325.6 | 6094.0 | 6119.7 | 6352.2 | 8769.4 | 6860.9 |

## Table 4-11 SSS HEAT RATES, VAPOR-COOLED $LO_2$ TANK (mW)

| Hot Boundary Temperaiure (K) | Tank Components | POOS-III Initial Tank Condition | | | | | | SOTA Initial Tank Condition | |
|---|---|---|---|---|---|---|---|---|---|
| | | Full: 28155.9 kg (62,072 lb) Struts = 12 | | | Empty: 873.6 kg (1926 lb) Struts = 6 | | | Full 28,155.9 kg (62,072 lb) | Empty 873.6 kg (1926 lb) |
| | | Orbital Resonance | | | Orbital Resonance | | | Struts | Struts |
| | | 1 Hz | 10 Hz | 20 Hz | 1 Hz | 10 Hz | 20 Hz | 12 | 6 |
| 150 | Supports | 2.9 | 27.9 | 108.2 | 1.4 | 1.4 | 5.3 | 340.8 | 23.5 |
| | MLI | 1209.1 | 1206.9 | 1199.7 | 1209.3 | 1209.3 | 1208.9 | 1179.0 | 1207.3 |
| | Fill Line | 10.2 | 10.2 | 10.1 | 10.2 | 10.2 | 10.2 | 9.9 | 10.2 |
| | Vent Line | 1.5 | 1.5 | 1.5 | 1.5 | 1.5 | 1.5 | 1.5 | 1.5 |
| | Total | 1223.8 | 1246.5 | 1319.5 | 1222.4 | 1222.4 | 1225.9 | 1531.3 | 1242.5 |
| 200 | Supports | 6.8 | 65.1 | 251.5 | 3.2 | 3.2 | 12.3 | 783.8 | 52.3 |
| | MLI | 2979.5 | 2969.9 | 2939.3 | 2980.1 | 2980.1 | 2978.6 | 2853.1 | 2972.0 |
| | Fill Line | 23.6 | 23.5 | 23.3 | 23.6 | 23.6 | 23.6 | 22.7 | 23.5 |
| | Vent Line | 3.5 | 3.5 | 3.5 | 3.5 | 3.5 | 3.5 | 3.4 | 3.5 |
| | Total | 3013.4 | 3062.1 | 3217.6 | 3010.4 | 3010.4 | 3028.0 | 3663.0 | 3051.4 |
| 250 | Supports | 12.5 | 119.5 | 460.2 | 5.9 | 5.9 | 22.6 | 1417.2 | 95.7 |
| | MLI | 5867.3 | 5842.4 | 5763.5 | 5868.9 | 5868.9 | 5865.0 | 5544.8 | 5848.0 |
| | Fill Line | 42.7 | 42.5 | 42.0 | 42.7 | 42.7 | 42.6 | 40.7 | 42.5 |
| | Vent Line | 6.4 | 6.4 | 6.3 | 6.4 | 6.4 | 6.4 | 6.1 | 6.4 |
| | Total | 5928.9 | 6010.8 | 6272.0 | 5923.9 | 5923.9 | 5936.6 | 7008.7 | 5992.6 |

## Table 4-12 SSS HEAT RATES, VAPOR-COOLED $LH_2$ TANK (mW)

| Hot Boundary Temperature (K) | Tank Components | PODS-III Initial Tank Condition | | | | | | SOTA Initial Tank Condition | |
|---|---|---|---|---|---|---|---|---|---|
| | | Full: 10654.6 kg (23,489 lb) Struts = 12 | | | Empty: 2665.8 kg (5877 lb) Struts = 12 | | | Full 10,654.6 kg (23,489 lb) | Empty 2665.8 kg (5877 lb) |
| | | Orbital Resonance | | | Orbital Resonance | | | Struts | Struts |
| | | 1 Hz | 10 Hz | 20 Hz | 1 Hz | 10 Hz | 20 Hz | 12 | 12 |
| 150 | Supports | 4.0 | 21.0 | 81.0 | 3.9 | 6.0 | 24.3 | 252.1 | 100.7 |
| | MLI | 569.4 | 561.2 | 532.7 | 569.5 | 568.4 | 559.6 | 454.9 | 523.4 |
| | Fill Line | 11.3 | 11.2 | 10.6 | 11.3 | 11.3 | 11.1 | 9.1 | 10.4 |
| | Vent Line | 1.7 | 1.7 | 1.6 | 1.7 | 1.7 | 1.7 | 1.4 | 1.6 |
| | Total | 586.4 | 595.0 | 625.9 | 586.4 | 587.4 | 596.7 | 717.5 | 636.1 |
| 200 | Supports | 6.1 | 32.4 | 126.0 | 6.0 | 9.3 | 37.8 | 393.1 | 156.2 |
| | MLI | 983.1 | 968.4 | 916.6 | 983.2 | 981.3 | 965.4 | 774.4 | 900.1 |
| | Fill Line | 18.6 | 18.3 | 17.5 | 18.6 | 18.5 | 18.3 | 15.1 | 17.2 |
| | Vent Line | 2.8 | 2.7 | 2.6 | 2.8 | 2.8 | 2.7 | 2.3 | 2.6 |
| | Total | 1010.6 | 1021.9 | 1062.7 | 1010.5 | 1011.9 | 1024.2 | 1184.8 | 1076.0 |
| 250 | Supports | 9.2 | 48.2 | 185.5 | 8.9 | 13.8 | 55.3 | 587.5 | 233.6 |
| | MLI | 1581.5 | 1557.3 | 1473.4 | 1581.6 | 1578.6 | 1553.0 | 1235.6 | 1444.2 |
| | Fill Line | 28.0 | 27.7 | 26.4 | 28.1 | 28.0 | 27.6 | 22.7 | 25.9 |
| | Vent Line | 4.2 | 4.2 | 4.0 | 4.2 | 4.2 | 4.1 | 3.4 | 3.9 |
| | Total | 1622.9 | 1637.4 | 1689.2 | 1622.8 | 1624.6 | 1640.0 | 1849.2 | 1707.7 |

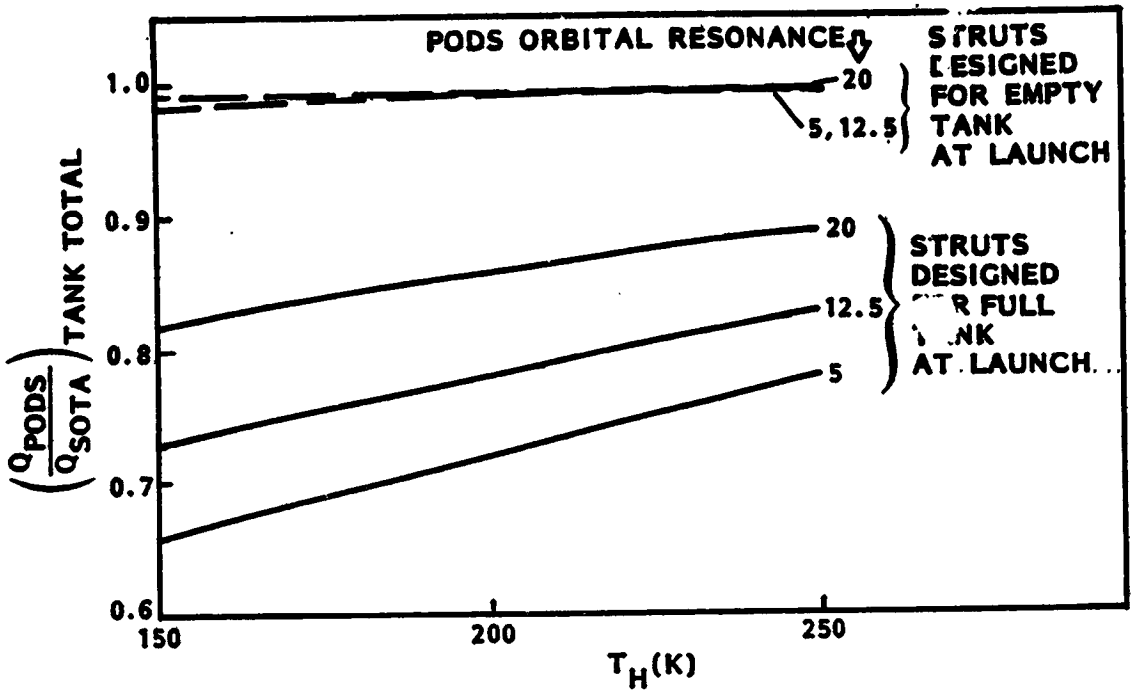


Fig. 4-7 Relative Reduction in Tank Heat Rate for the OTV $LO_2$ Tank (PODS Versus SOTA Struts)

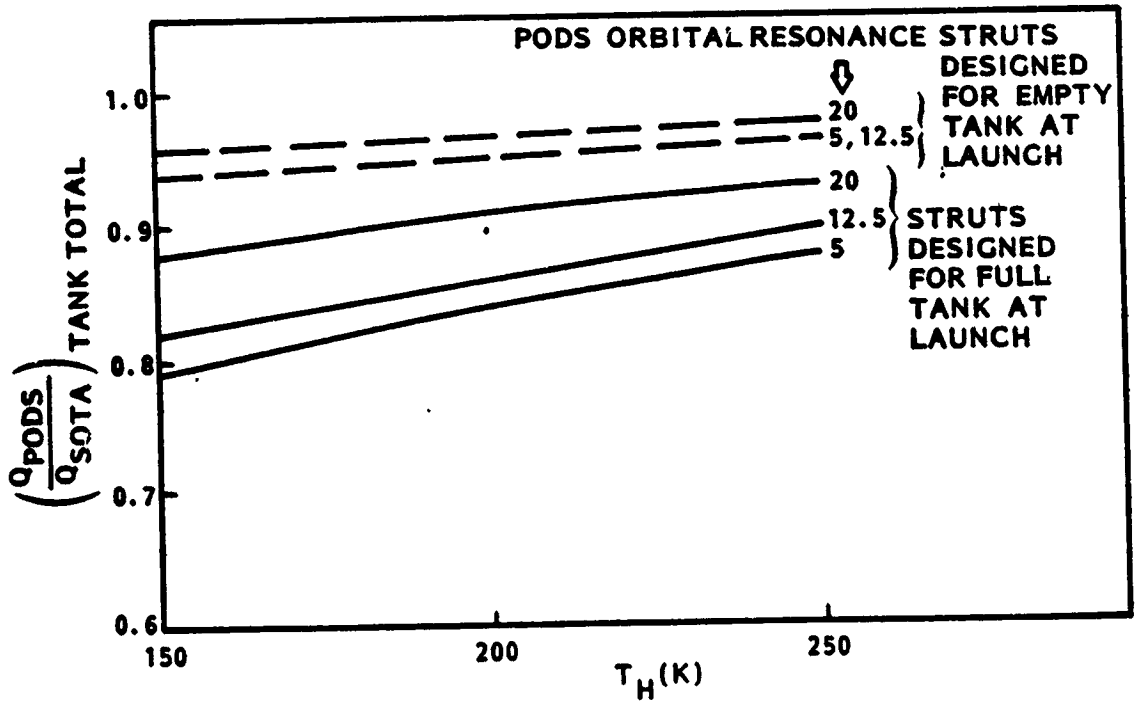


Fig. 4-8 Relative Reduction in Tank Heat Rate for the OTV $LH_2$ Tank (PODS Versus SOTA Struts)

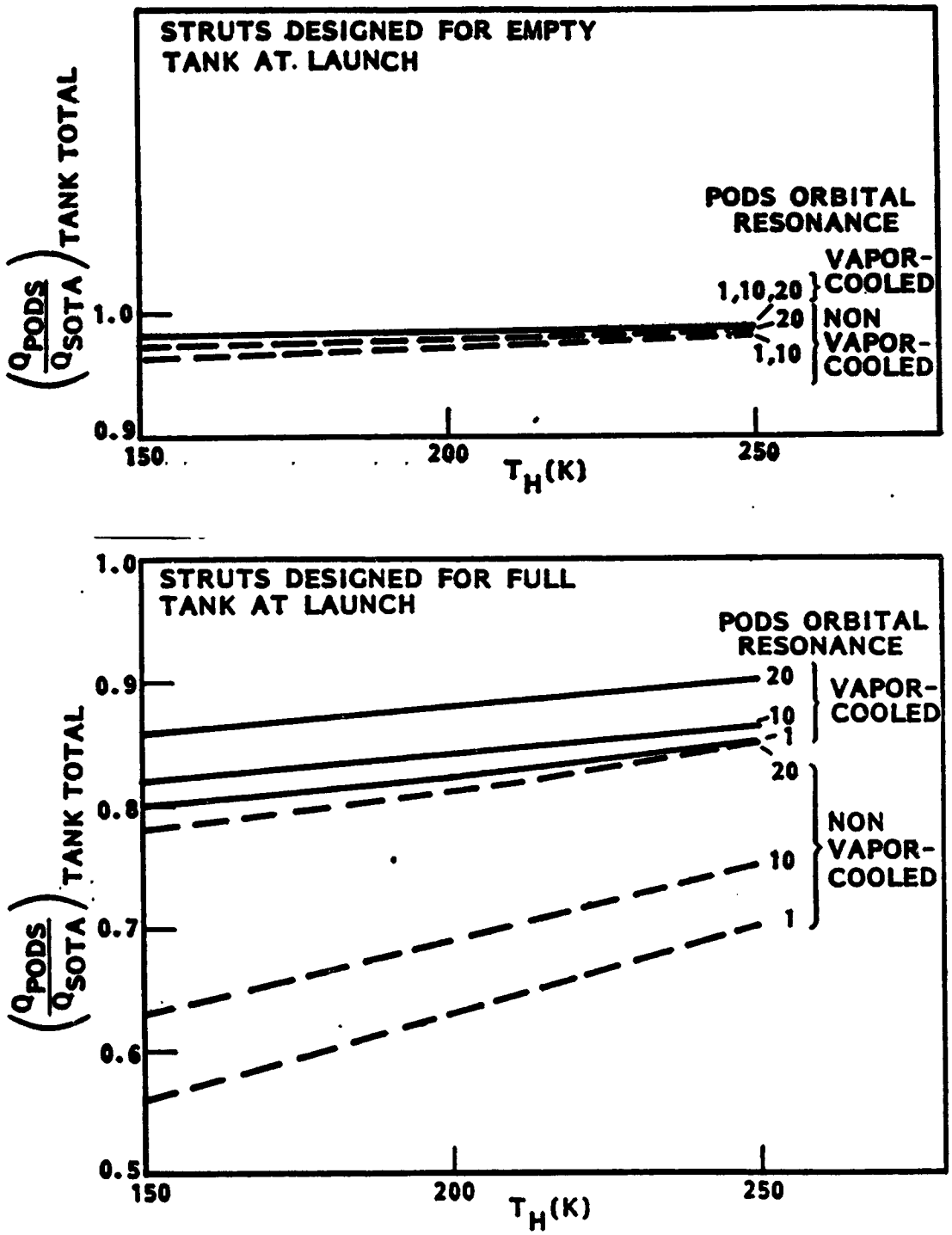


Fig. 4-9 Relative Reduction in Tank Heat Rate for the Space Station $LO_2$ Tank (PODS Versus SOTA Struts)

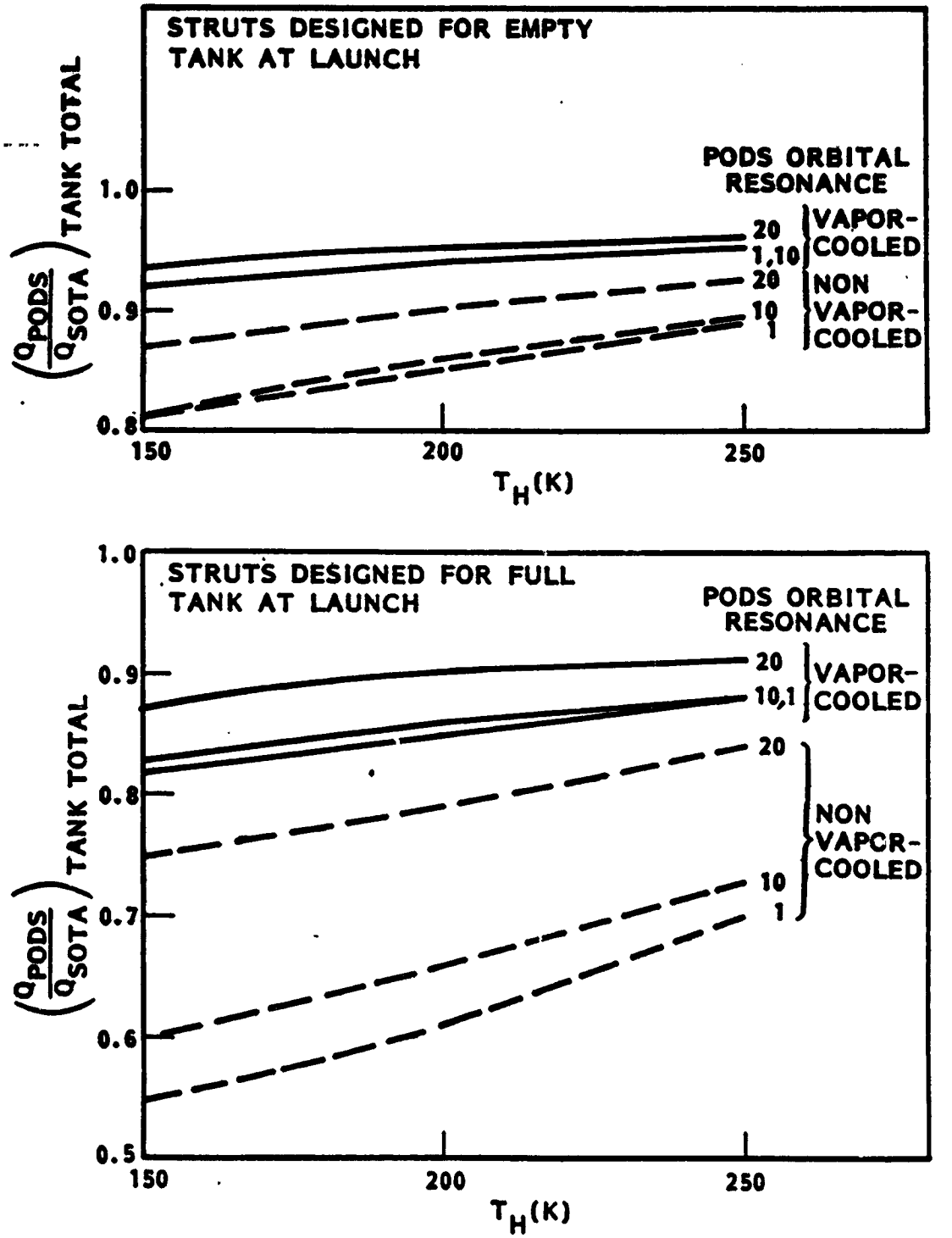


Fig. 4-10 Relative Reduction in Tank Heat Rate for the Space Station $LH_2$ Tank (PODS Versus SOTA Struts)

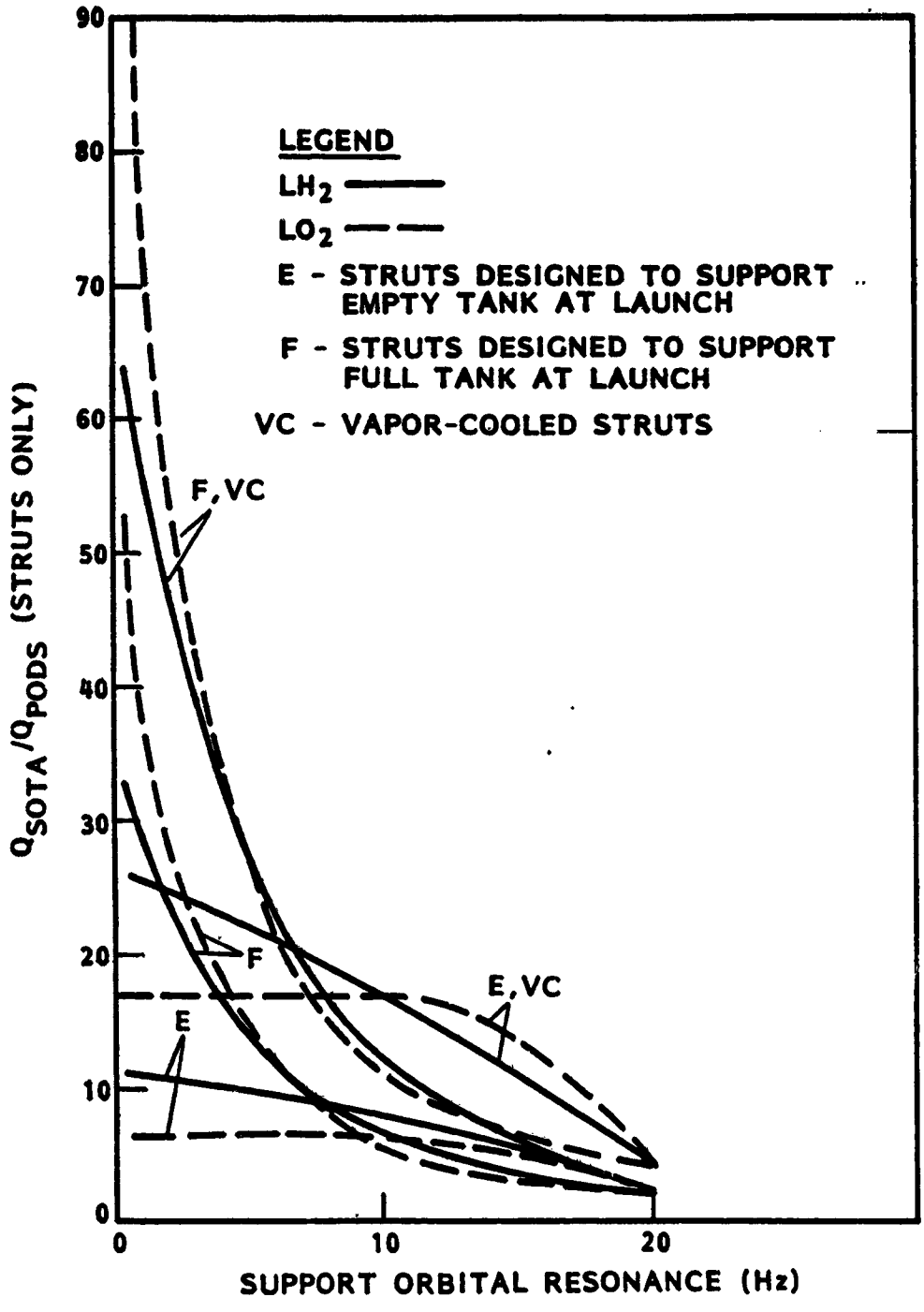


Fig. 4-11 Ratio of Strut Heat Rate for the Space Station Tanks (PODS Versus SOTA Struts)

The support heat rates can be kept equal between the PODS-III supports (designed for 35 Hz during launch with a full tank) and the SOTA struts (designed for 35 Hz during launch with an empty tank) by lowering the PODS-III orbital resonances to the following values.

| Tank | Vapor Cooled | Full Tank PODS-III Orbital Resonance, Hz (Designed for Full Tank at Launch) | Full Tank SOTA Strut Orbital Resonance, Hz (Designed for Empty Tank at Launch) |
|---|---|---|---|
| OTV-$LO_2$ | No | 4 | 4 |
| OTV-$LH_2$ | No | 15 | 16 |
| SSS-$LO_2$ | No | 3 | 6 |
| SSS-$LO_2$ | Yes | 8 | 6 |
| SSS-$LH_2$ | No | 15 | 16 |
| SSS-$LH_2$ | Yes | 23 | 18 |

The orbital resonances for the SOTA struts and PODS-III are comparable. However, the PODS-III strut-supported tanks can be launched full or empty, with potentially lower launch costs (1 versus 2 launches). For the OTV $LO_2$ tank, orbit resonances of 4 to 8 Hz would probably not be acceptable during orbital engine firings. The $LO_2$ PODS supports with low orbital resonances would short and drive the strut resonance higher to "launch values" during orbital engine firings. The difference in fabrication costs between PODS-III supports and SOTA struts is insignificant compared to the total costs of a cryogen system (Ref. 2).

The calculated heat rates were translated into cryogen left for vented systems (Figs. 4-12, 4-13) and pressure rise versus time for nonvented systems (Figs. 4-14 through 4-17). An orbital resonance of 20 Hz was arbitrarily selected for the OTV tanks due to the higher orbital accelerations they experience. A lower 10-Hz orbital resonance was arbitrarily selected for the SSS tanks due to minimal accelerations they experience in orbit.

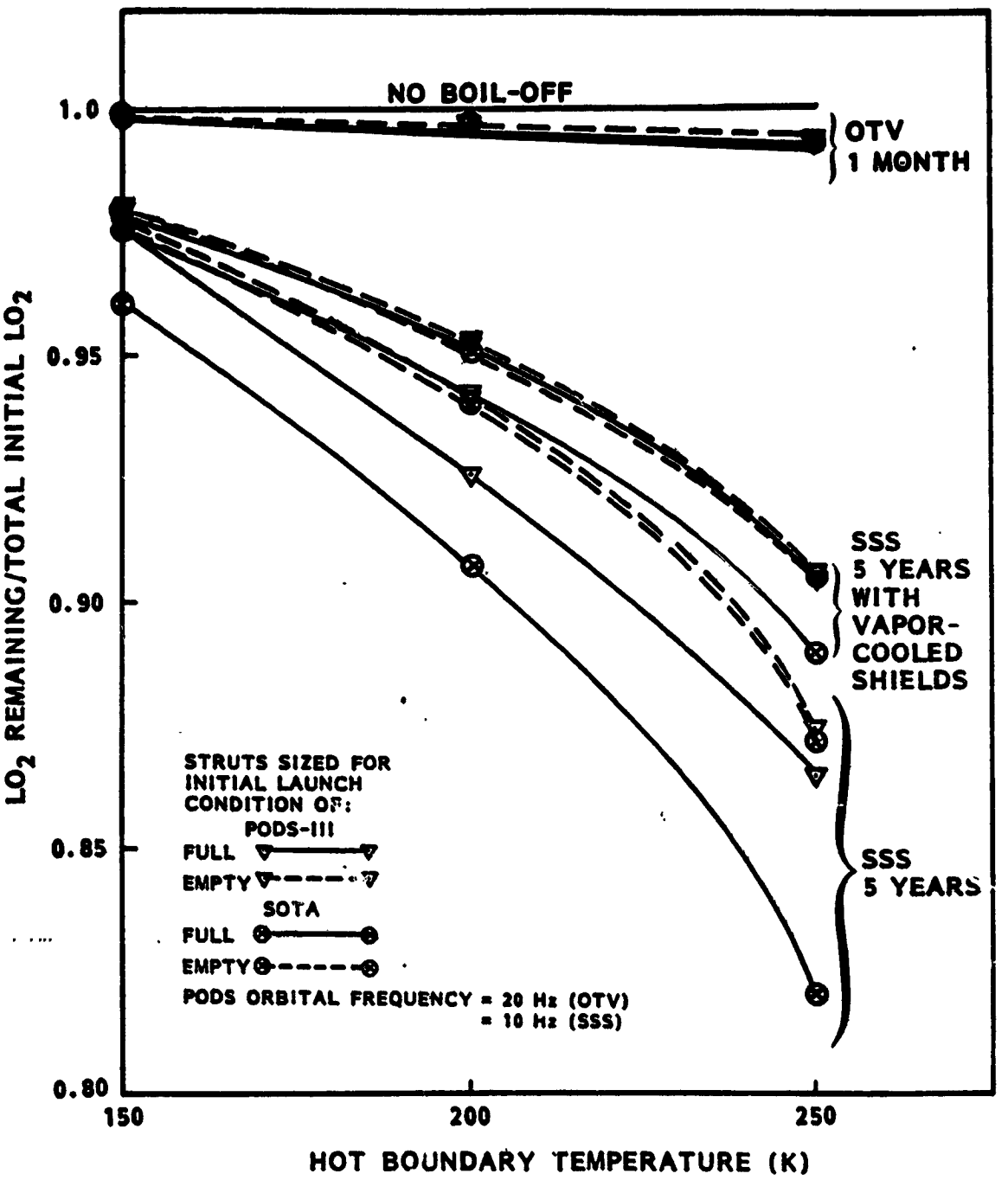


Fig. 4-12 $LO_2$ Loss for Vented Tanks

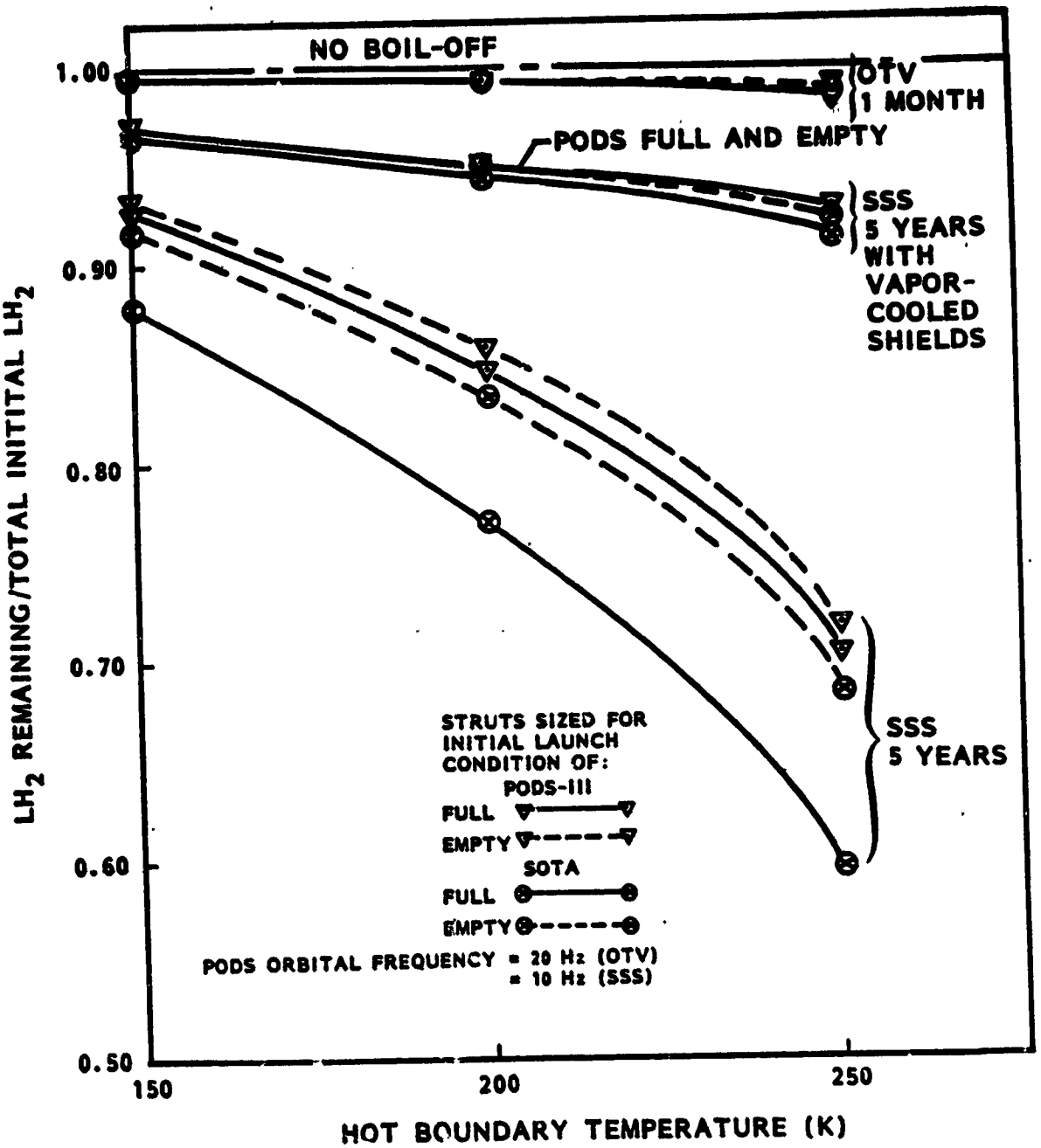


Fig. 4-13 $LH_2$ Loss for Vented Tanks

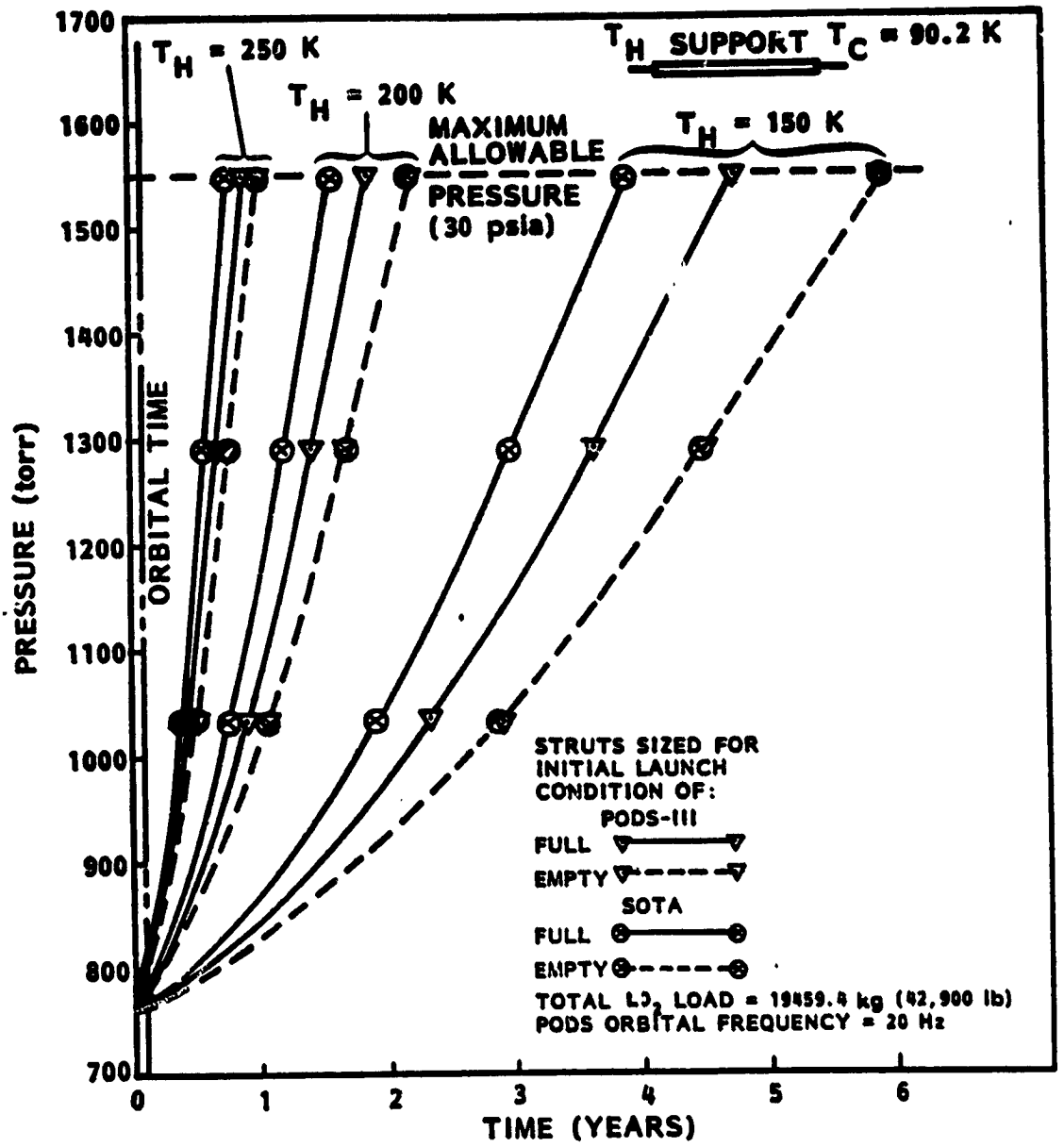


Fig. 4-14 $LO_2$ OTV Tank No-Vent Pressure History

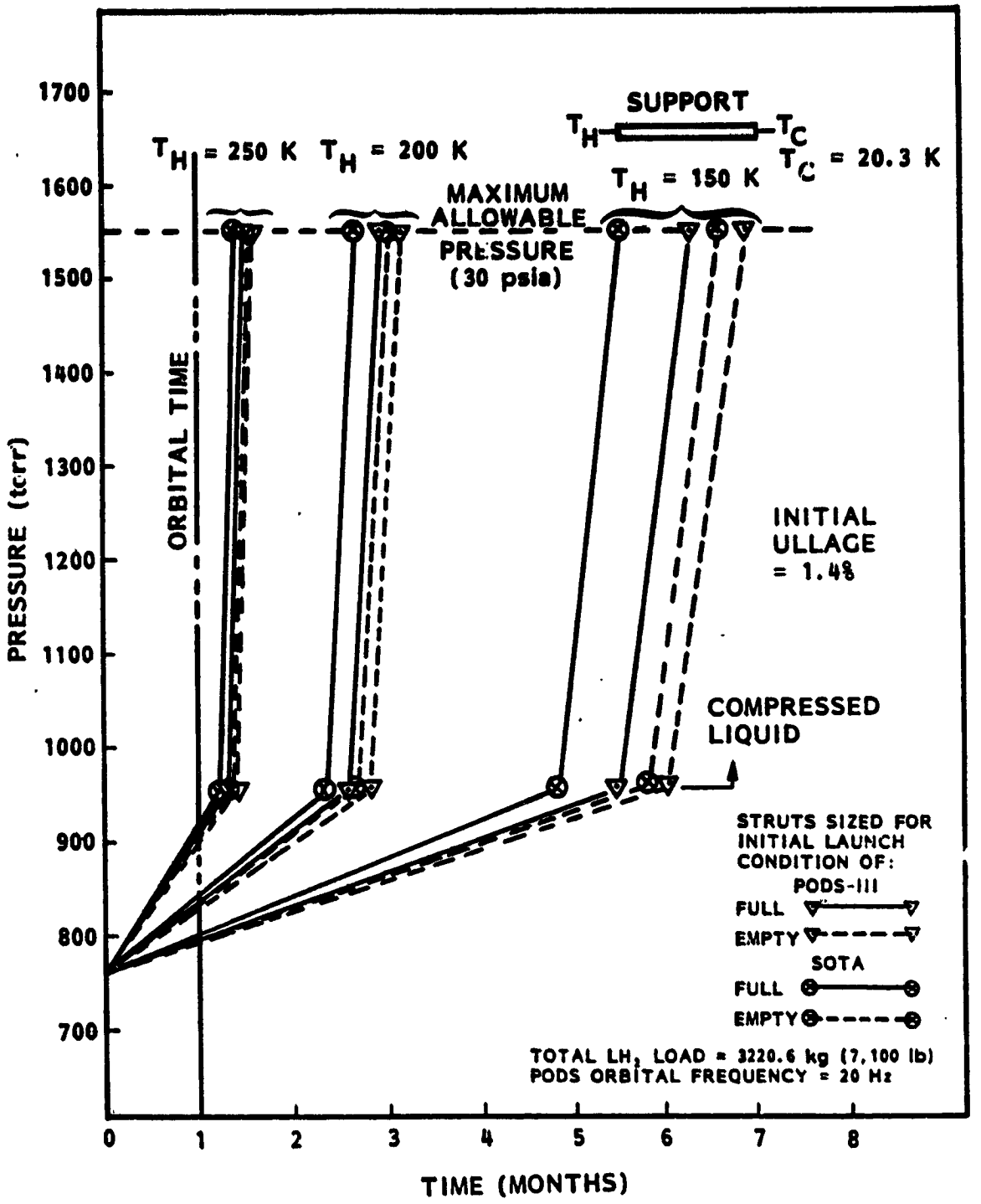


Fig. 4-15 $LH_2$ OTV Tank No-Vent Pressure History

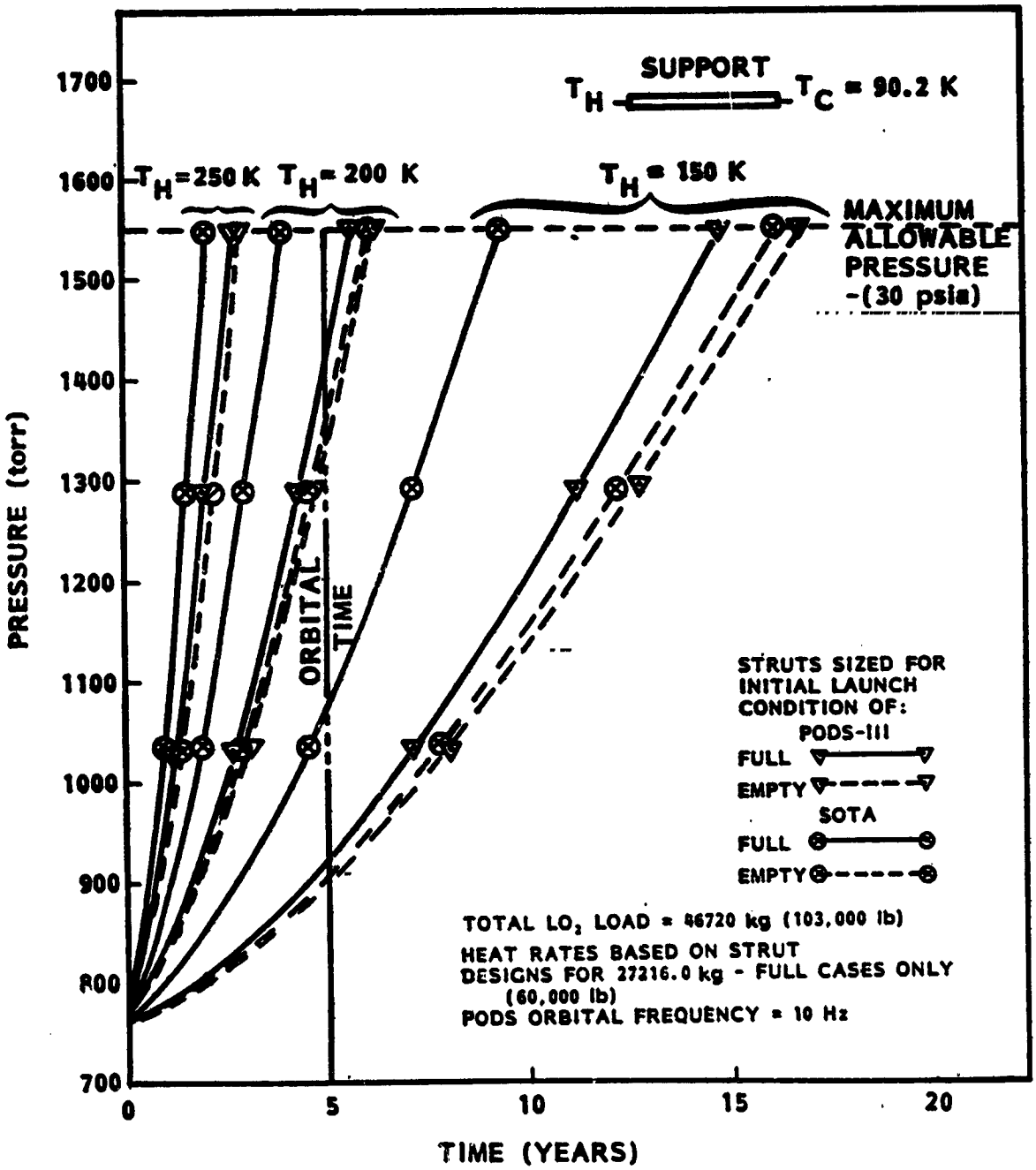


Fig. 4-16 $LO_2$ SSS Tank No-Vent Pressure History

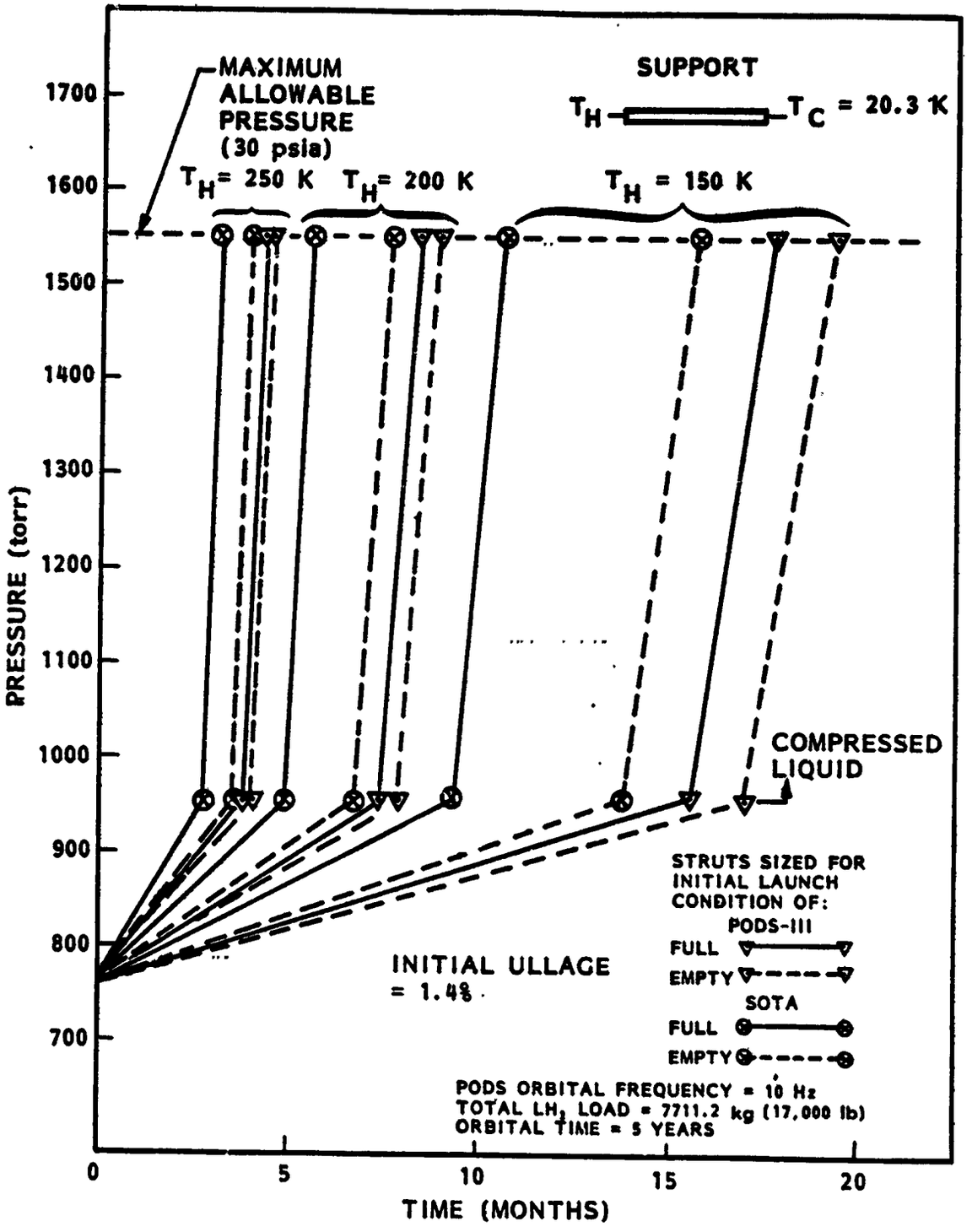


Fig. 4-17 $LH_2$ SSS Tank No-Vent Pressure History

# Section 5
# CONCLUSIONS AND RECOMMENDATIONS

## 5.1 TASK 1 - MODAL VIBRATION TESTS

Modal vibration tests were performed on the PODS-III assembly, and single strut frequencies were determined under various preload conditions. These test data were compared with analytical results obtained using linear finite element analysis theory, including the effects of preload.

The analytical models simulated the test configuration by including the accelerometer/clamp assembly that was attached to the fiberglass tube to monitor the strut's modal vibration. The results obtained confirmed the initial assumption of the importance of the effects of this assembly on the fundamental frequency and associated mode shape. As-built frequencies were predicted by excluding the lumped weight and demonstrated a 10 percent increase in the fundamental frequency for each preload case. This latter set of frequencies represents the strut's actual, unencumbered, fundamental frequency.

The fundamental modal response of the strut was dominated by the fiberglass tube for both orbit and launch strut configurations; however, in its orbit configuration, the strut's graphite tube also contributed. Analytical and test results compared favorably for all but one launch condition case. The analytical results differ most significantly from the test results for the orbit configuration due to "rattling" of the strut under low preload test conditions. Because of this phenomena and the excellent comparisons between other analytical and test cases, it is concluded that the analytical frequencies determined are accurate representations of the strut's fundamental frequencies.

The finite element model developed within the scope of this project is a basic model and is only adequate to represent fundamental strut behavior. The tests, however, demonstrated higher, more complex modal response including torsion and bending. No attempt was made to predict these higher modes of vibration. However, it is concluded, based on the strut's design, that the torsional vibration reported during the tests was a result of the accelerometer/clamp offset mass and not due to the strut's structural configuration.

Should the higher modes of the strut be of interest, it is recommended that a more detailed model be developed to determine the "range of interest" frequencies and associated mode shapes to assess the overall strut dynamic response under various preload conditions. In addition, tests should be performed at more preload points to compare with the analytical results and better define the strut's behavior under these conditions.

## 5.2 TASK 2 - BENEFIT STUDY

For the OTV, the largest benefits of using the PODS-III struts occur with fully loaded tanks at launch, at the lowest warm boundary temperatures, and at the lowest orbital resonances. Only minimal benefits accrue when the PODS-III supports are designed for an empty $LO_2$ tank at launch. However, the orbital resonances are so low, 4 Hz, the SOTA strut resonance value probably will have to be increased substantially (i.e., to 20 Hz) due to engine firings in orbit. On the other hand, the PODS-III nonshorted, orbit support resonance may not have to be increased since the orbit resonance rises to 35 Hz when shorted under typical orbital engine acceleration loads. If this occurs, the PODS-III support heat leak advantage will increase over the SOTA strut for an empty tank launch.

For the SSS tanks the same trends hold true. In addition, the non-vapor-cooled PODS-III supports have a larger relative advantage over the SOTA struts than when they are vapor cooled.

Since the cost differential is small between fabricating PODS-III or SOTA struts (Ref. 2) and the differential is an insignificant fraction of the total cryogen tank costs, it is recommended that the PODS supports be used for all OTV and SSS tank applications. The PODS-IV version currently being developed with potentially a side-load shorting resistance ten times that of PODS-III is the recommended design choice for these large tank applications.

## Section 6
## REFERENCES


1. Parmley, R. T., Feasibility Study for Long Lifetime Helium Dewar, NASA CR 166254, Dec 1981.

2. Parmley, R. T., Passive Orbital Disconnect Strut (PODS-III) Structural and Thermal Test Program, NASA CR 166473, Mar 1983.

3. Parmley, R. T., Passive Orbital Disconnect Strut (PODS-III) Structural Test Program, NASA CR 177325, Jan 1985.

4. Vanderplaats, G. N., and Moses, F., "Structural Optimization by Methods of Feasible Directions," Computers & Structures, Vol. 3, pp. 739-755, 1973.

5. Vanderplaats, G. N., "COMNIN-A FORTRAN Program for Constrained Function Minimization; User's Manual," NASA TM X-62,282, Ames Research Center, Moffett Field, CA, Aug 1973; version updated in Mar 1975.

6. Zoutendijk, G., Methods of Feasible Directions, Elsevier Publishing Co., Amsterdam, 1960.

7. Inhouse communication with Space Station Group.

8. Advanced Maneuvering Propulsion System, LMSC-687208, 1969.

9. Havas, T. W., ASTRO Program Manual, Lockheed Missiles & Space Company, Inc., Version J (J-073185).

# Section 7
## APPENDIX A - MODAL RESONANCE TEST RESULTS

The admittance function and phase plots given here are test data from Section 3.3. The test numbers shown on the curves refer to Table 3-2. The axes shown give the accelerometer locations and directions. For the phase plots, when the curve hits the +180 deg or -180 deg line and jumps abruptly to the other extreme, it is only an artifact of the plot routine and does not represent a phase shift.

ORIGINAL PAGE IS
OF POOR QUALITY

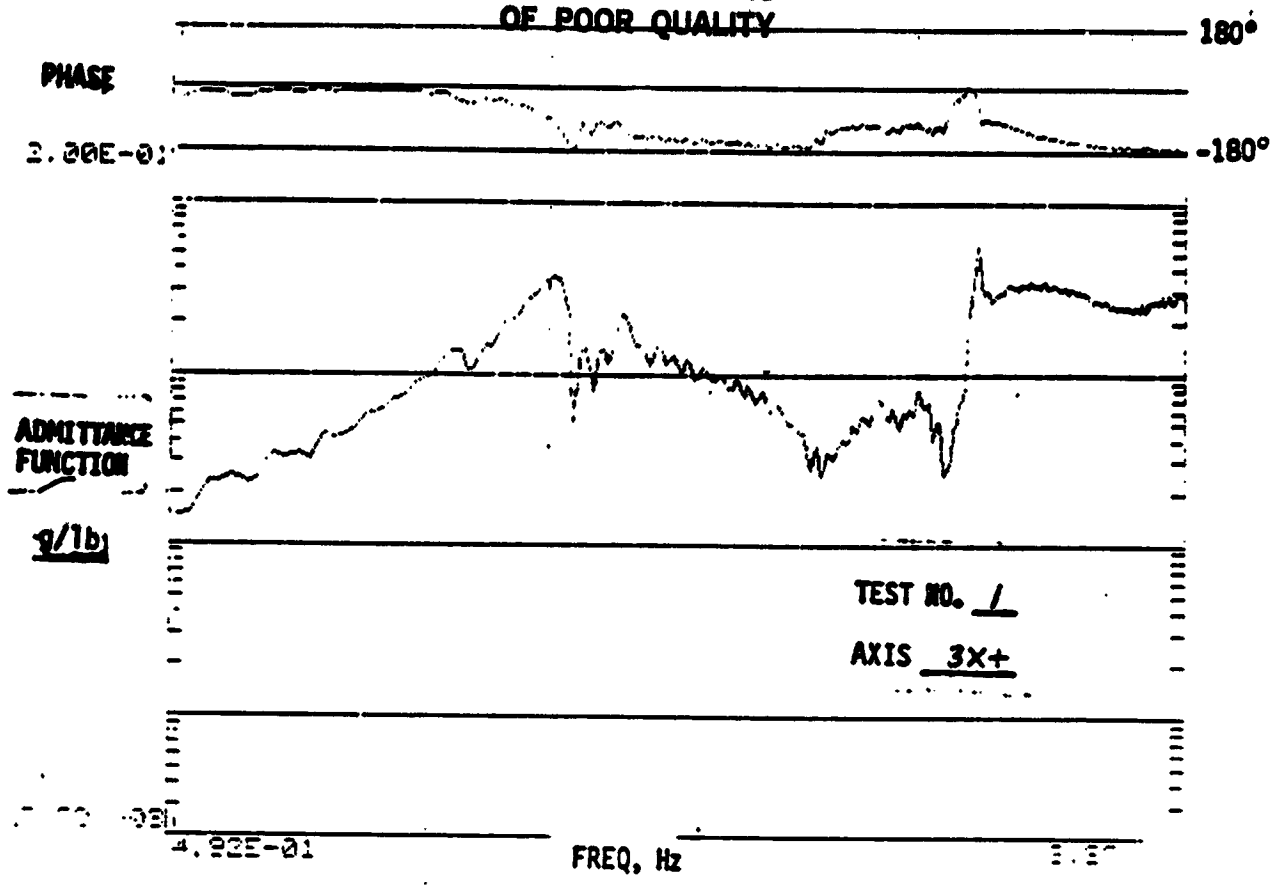


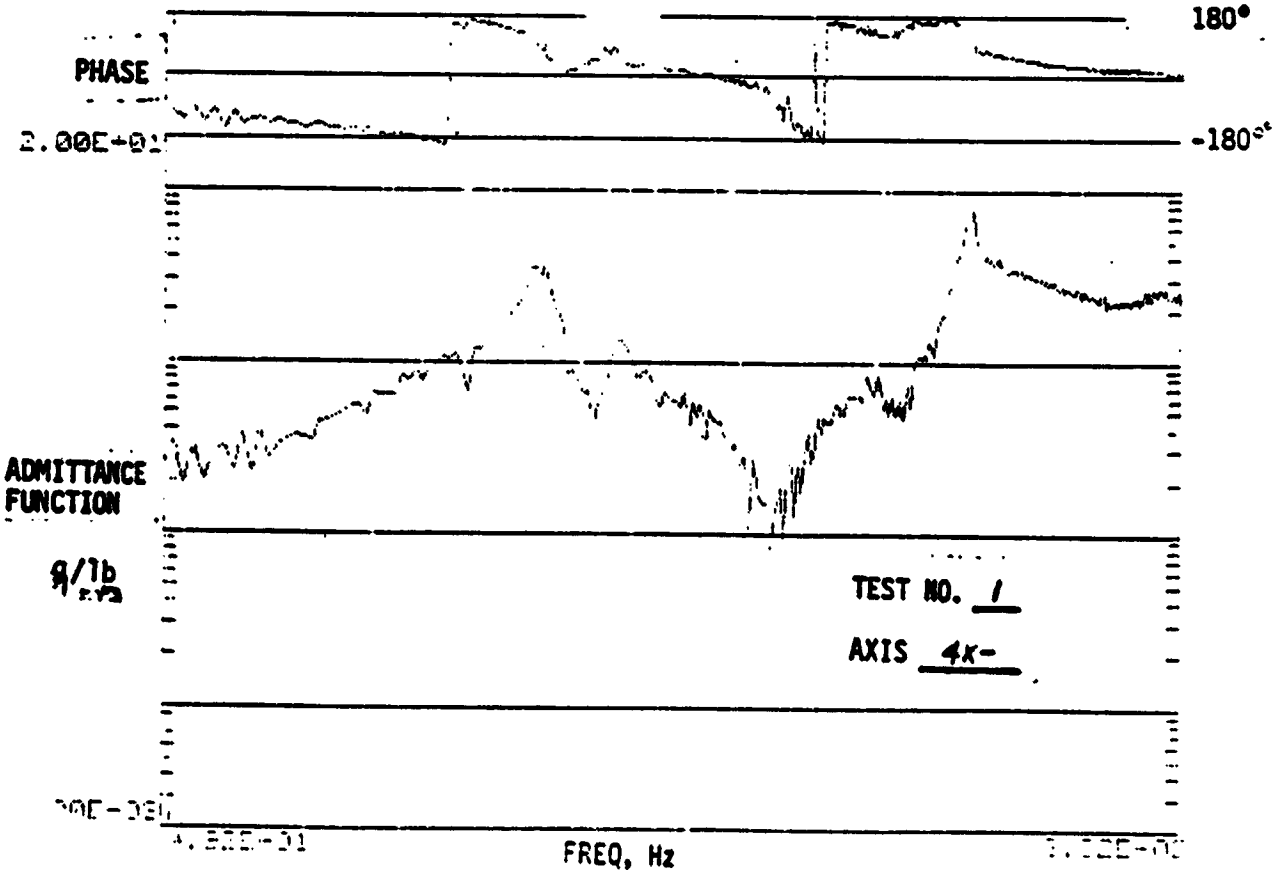

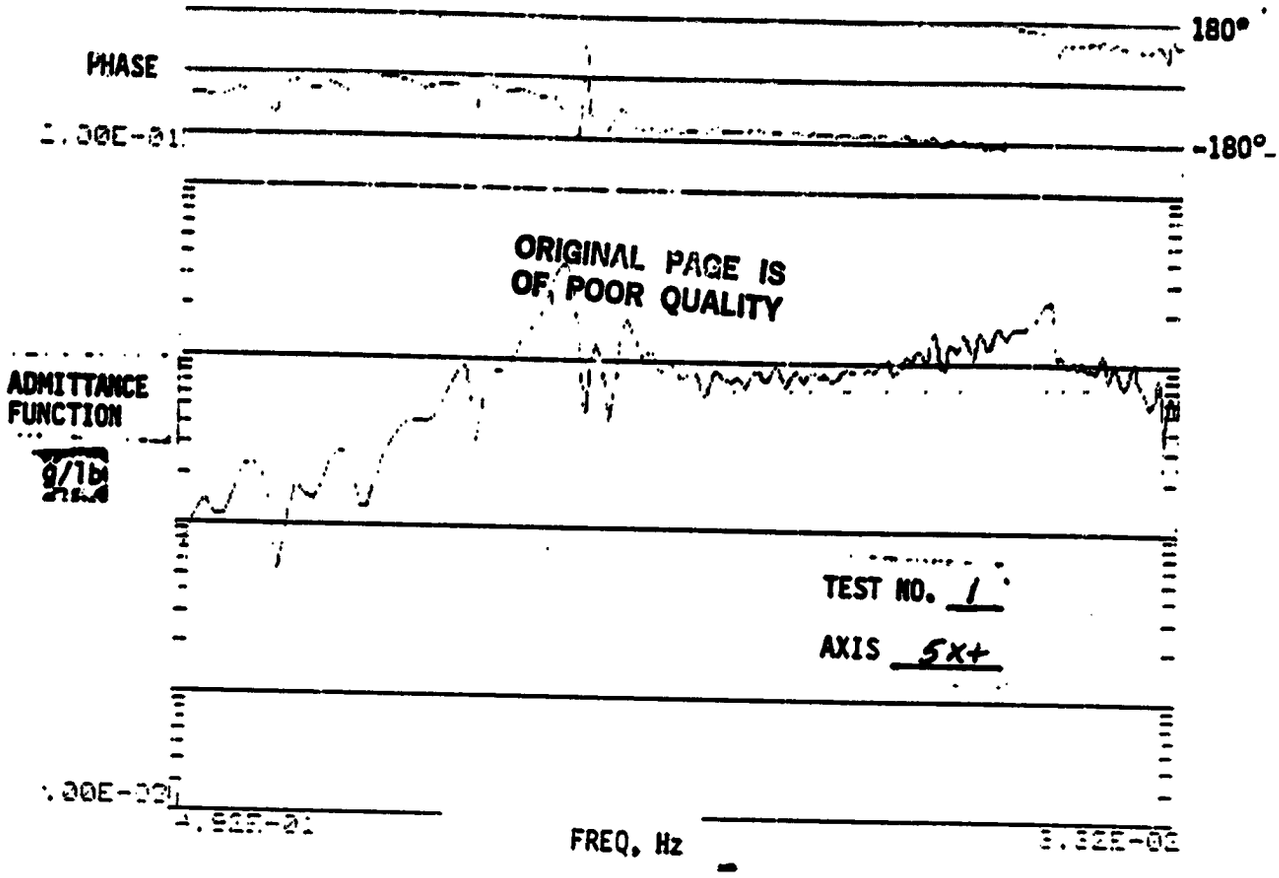




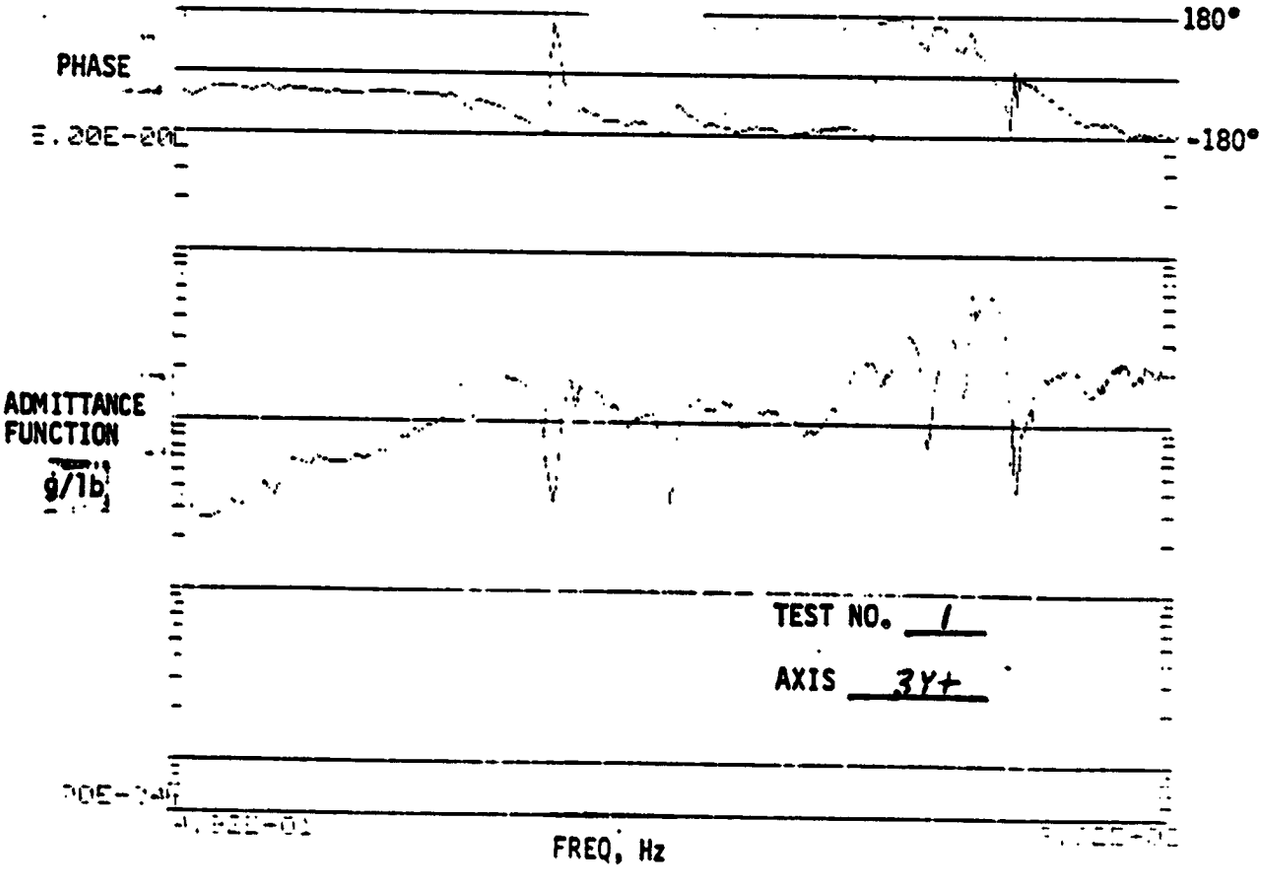

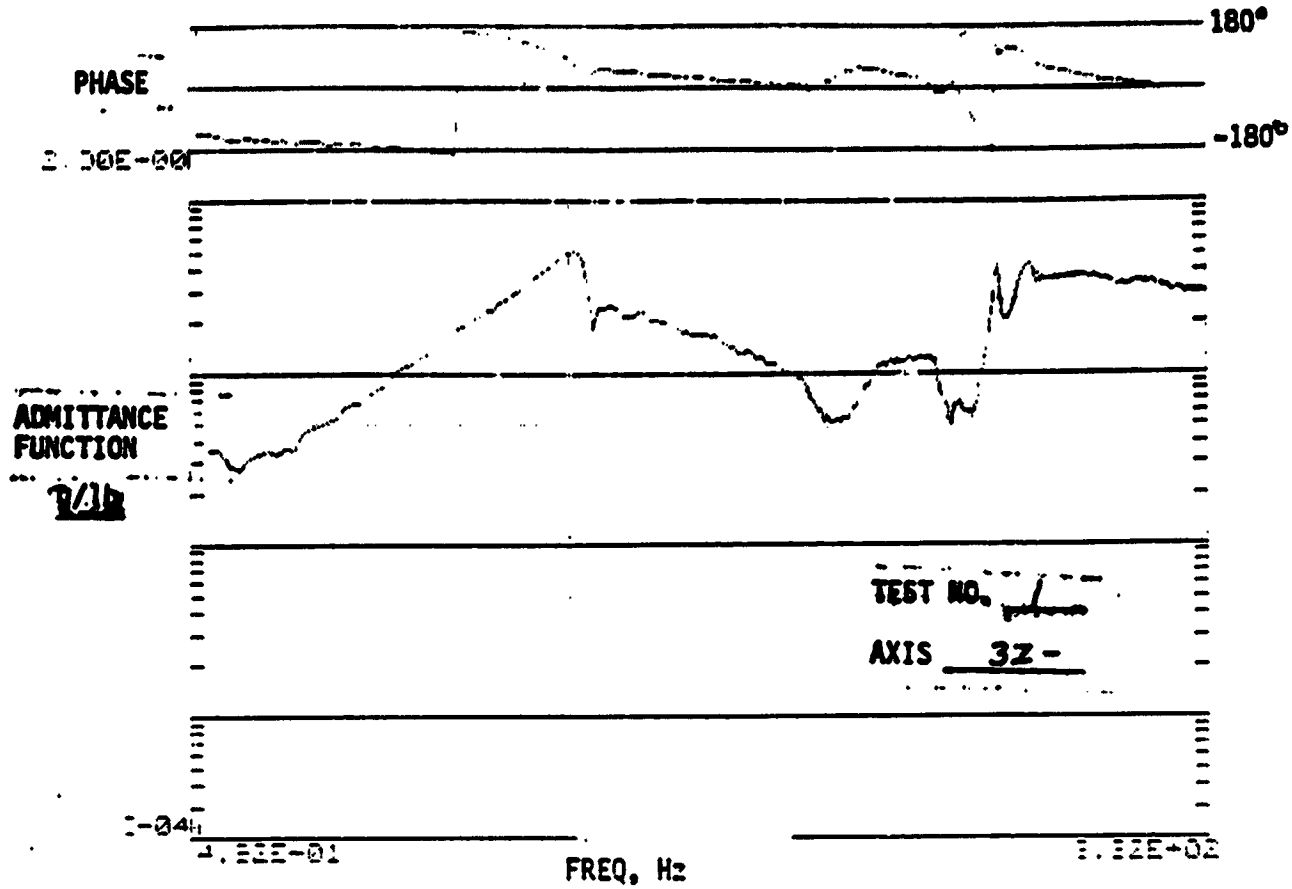


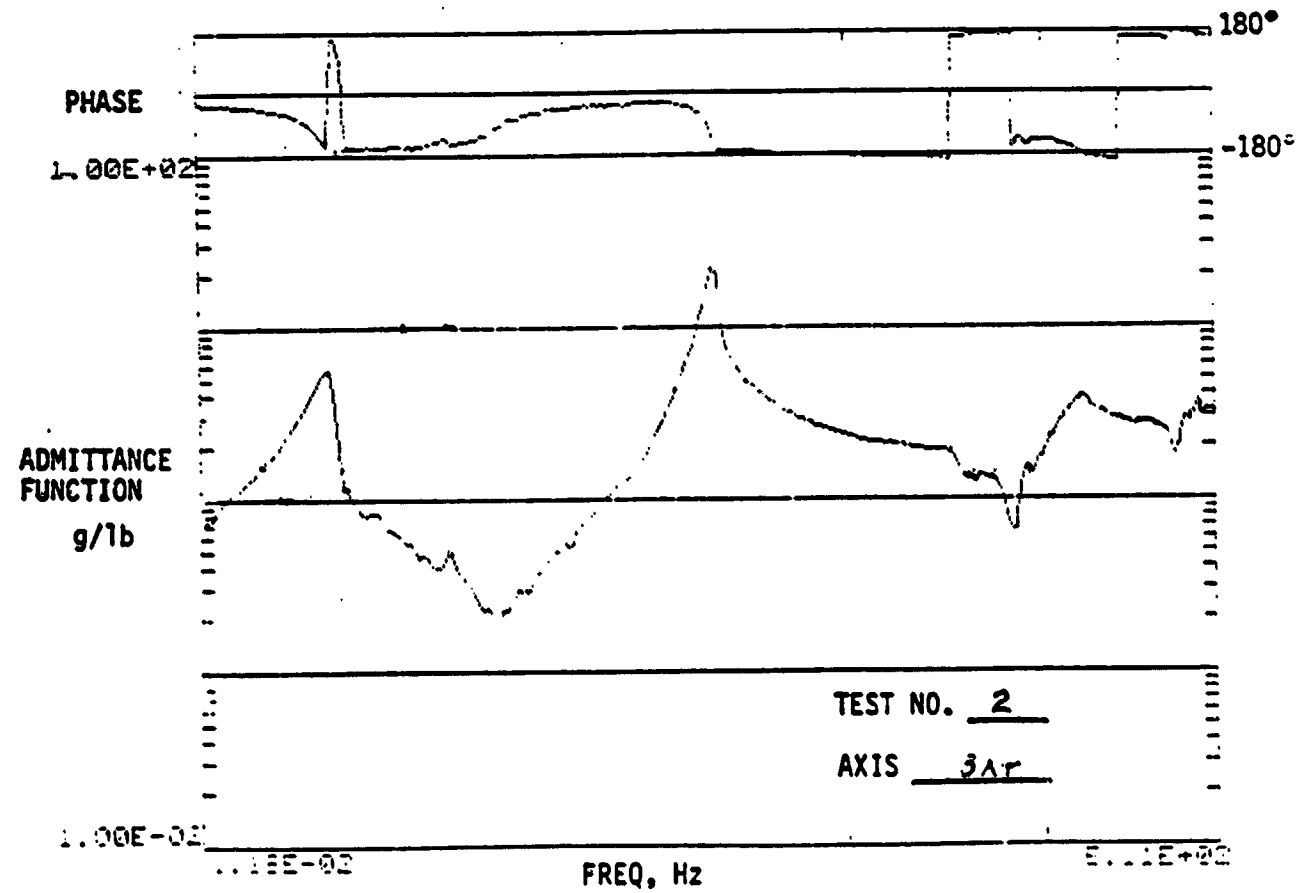

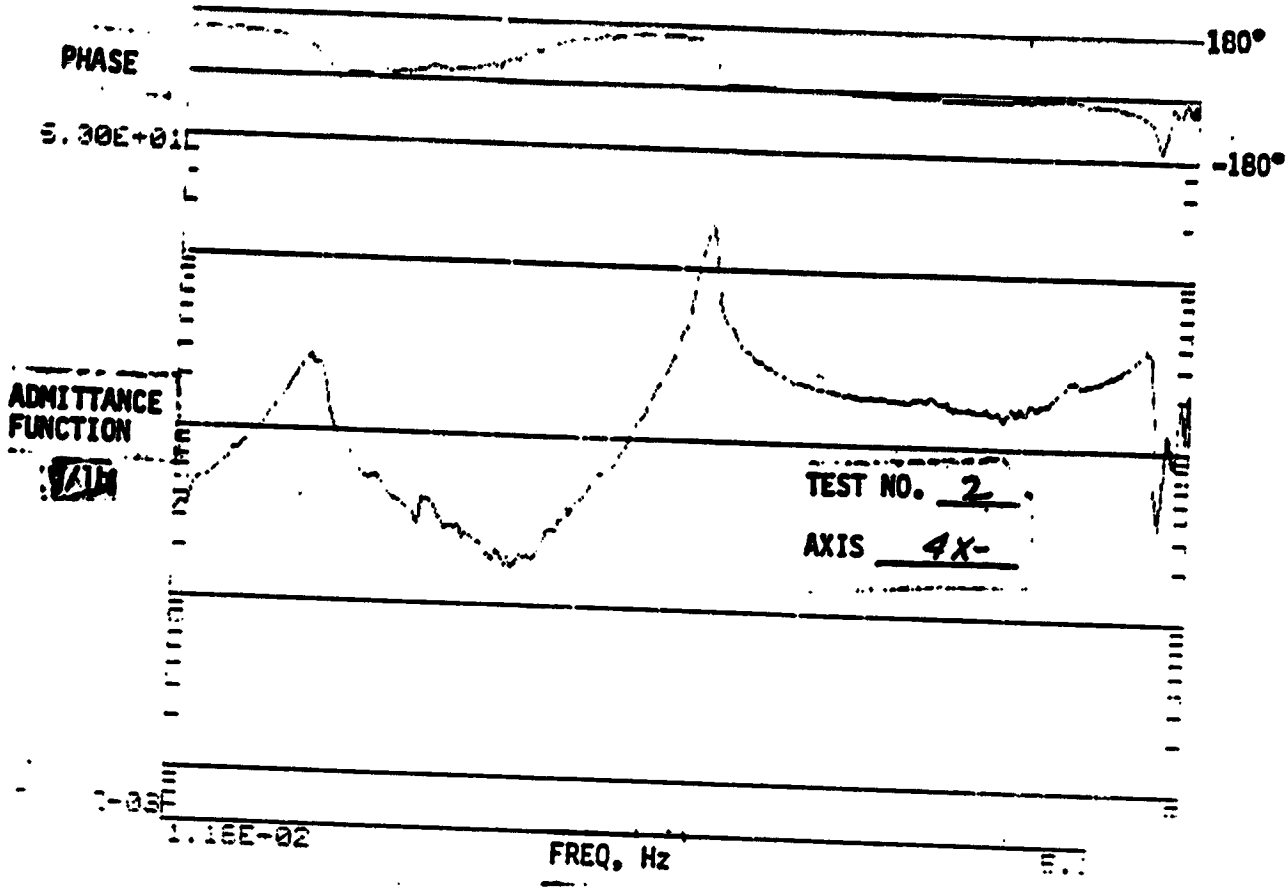


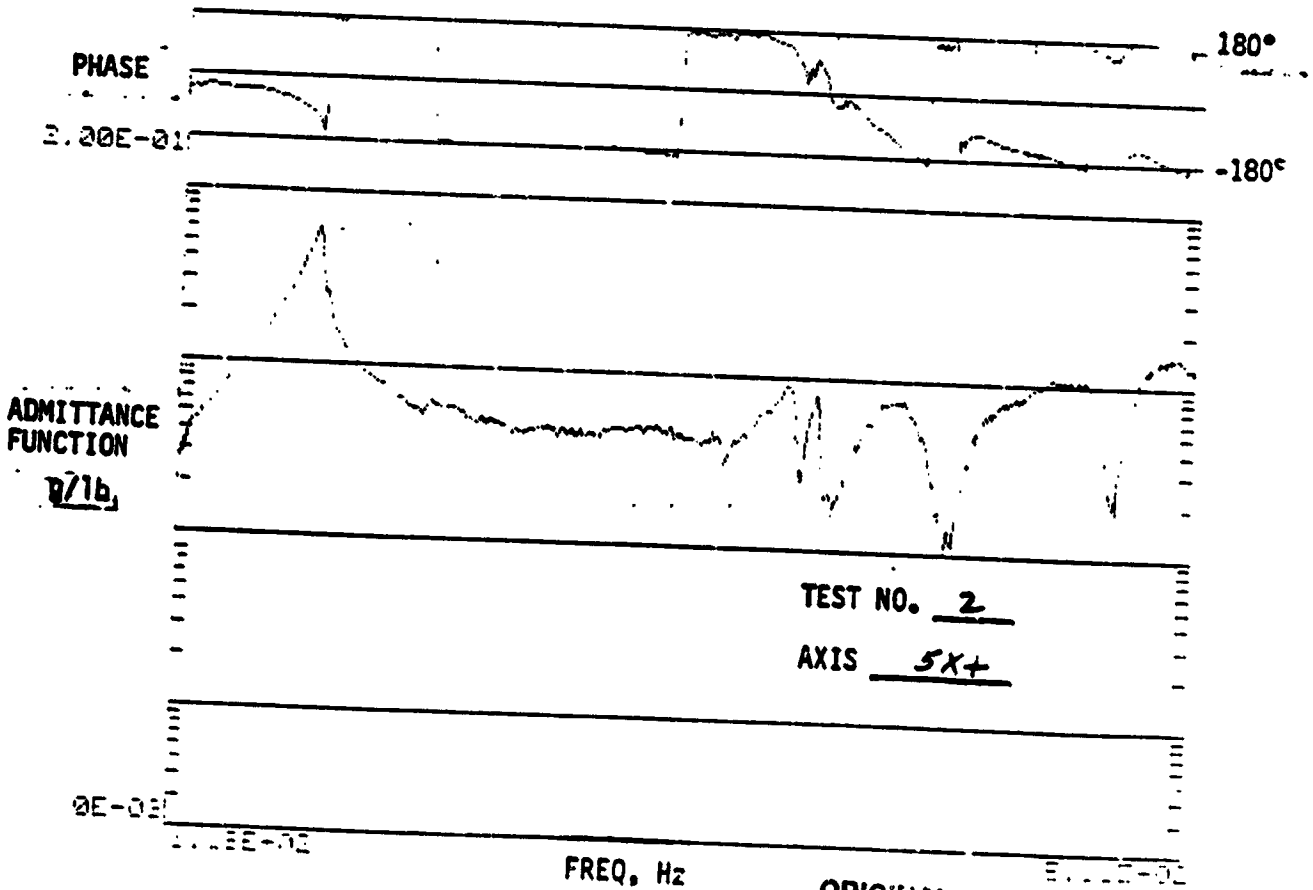

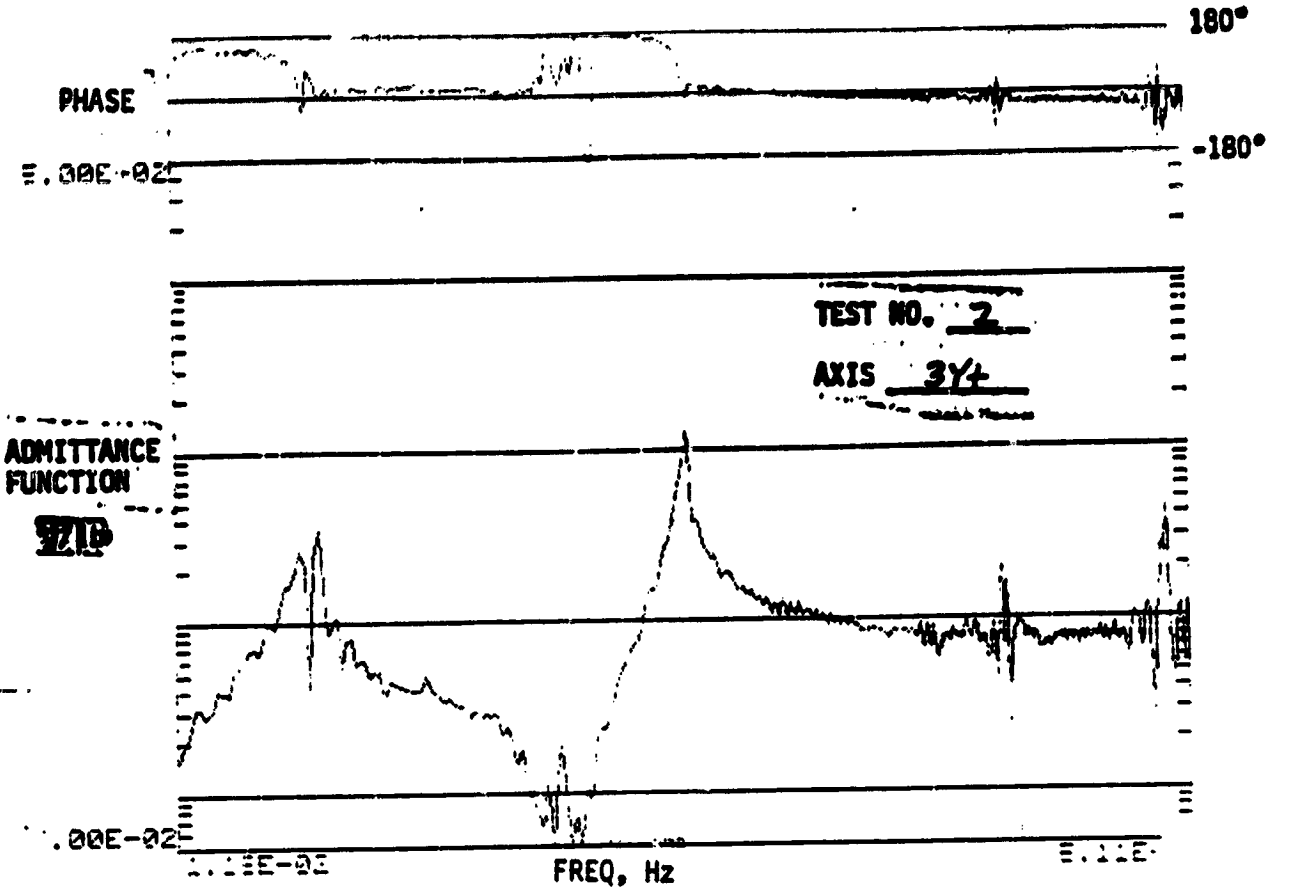
180°
PHASE
-180°
TEST NO. 2
AXIS 3Y+
ADMITTANCE FUNCTION
FREQ, Hz

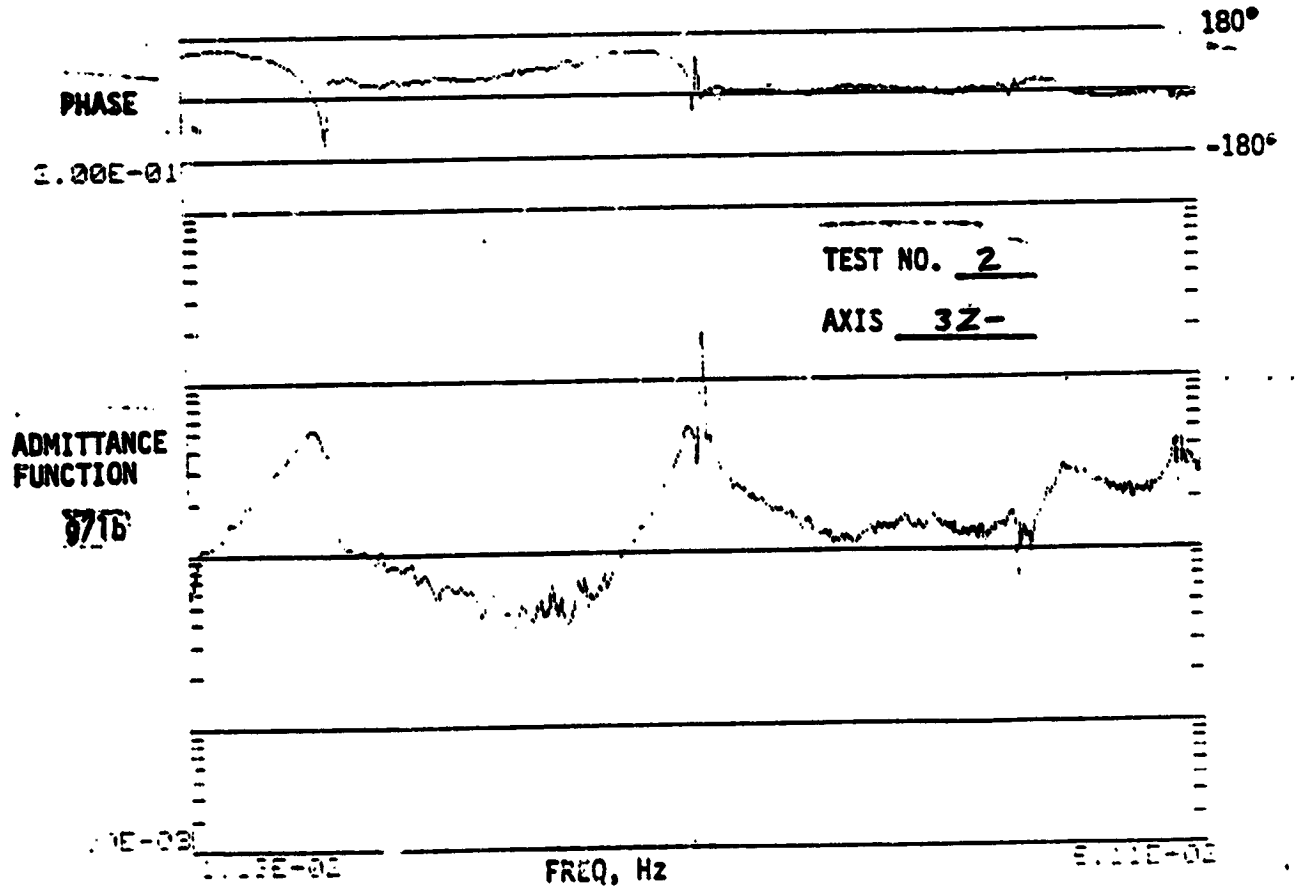
180°
PHASE
-180°
TEST NO. 2
AXIS 3Z-
ADMITTANCE FUNCTION
FREQ, Hz

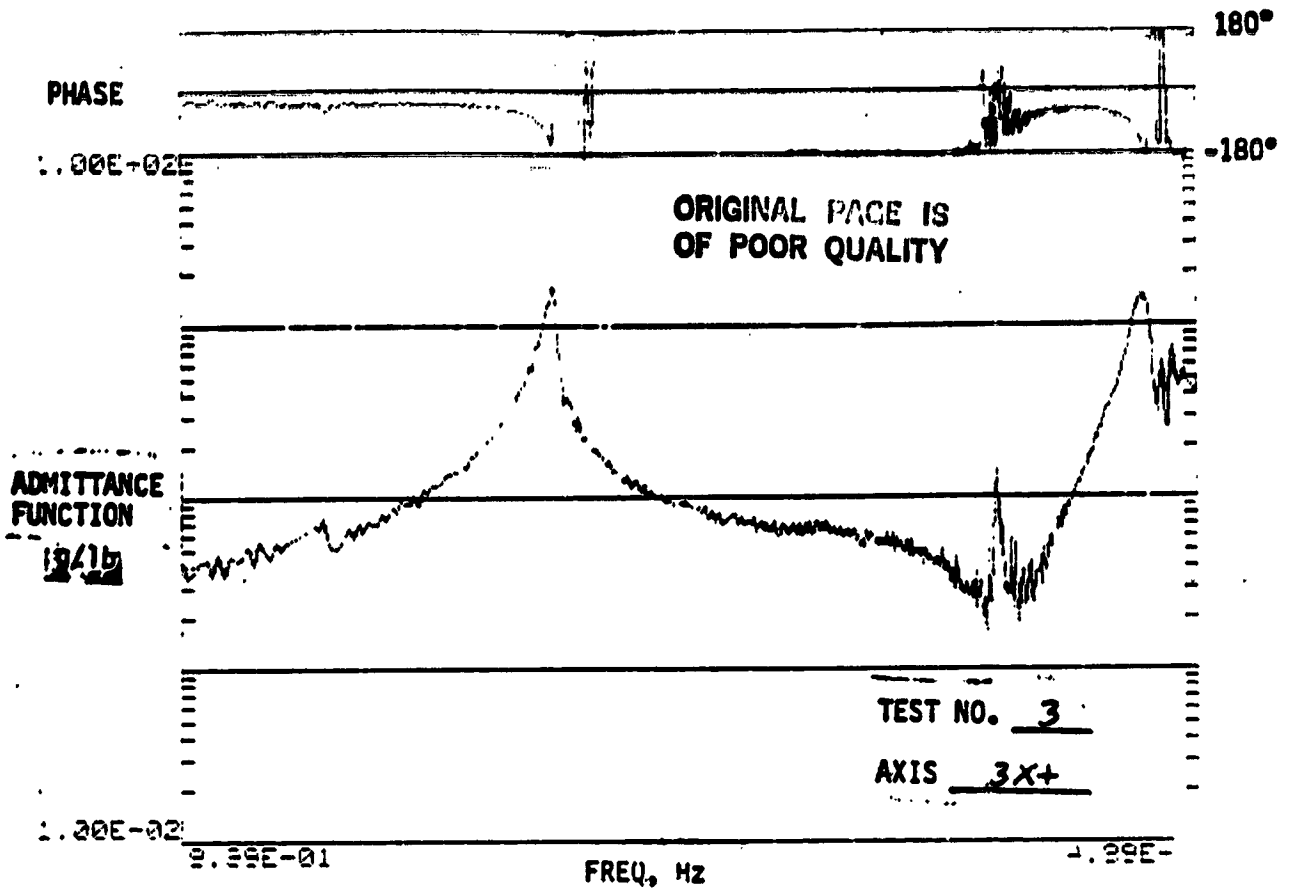
180°
PHASE
-180°
1.00E+02
ORIGINAL PAGE IS
OF POOR QUALITY
ADMITTANCE
FUNCTION
g/lb
TEST NO. 3
AXIS 3X+
1.00E-02
9.99E-01
FREQ, Hz

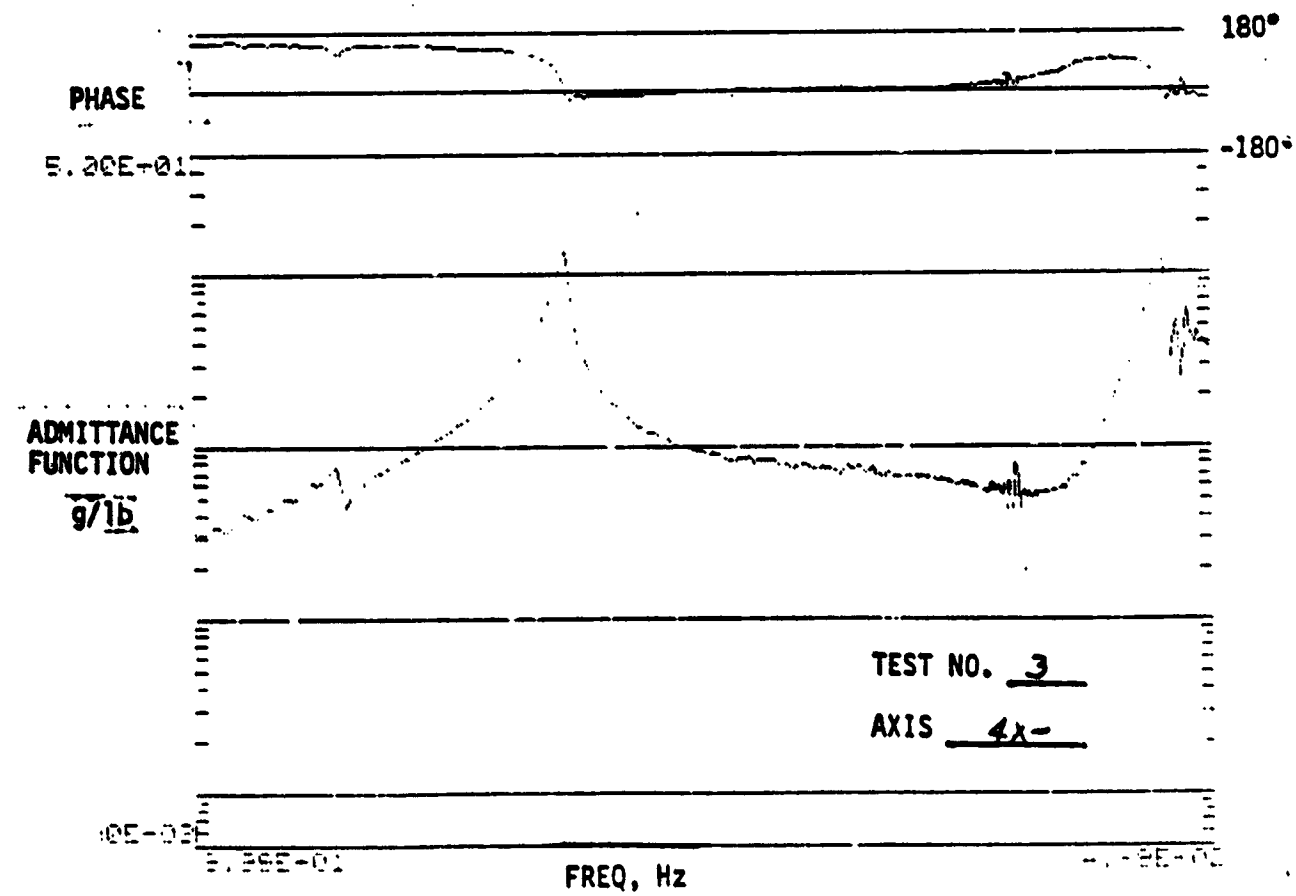
180°
PHASE
-180°
5.00E+01
ADMITTANCE
FUNCTION
g/lb
TEST NO. 3
AXIS 4X-
FREQ, Hz

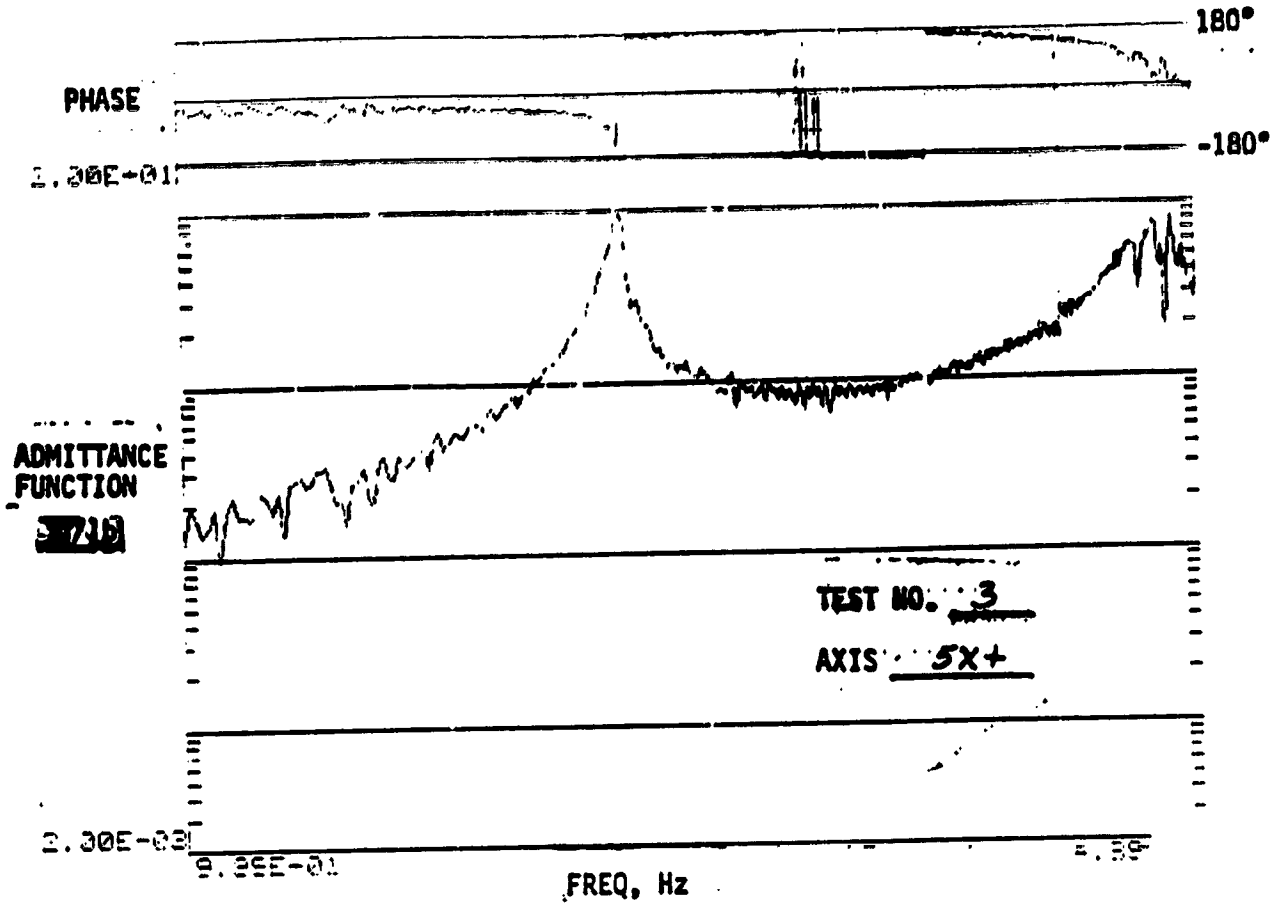
180°
PHASE
-180°
1.00E-01
ADMITTANCE
FUNCTION
g/lb
TEST NO. 3
AXIS 5X+
2.30E-03
FREQ, Hz

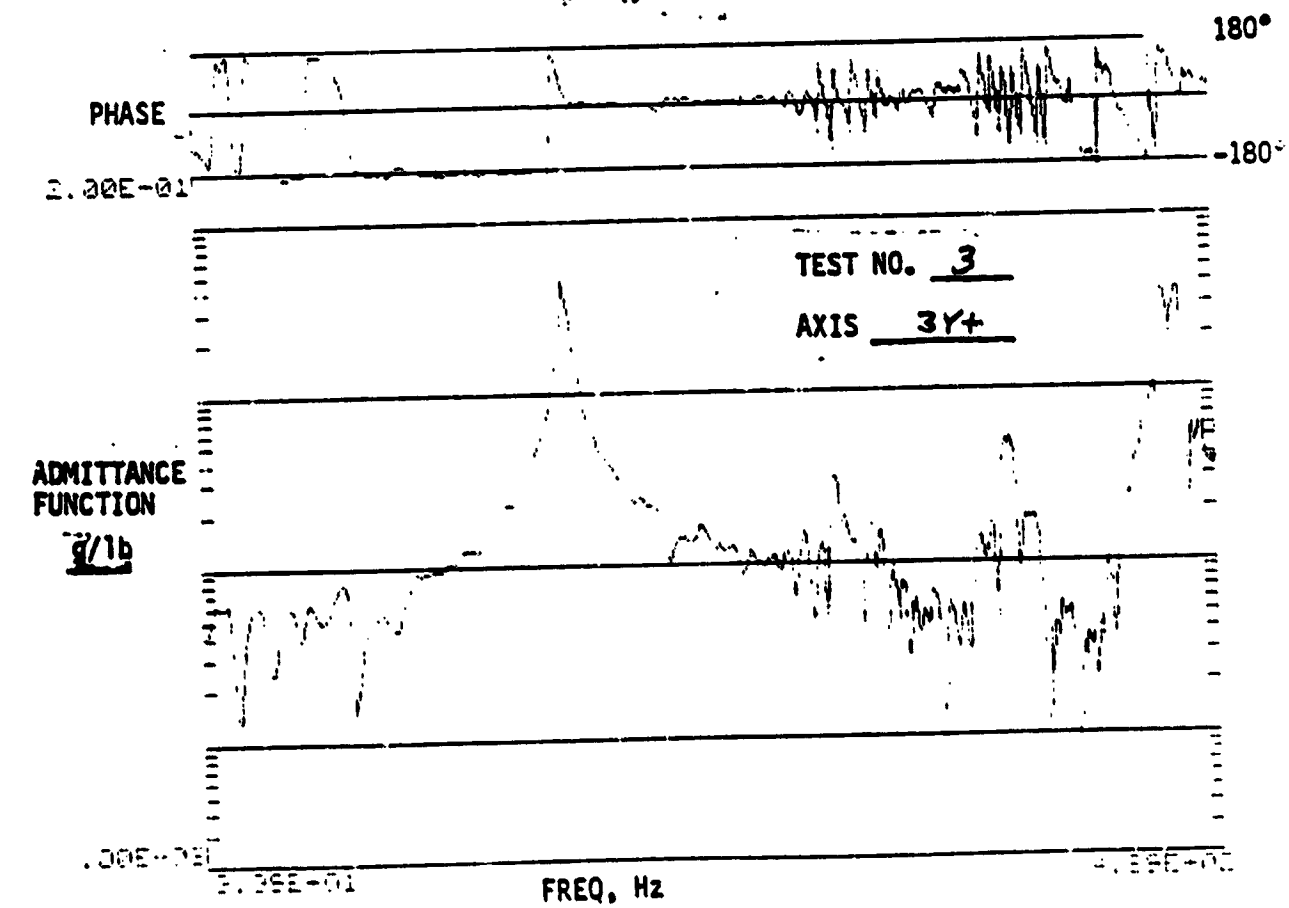
180°
PHASE
-180°
1.00E-01
TEST NO. 3
AXIS 3Y+
ADMITTANCE
FUNCTION
g/lb
FREQ, Hz

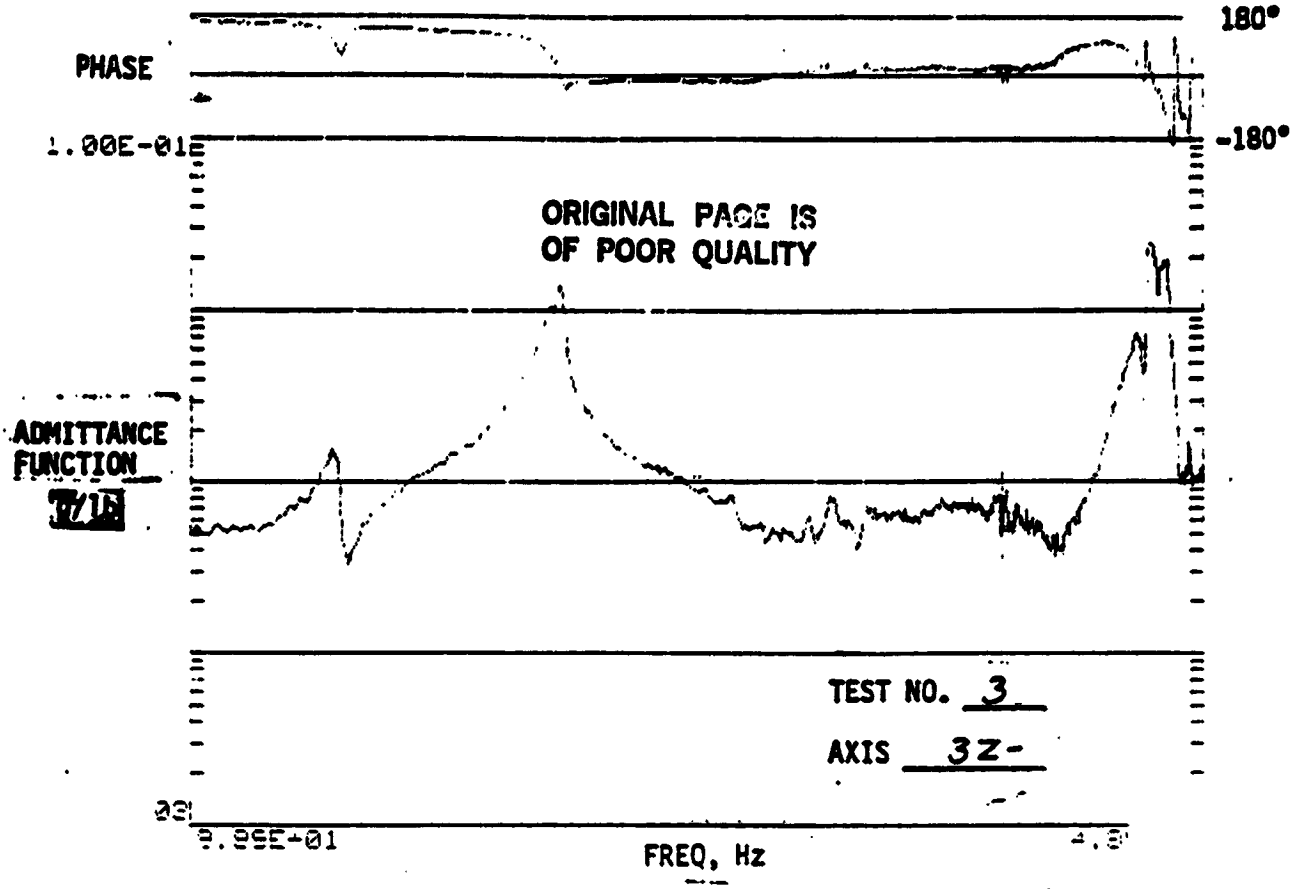
PHASE
180°
-180°
1.00E-01
ORIGINAL PAGE IS
OF POOR QUALITY
ADMITTANCE
FUNCTION
g/lb
TEST NO. 3
AXIS 3Z-
FREQ, Hz

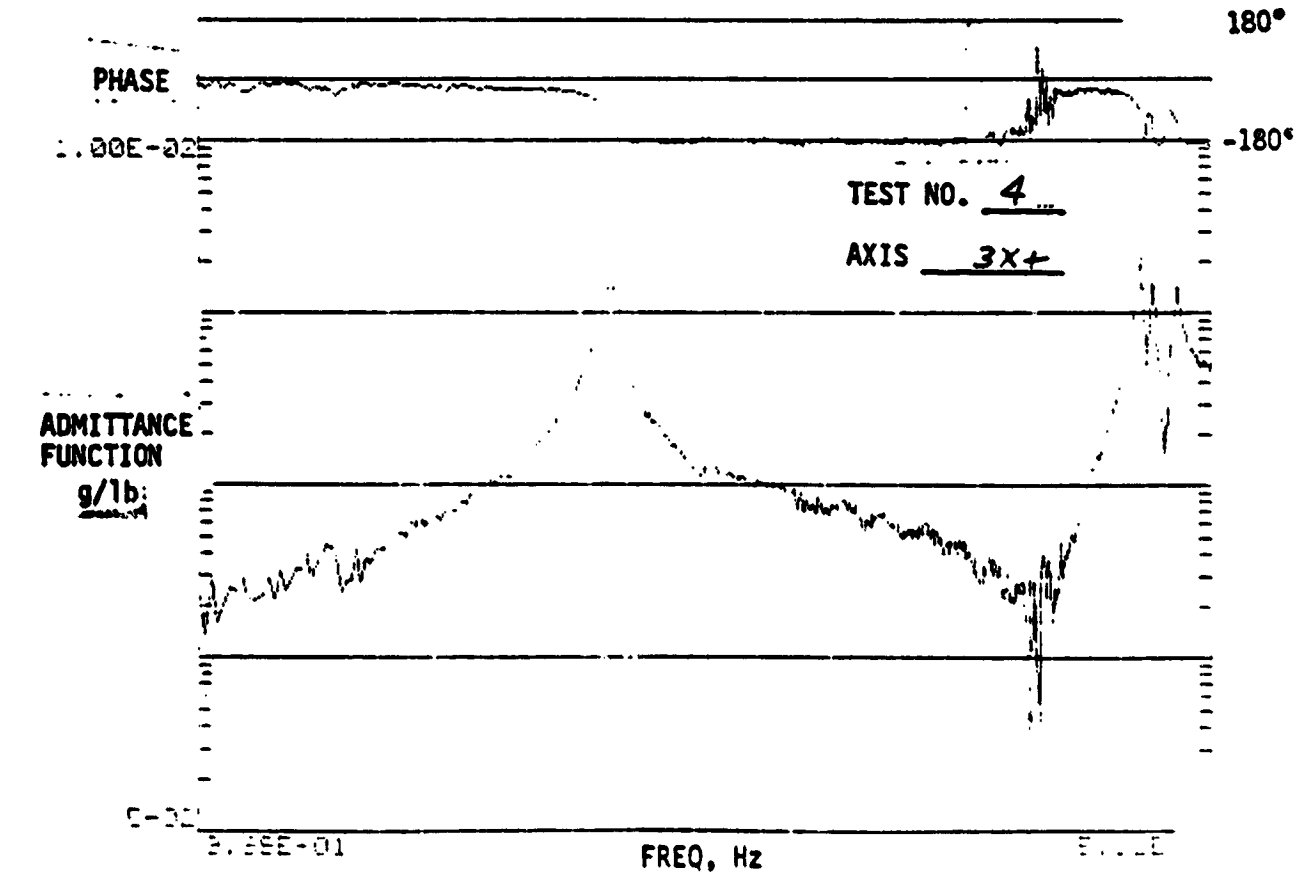
PHASE
180°
-180°
1.00E-02
TEST NO. 4
AXIS 3X+
ADMITTANCE
FUNCTION
g/lb
FREQ, Hz

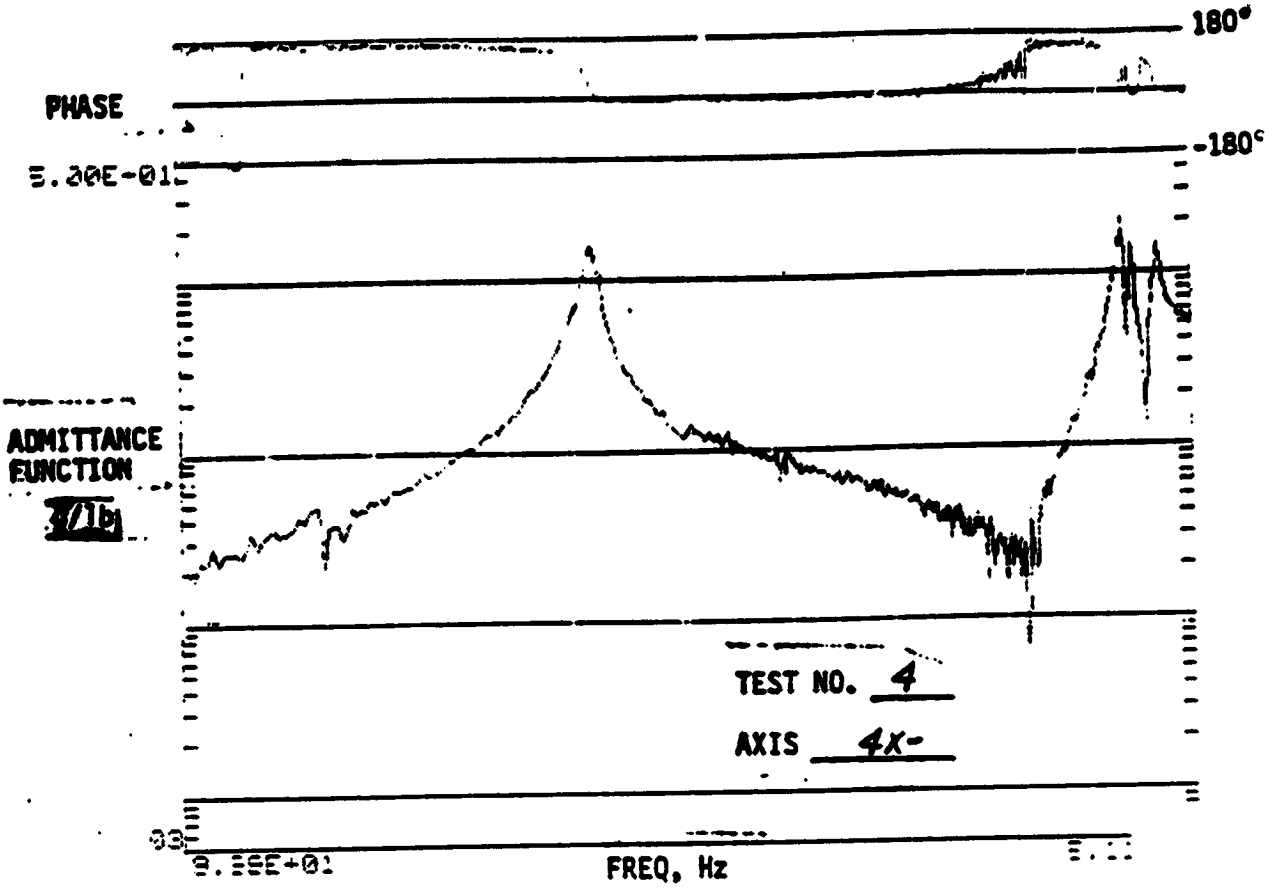
180°
PHASE
-180°
5.00E-01
ADMITTANCE FUNCTION
g/lb
TEST NO. 4
AXIS 4X-
FREQ, Hz

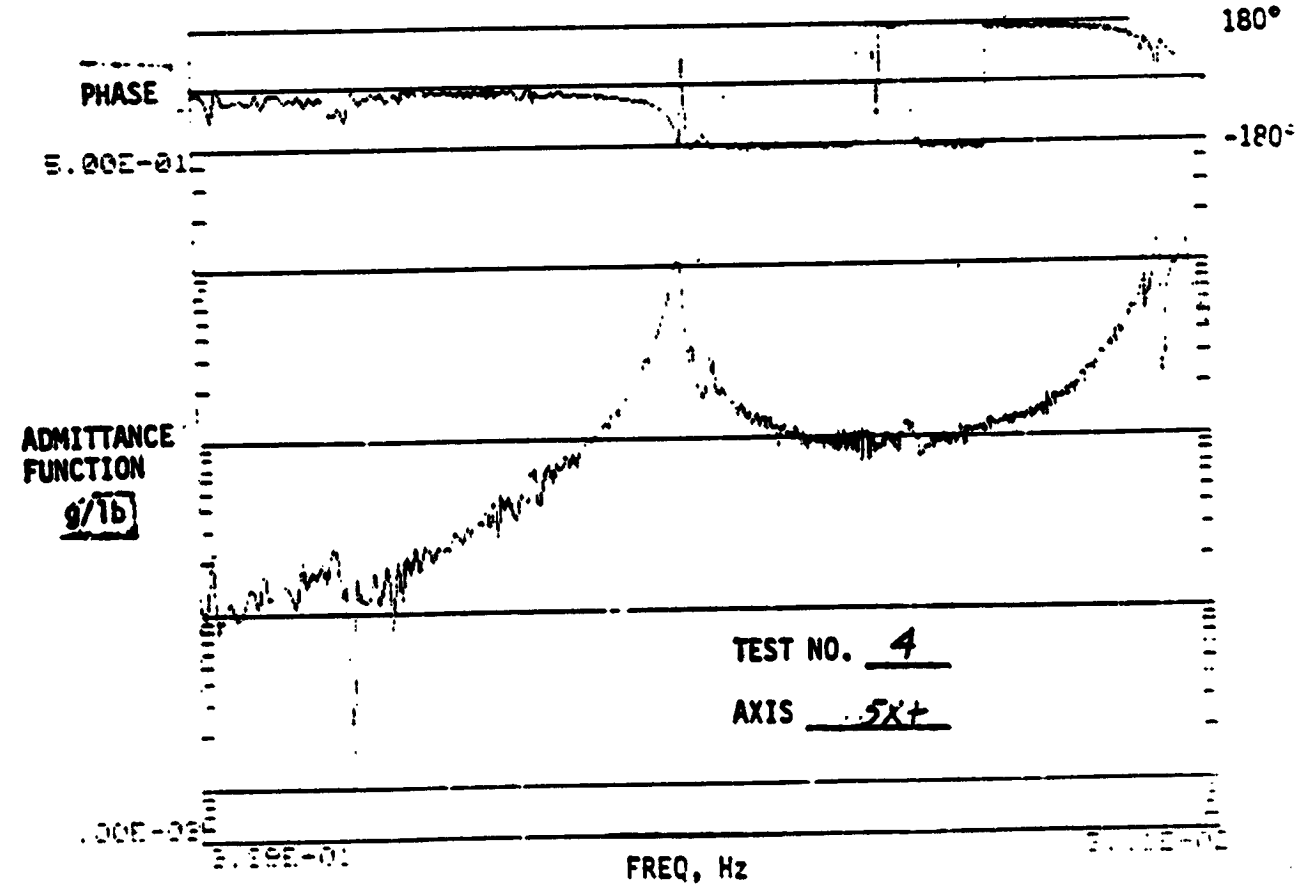
180°
PHASE
-180°
5.00E-01
ADMITTANCE FUNCTION
g/lb
TEST NO. 4
AXIS 5X+
FREQ, Hz

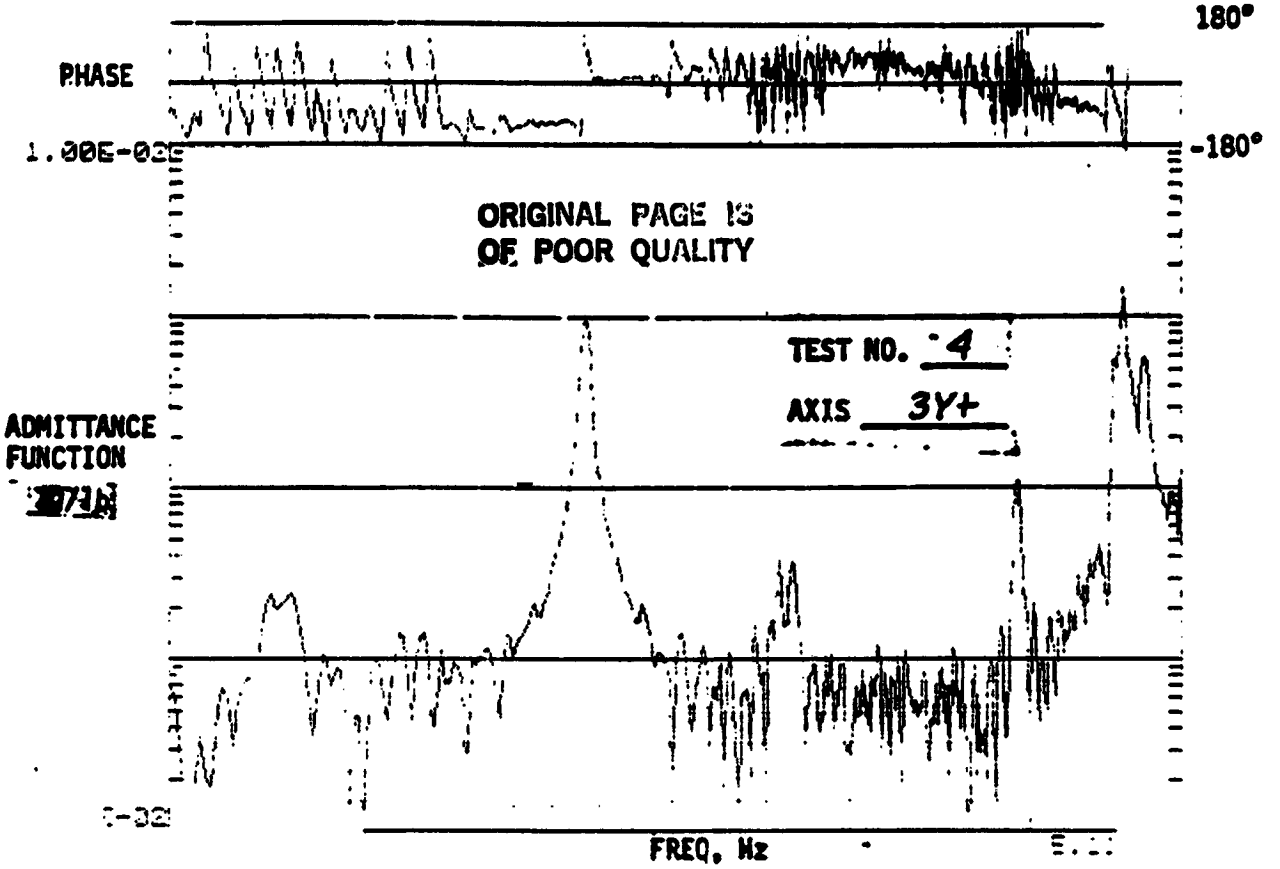
PHASE
180°
-180°
ORIGINAL PAGE IS
OF POOR QUALITY
TEST NO. 4
AXIS 3Y+
ADMITTANCE
FUNCTION
FREQ, Hz

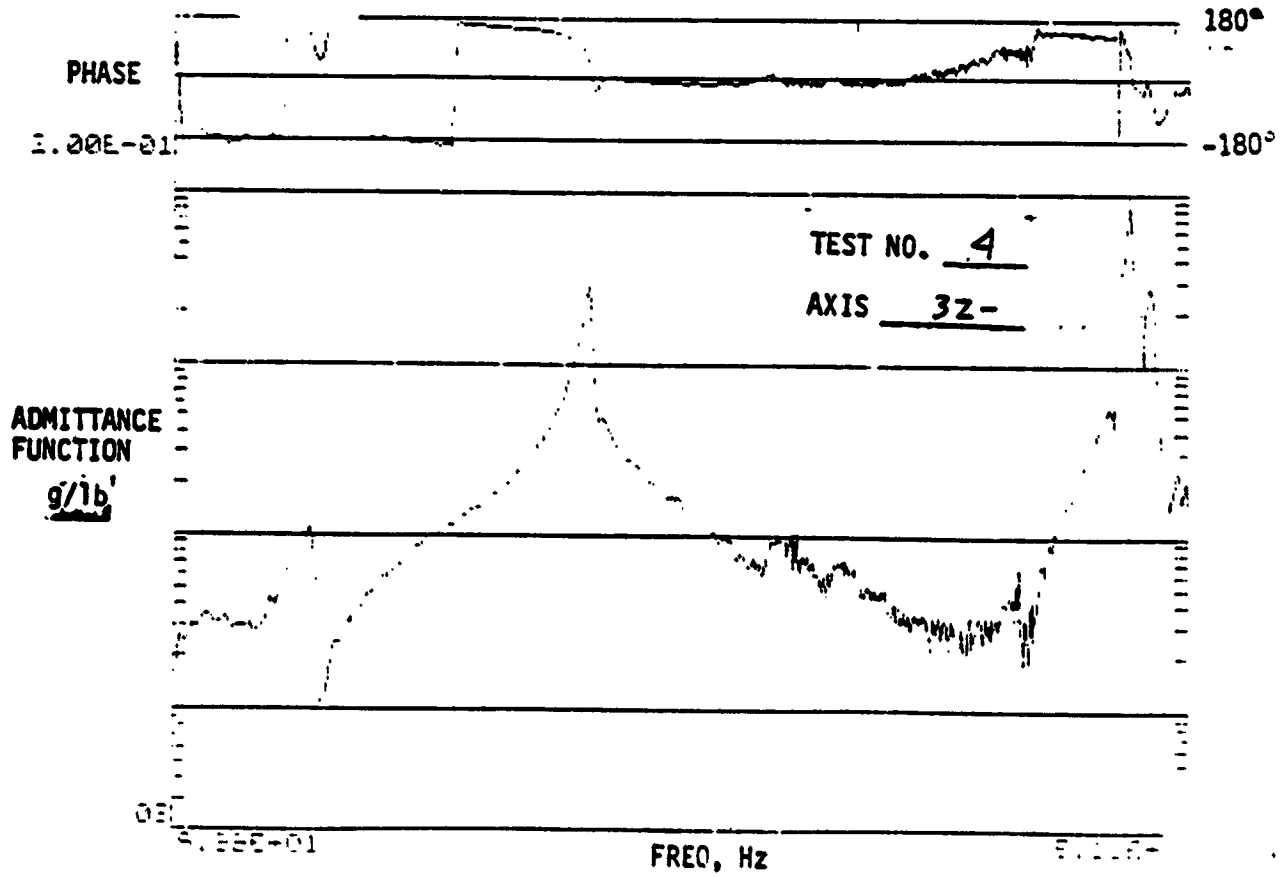
PHASE
180°
-180°
TEST NO. 4
AXIS 3Z-
ADMITTANCE
FUNCTION
g/lb
FREQ, Hz

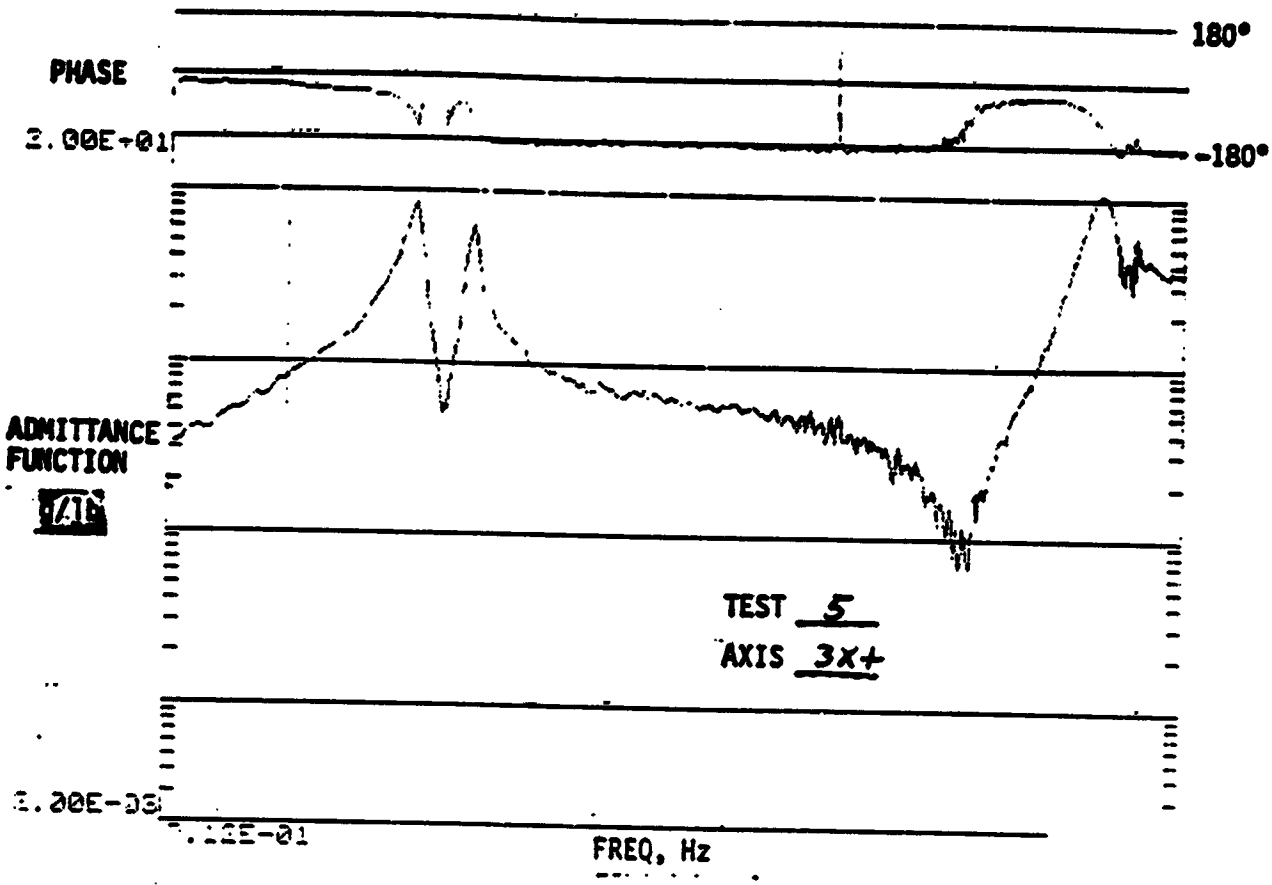
PHASE
180°
-180°
2.00E+01
ADMITTANCE FUNCTION
g/lb
TEST 5
AXIS 3x+
FREQ, Hz

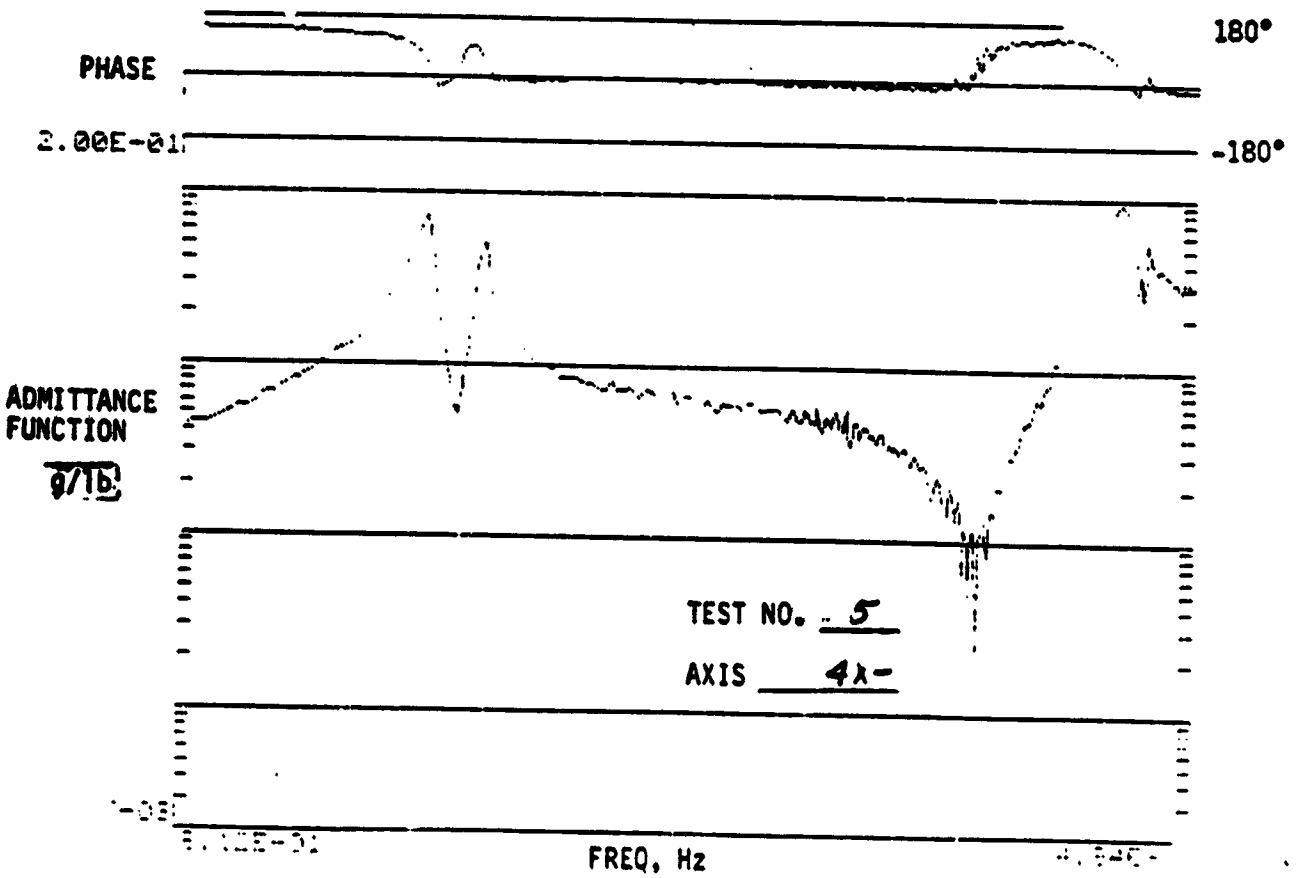
PHASE
180°
-180°
2.00E-01
ADMITTANCE FUNCTION
g/lb
TEST NO. 5
AXIS 4x-
FREQ, Hz

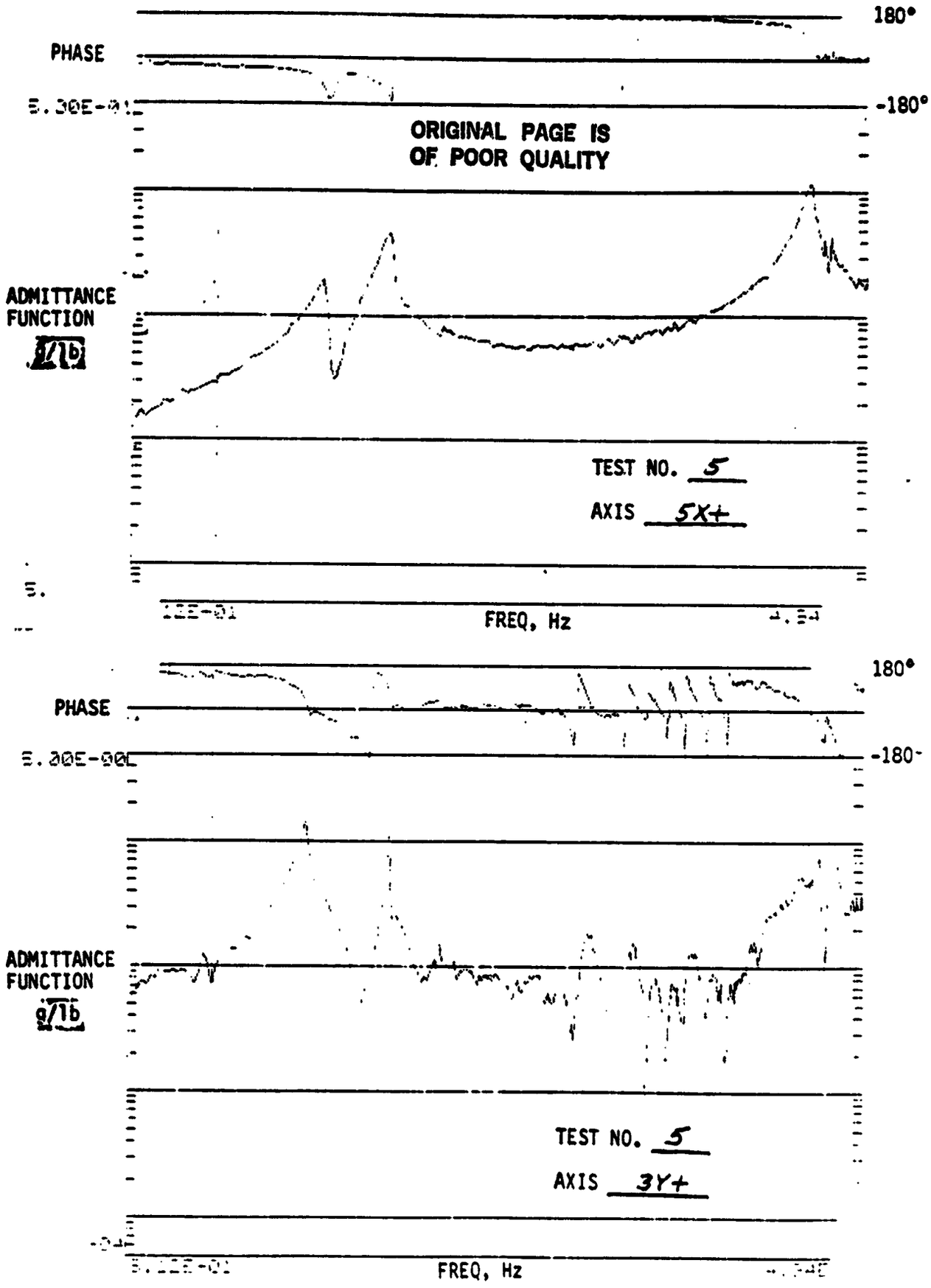
180°
PHASE
-180°
ORIGINAL PAGE IS
OF POOR QUALITY
ADMITTANCE
FUNCTION
g/lb
TEST NO. 5
AXIS 5X+
FREQ, Hz
180°
PHASE
-180°
ADMITTANCE
FUNCTION
g/lb
TEST NO. 5
AXIS 3Y+
FREQ, Hz

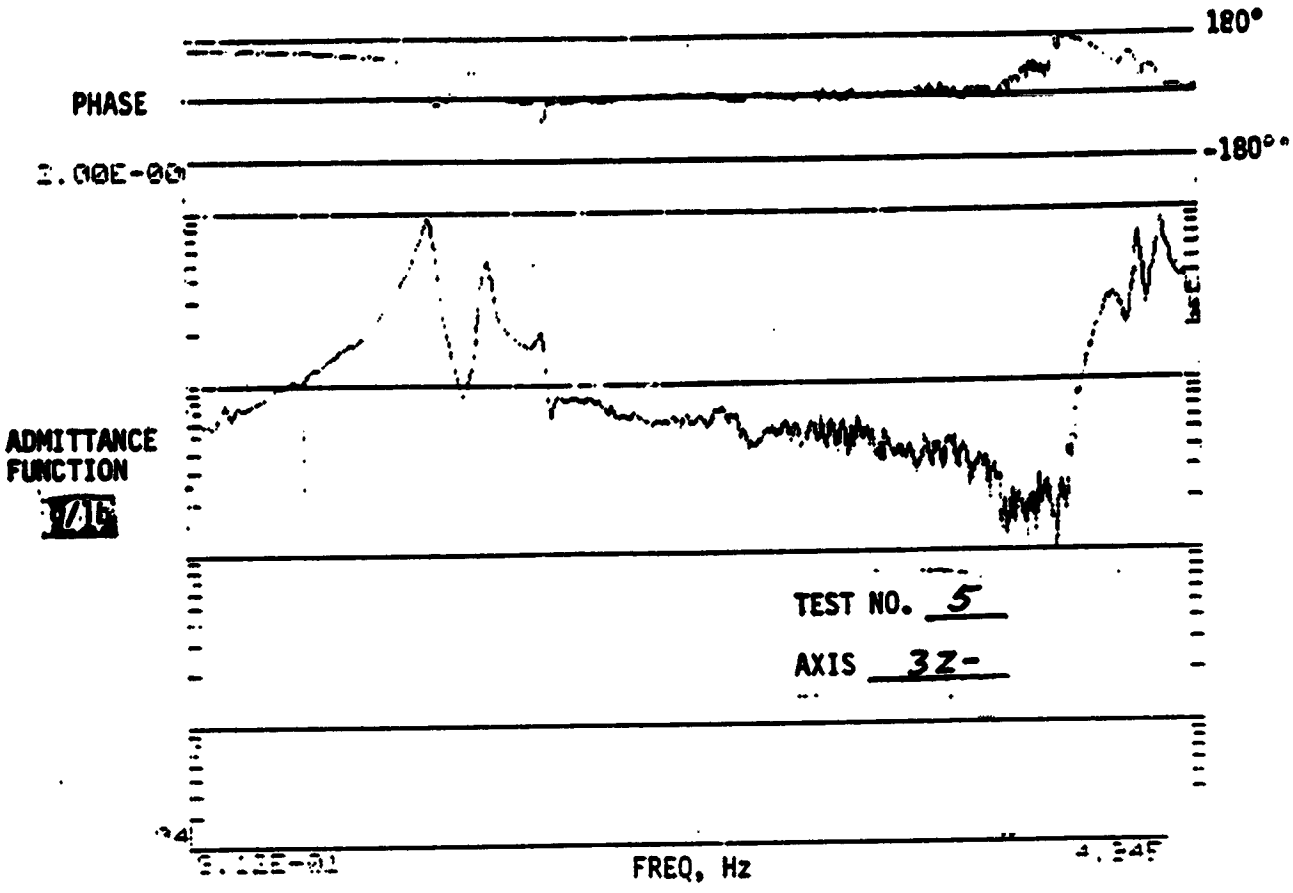
180°
PHASE
-180°
ADMITTANCE
FUNCTION
TEST NO. 5
AXIS 3Z-
FREQ, Hz

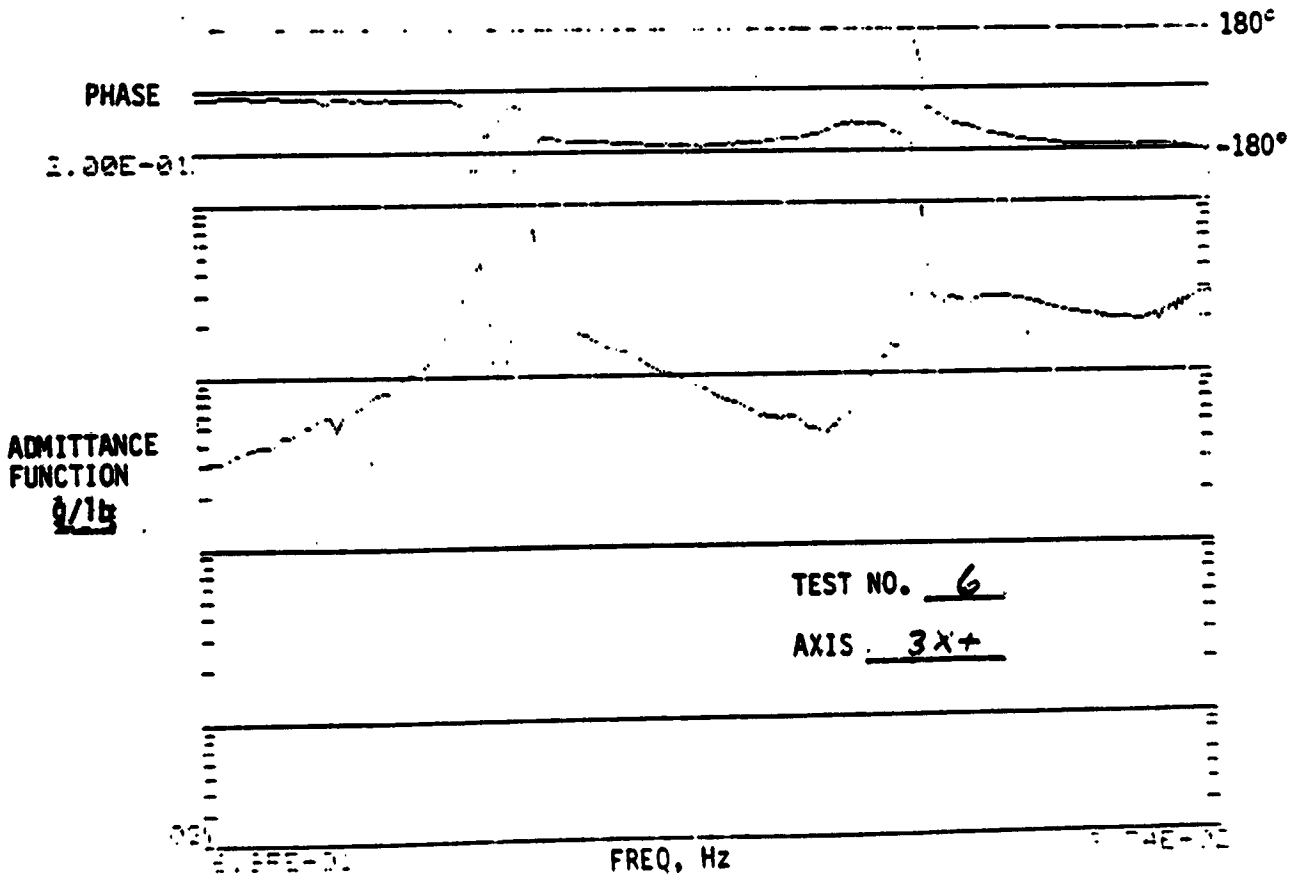
180°
PHASE
-180°
ADMITTANCE
FUNCTION
TEST NO. 6
AXIS 3X+
FREQ, Hz

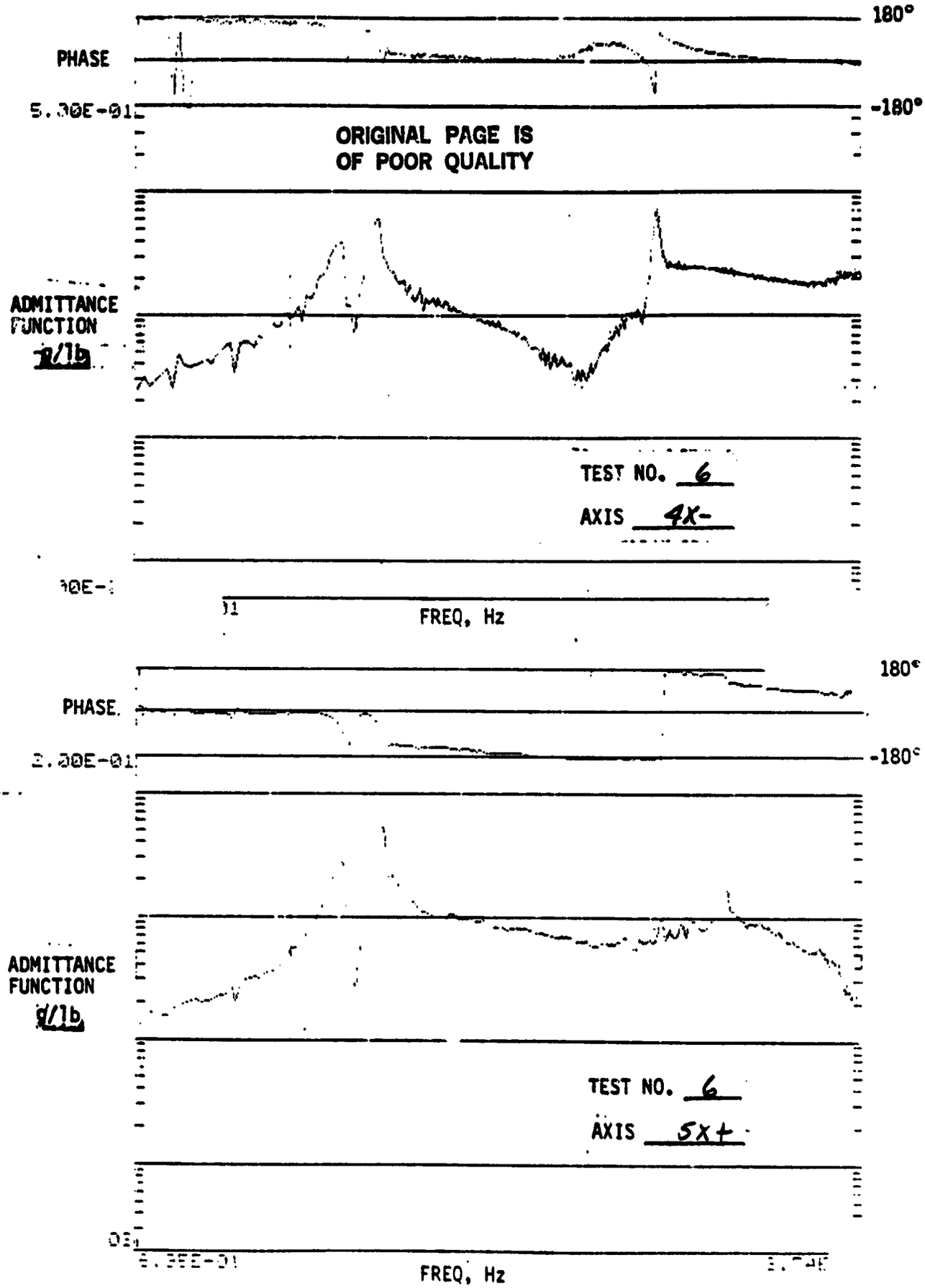
180°
PHASE
-180°
ORIGINAL PAGE IS
OF POOR QUALITY
ADMITTANCE
FUNCTION
g/lb
TEST NO. 6
AXIS 4X-
FREQ, Hz
180°
PHASE
-180°
ADMITTANCE
FUNCTION
g/lb
TEST NO. 6
AXIS 5X+
FREQ, Hz

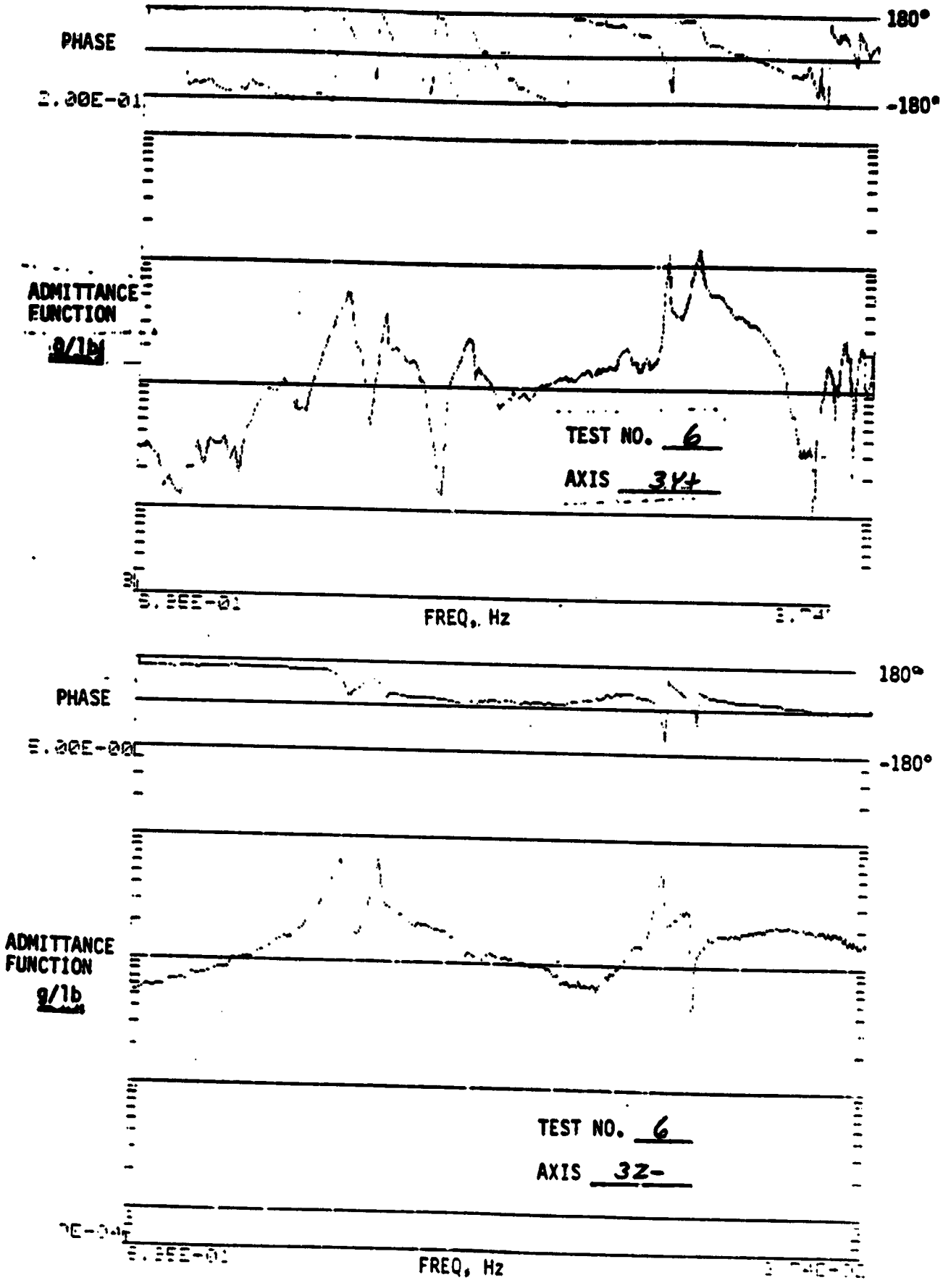
PHASE
180°
-180°
ADMITTANCE FUNCTION g/lb
TEST NO. 6
AXIS 3Y+
FREQ, Hz
PHASE
180°
-180°
ADMITTANCE FUNCTION g/lb
TEST NO. 6
AXIS 3Z-
FREQ, Hz

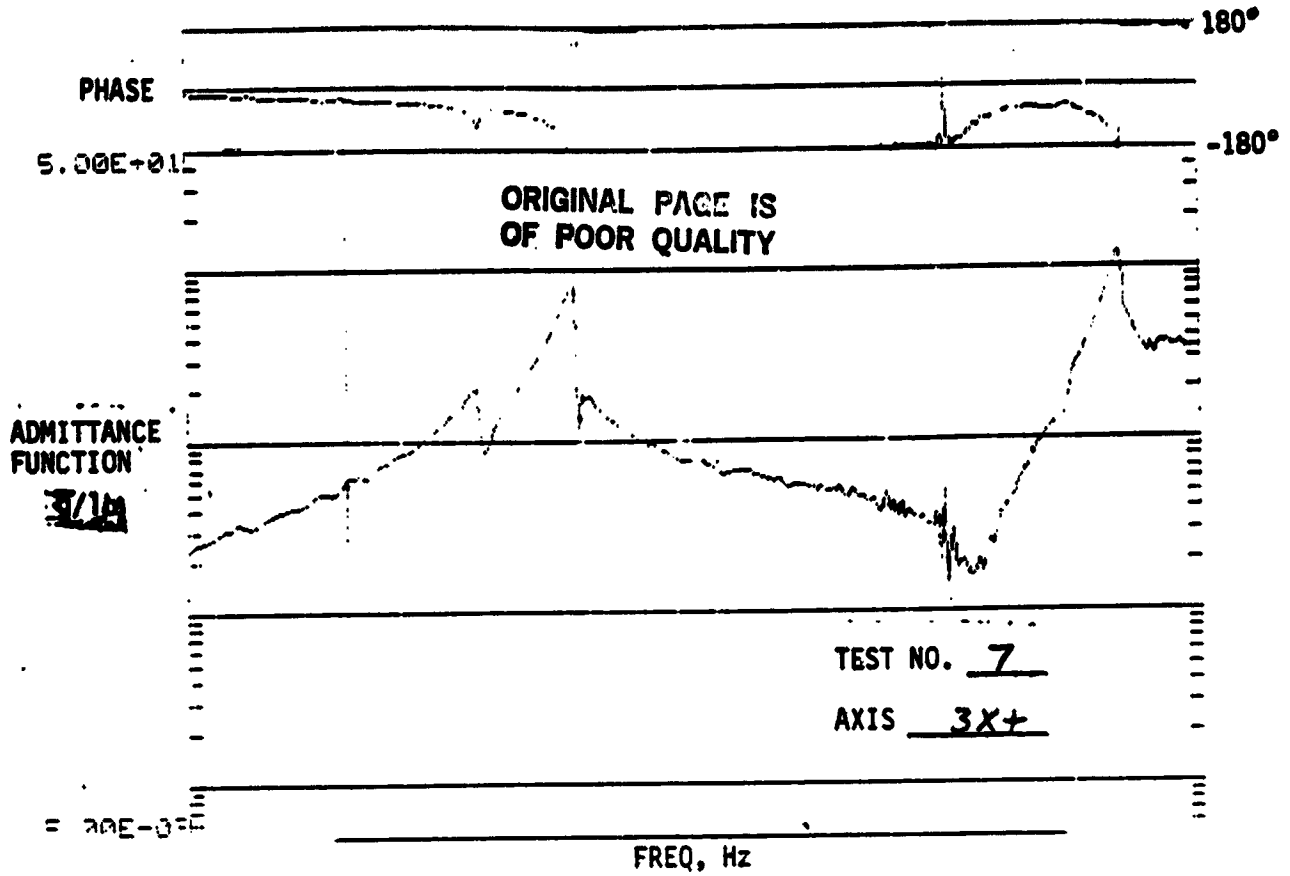




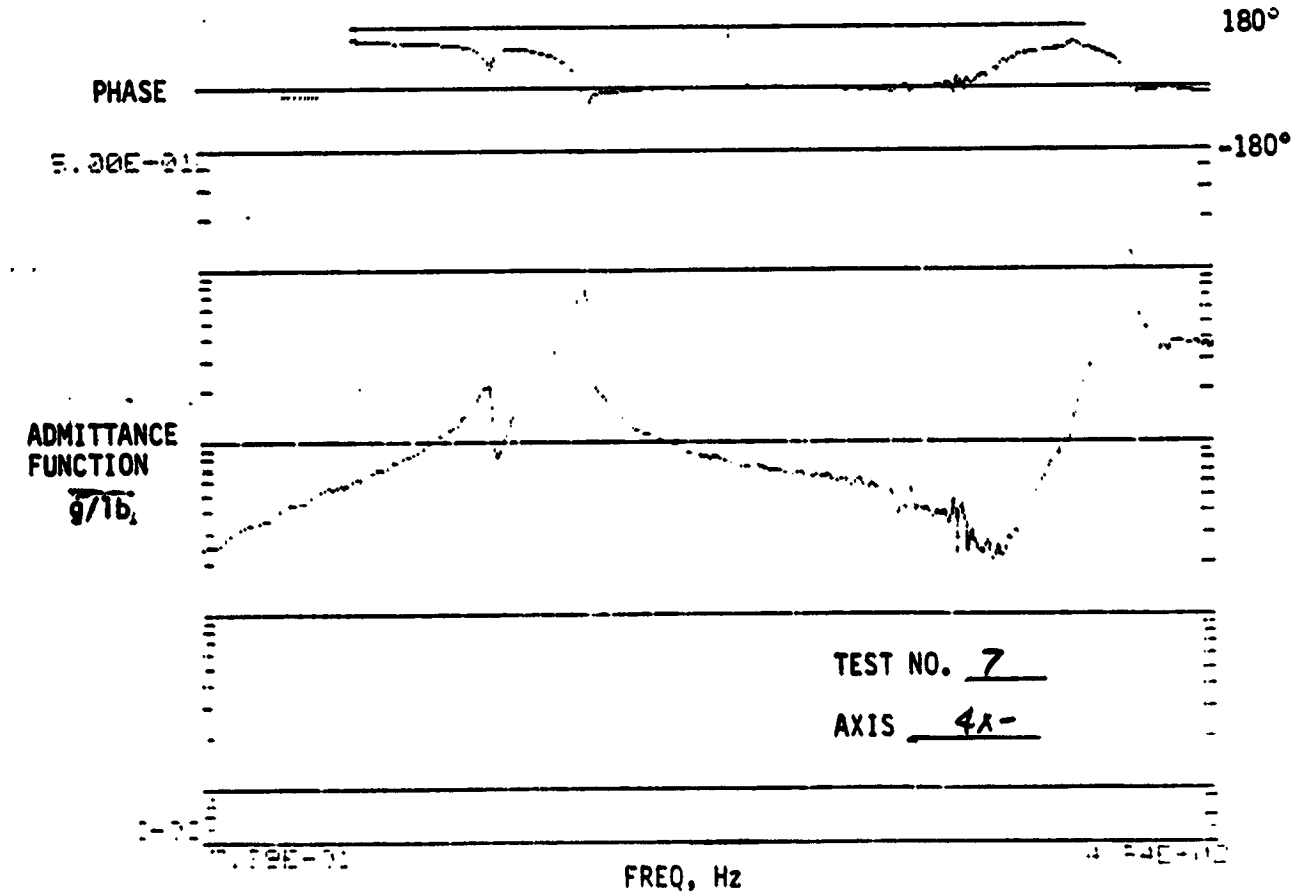

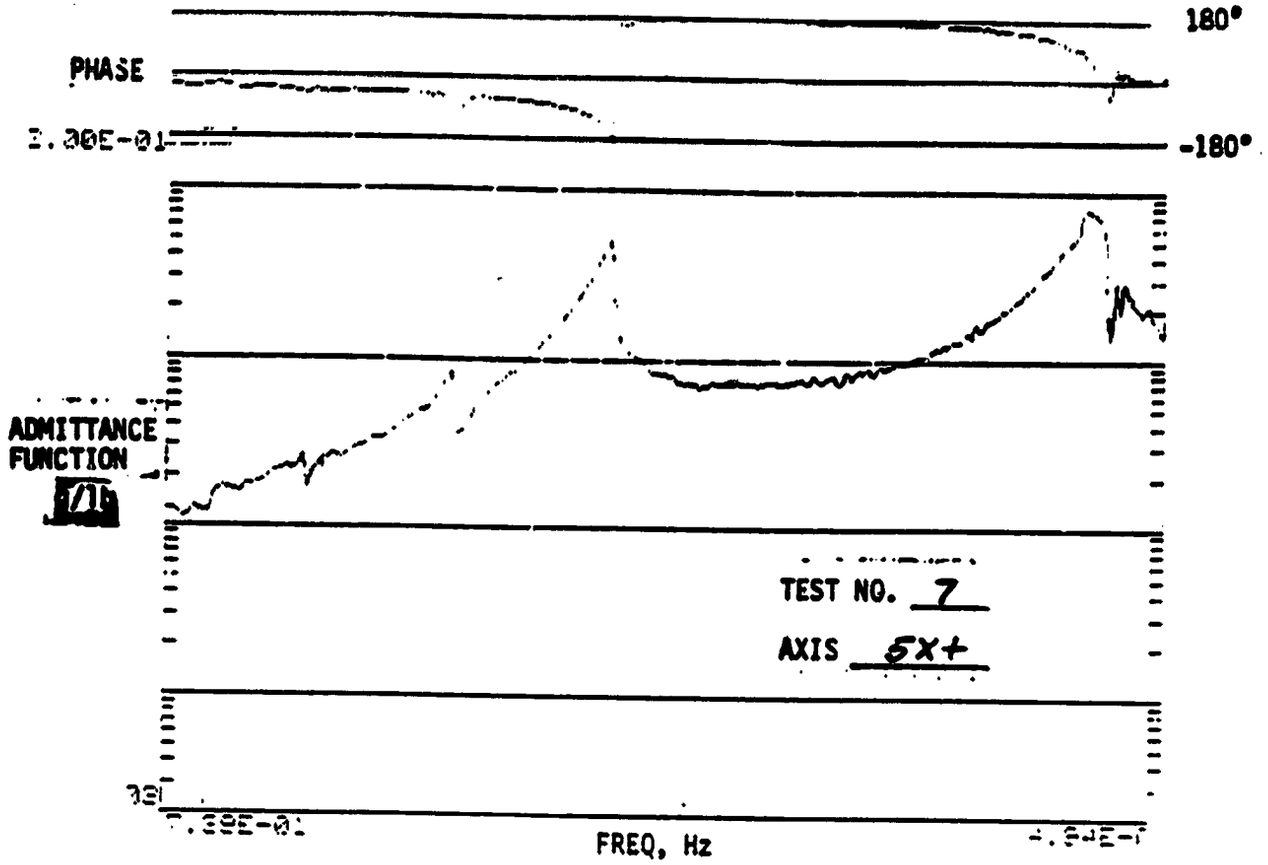
180°
PHASE
-180°
ADMITTANCE
FUNCTION
5/1b
TEST NO. 7
AXIS 5X+
FREQ, Hz

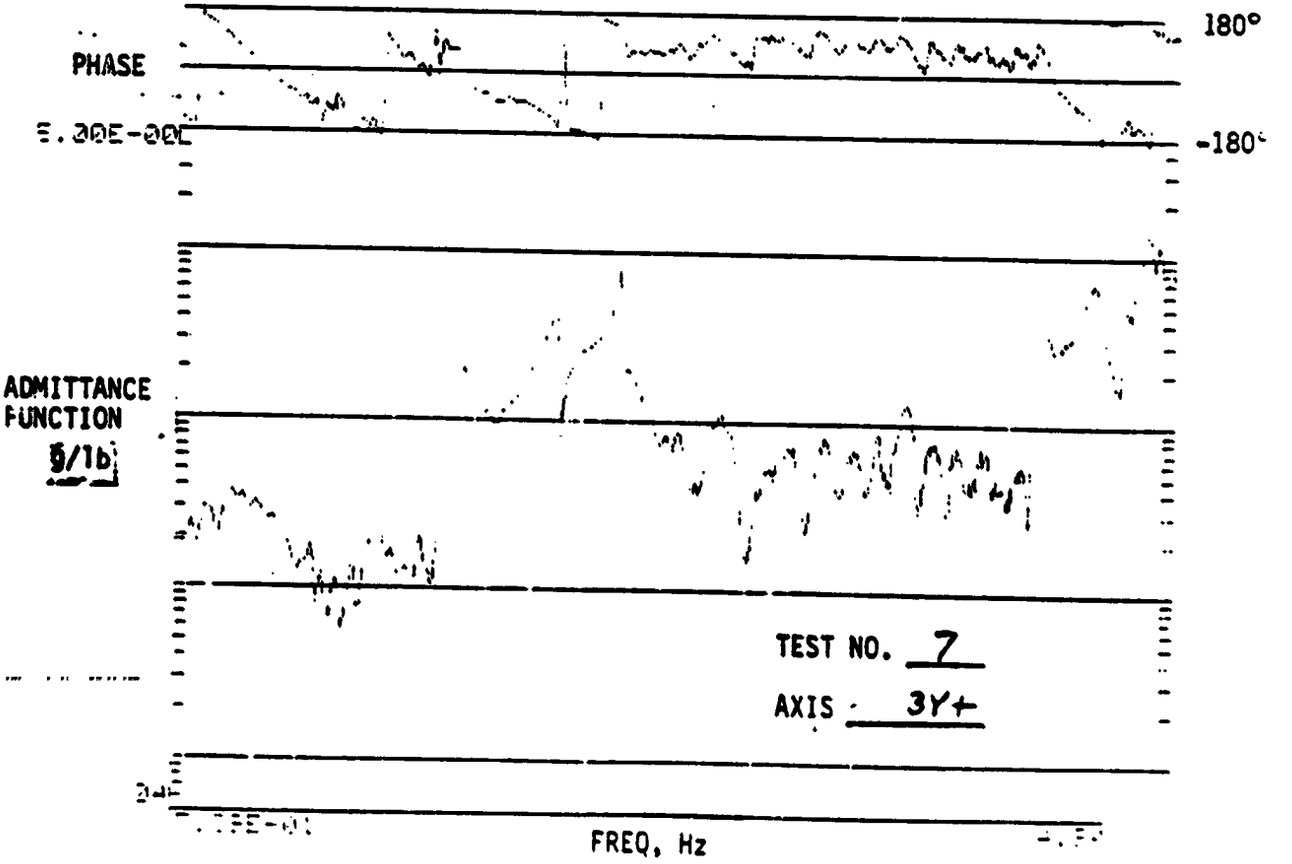
180°
PHASE
-180°
ADMITTANCE
FUNCTION
5/1b
TEST NO. 7
AXIS 3Y+
FREQ, Hz

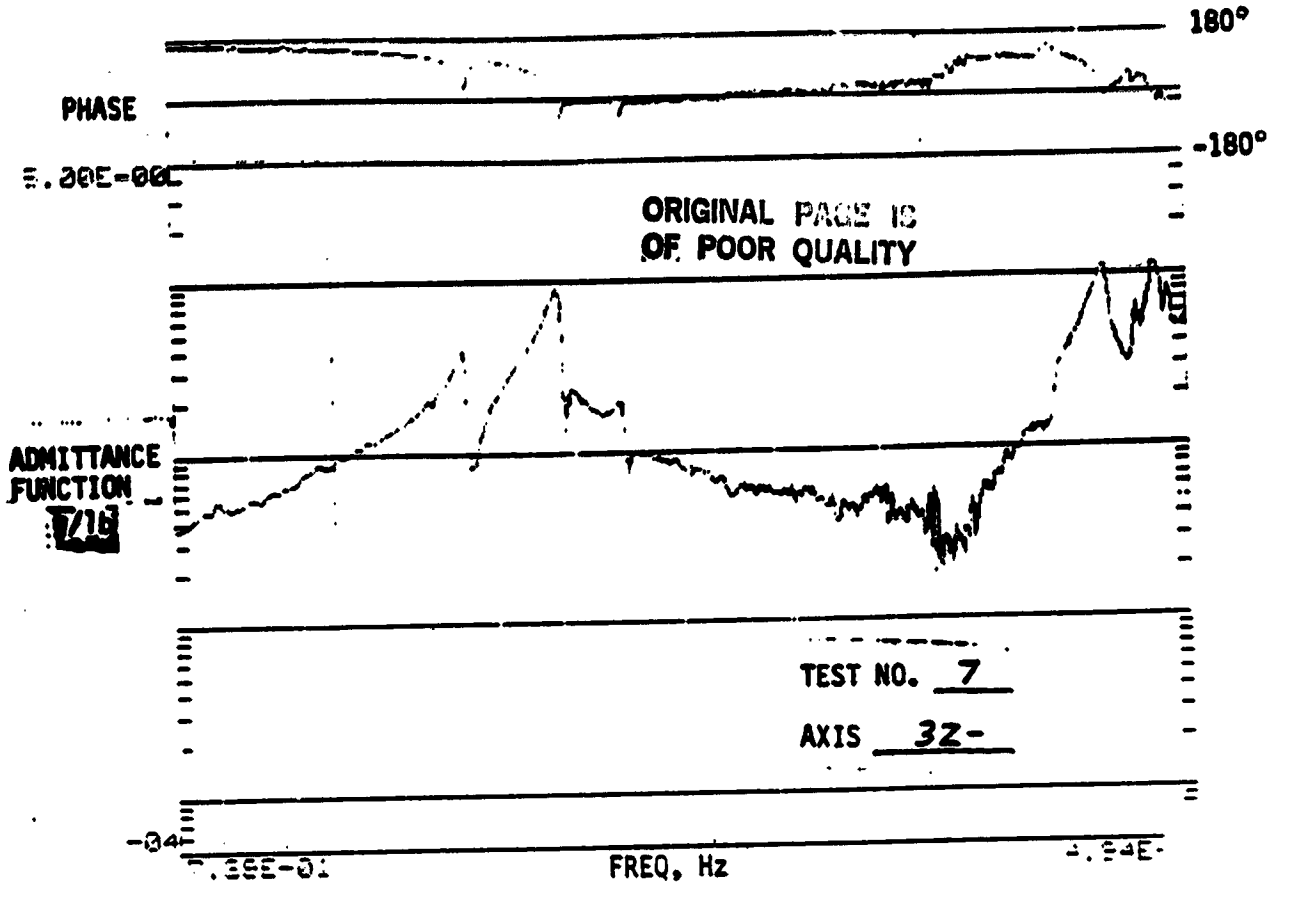
180°
PHASE
-180°
ORIGINAL PAGE IS
OF POOR QUALITY
ADMITTANCE
FUNCTION
9/1a
TEST NO. 7
AXIS 3Z-
FREQ, Hz

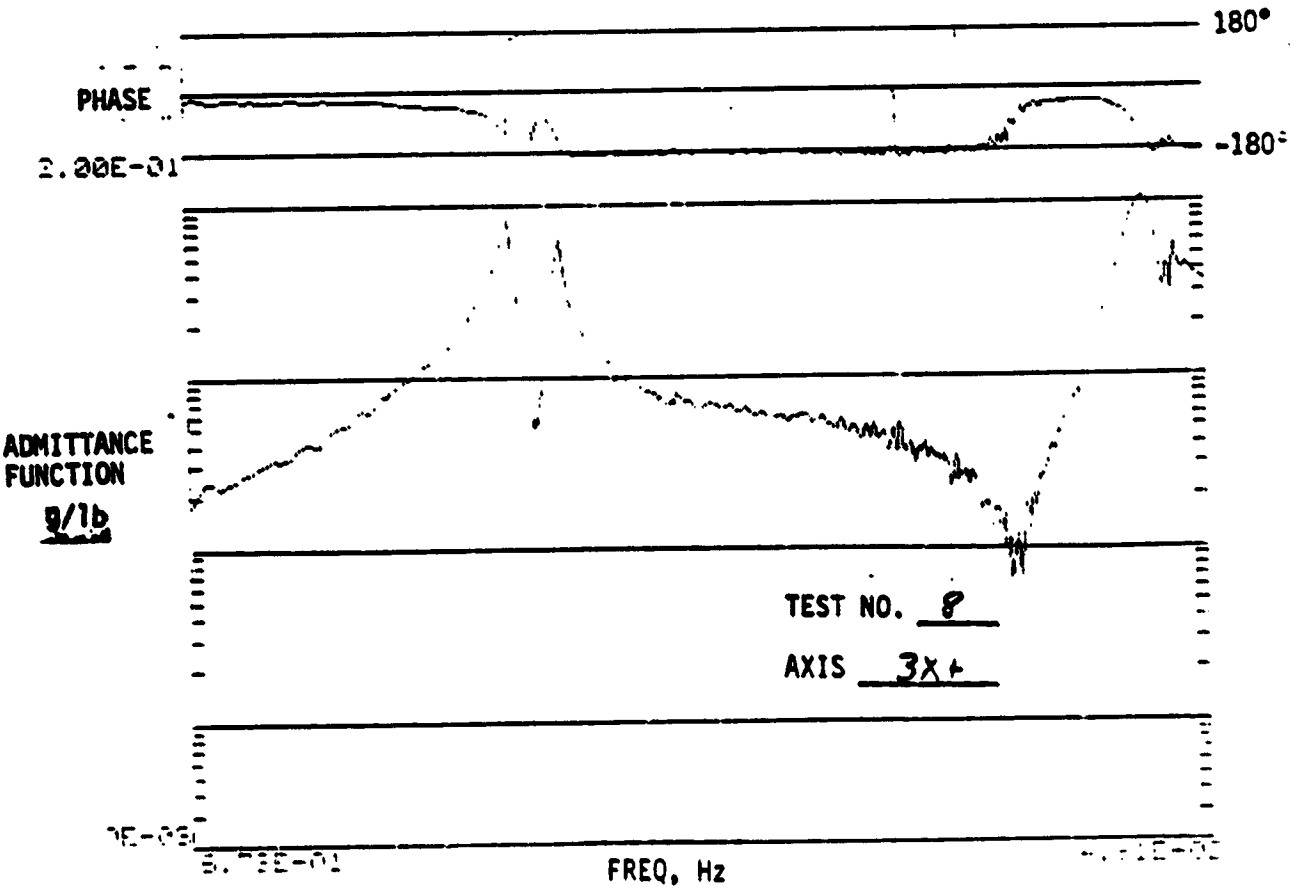
180°
PHASE
-180°
2.20E-01
ADMITTANCE
FUNCTION
9/1b
TEST NO. 8
AXIS 3X+
FREQ, Hz

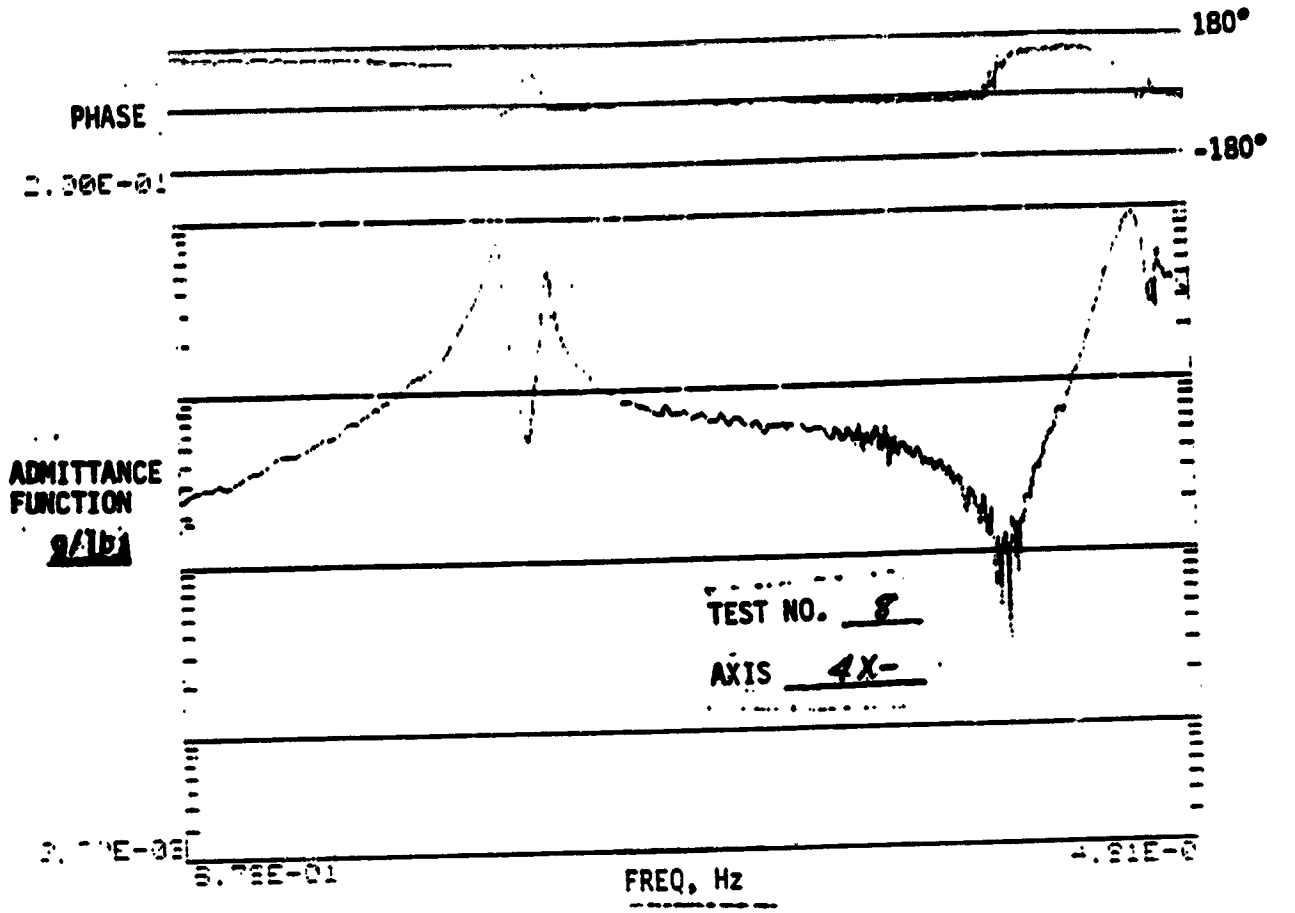
180°
PHASE
-180°
2.00E-01
ADMITTANCE FUNCTION
g/lb
TEST NO. 8
AXIS 4X-
FREQ, Hz

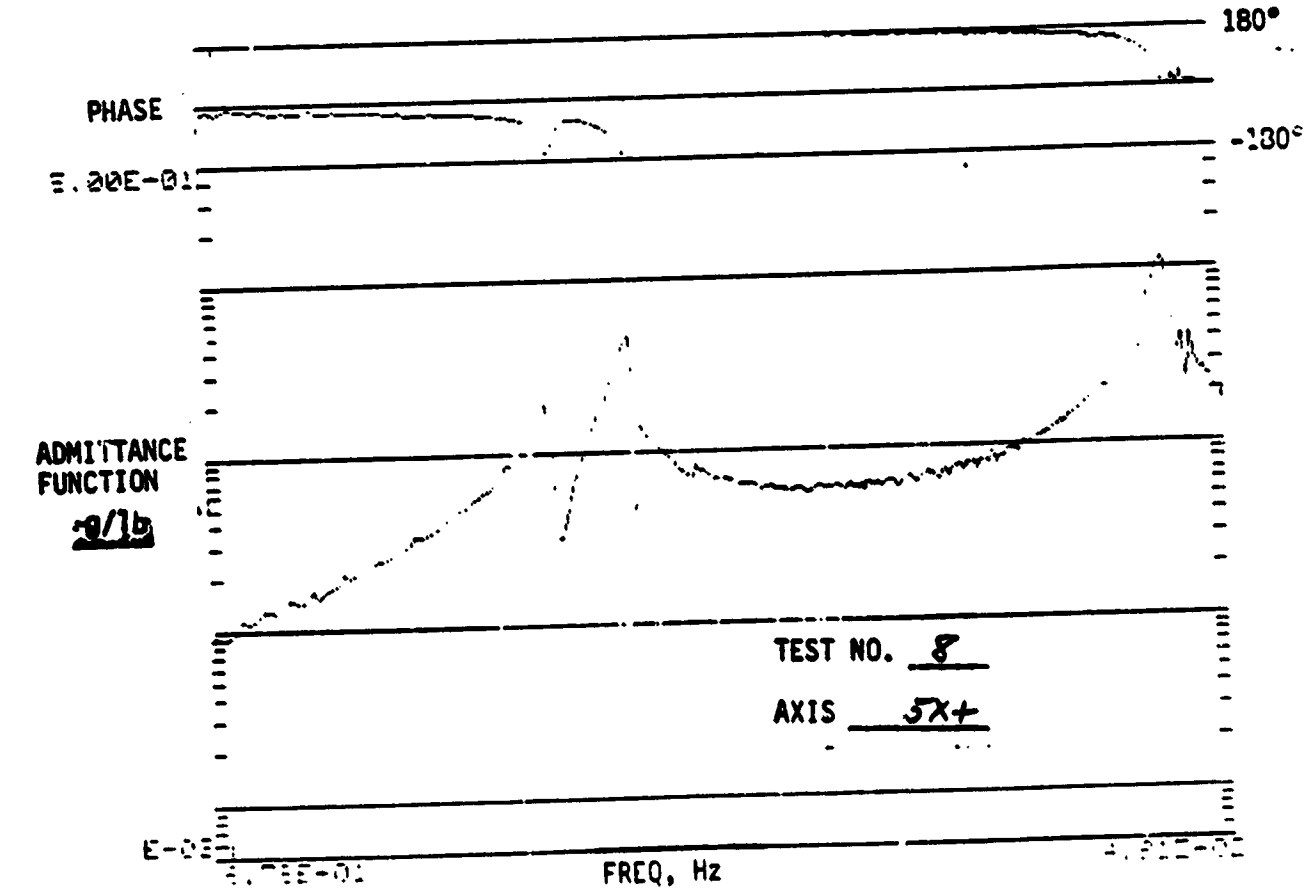
180°
PHASE
-180°
2.00E-01
ADMITTANCE FUNCTION
g/lb
TEST NO. 8
AXIS 5X+
FREQ, Hz

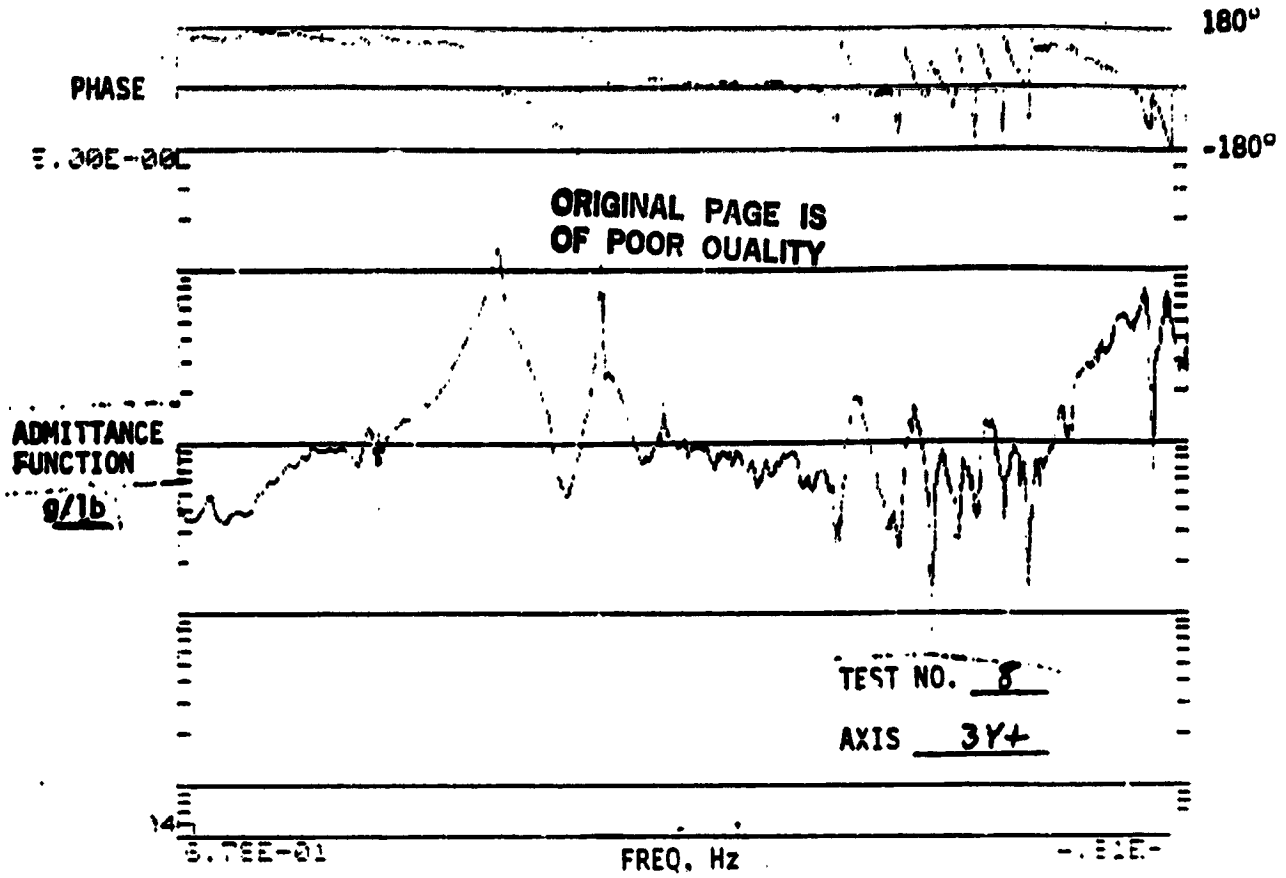
180°
PHASE
-180°
ORIGINAL PAGE IS
OF POOR QUALITY
ADMITTANCE
FUNCTION
g/lb
TEST NO. 8
AXIS 3Y+
FREQ, Hz

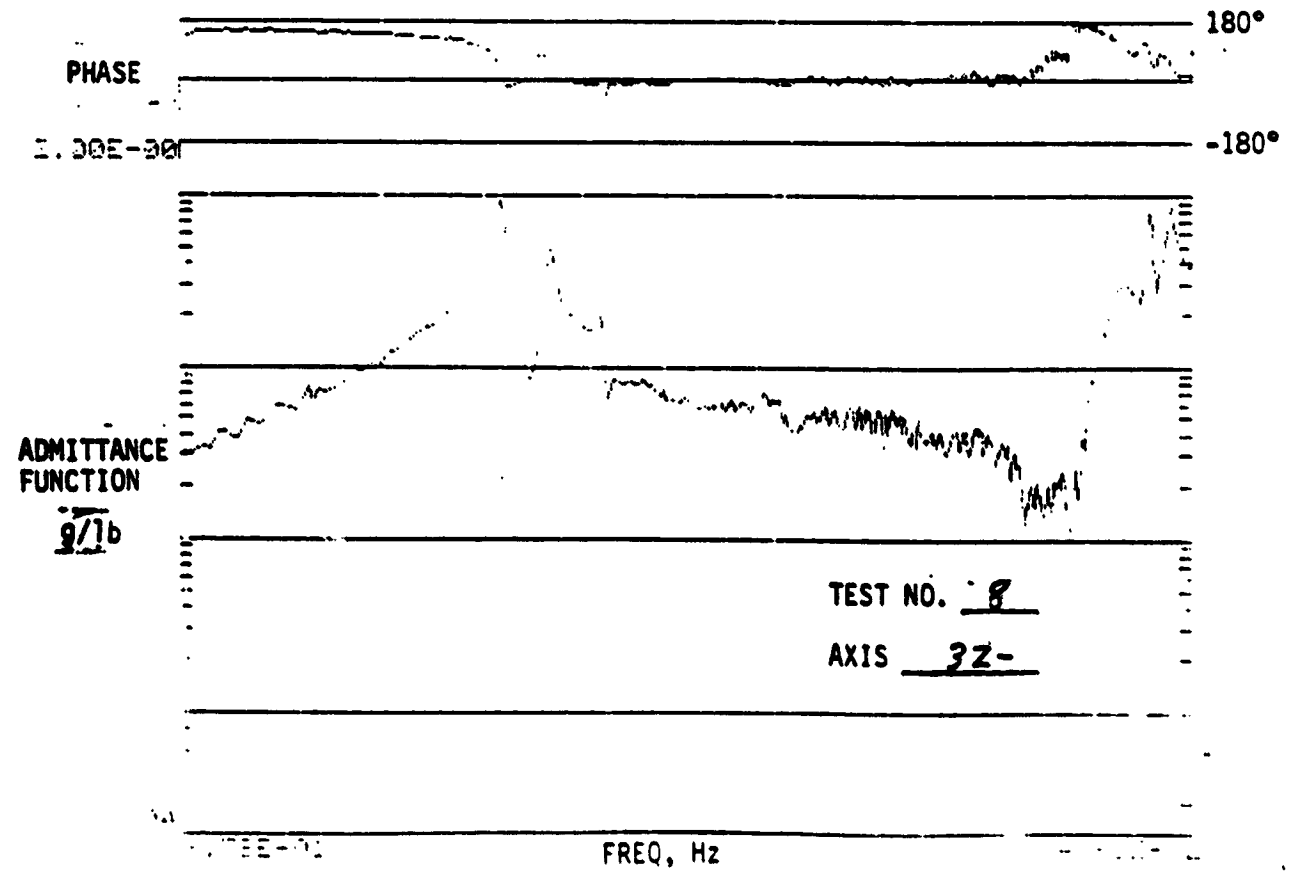
180°
PHASE
-180°
ADMITTANCE
FUNCTION
g/lb
TEST NO. 8
AXIS 3Z-
FREQ, Hz